MECHANISTIC CHARACTERIZATION OF MEMBERS OF THE AMIDOHYDROLASE SUPERFAMILY

A Dissertation

by

RICARDO MARTÍ ARBONA

Submitted to the Office of Graduate Studies of
Texas A&M University
in partial fulfillment of the requirements for the degree of

DOCTOR OF PHILOSOPHY

December 2006

Major Subject: Chemistry

MECHANISTIC CHARACTERIZATION OF MEMBERS OF THE AMIDOHYDROLASE SUPERFAMILY

A Dissertation

by

RICARDO MARTÍ ARBONA

Submitted to the Office of Graduate Studies of
Texas A&M University
in partial fulfillment of the requirements for the degree of

DOCTOR OF PHILOSOPHY

Approved by:

Chair of Committee,	Frank M. Raushel
Committee Members,	Paul A. Lindahl
	Eric E. Simanek
	Jerry Tsai
Head of Department,	Emile A. Schweikert

December 2006

Major Subject: Chemistry

ABSTRACT

Mechanistic Characterization of Members of the

Amidohydrolase Superfamily. (December 2006)

Ricardo Martí Arbona, B.S., Universidad de Puerto Rico, at Río Piedras

Chair of Advisory Committee: Dr. Frank M. Raushel

The amidohydrolase superfamily is a functionally diverse group of enzymes found in every organism sequenced to date. The landmark for this superfamily is the conservation of a $(\beta/\alpha)_8$-barrel structural fold. Isoaspartyl dipeptidase (IAD) from *Escherichia coli* catalyzes the hydrolytic cleavage of β-aspartyl dipeptides. Structural studies of the wild-type enzyme demonstrate that the active site consists of a binuclear metal center. Bell-shaped pH-rate profiles are observed for all four metal-substituted forms of the wild-type enzyme and the site-directed mutants, E77Q and Y137F. Structural analysis of IAD with the bound substrate and site-directed mutagenesis shows the importance of the side chains of residues Glu-77, Tyr-137, Arg-169, Arg-233, Asp-285, and Ser-289 in the substrate binding and hydrolysis. The reaction mechanism for the hydrolysis of dipeptides by IAD is initiated by the polarization of the amide bond via complexation to the β-metal and the hydrogen bond to Tyr-137. Asp-385 participates in the activation of the bridging hydroxide for nucleophilic attack at the peptide carbon center. The lately protonated Asp-285 donates the proton to the α-amino group of the leaving group, causing the collapse of the tetrahedral intermediate and cleavage of the carbon-nitrogen bond. *N*-formimino-L-glutamate iminohydrolase (HutF) from

Pseudomonas aeruginosa acts in the deimination of the fourth intermediate of the histidine degradation pathway, *N*-formimino-L-glutamate. An amino acid sequence alignment between HutF and other members of the amidohydrolase superfamily containing mononuclear metal centers suggests that the residues Glu-235, His-269, and Asp-320 are involved in substrate binding and deimination. Site-directed mutagenesis of Glu-235, His-269, and Asp-320, in conjunction with the analysis of the four metal-substituted enzyme forms and pH-rate profiles provides valuable information toward the proposal of a mechanism for deimination of *N*-formimino-L-glutamate by HutF. This information suggests that the reaction is initiated by the activation of the hydrolytic water through base catalysis via His-269. The enhanced nucleophile attacks the formimino carbon center. In a concerted reaction, Asp-320 deprotonates the hydroxide nucleophile, and His-269 donates a proton to the terminal amino of the iminium group resulting in the collapse of the tetrahedral intermediate, the cleavage of the carbon-nitrogen bond and the release of the products.

DEDICATION

To my wife, Denisse, my complement, inspiration and support, who makes me whole, and brings equilibrium and control to this chaos that people call life; to my parents, Angel and Josefina, who have been always there to laugh and cry with me, to share my achievements and disappointments, to listen, and help me through difficult times and to show me the way; to my brothers, Angel, Jonathan and Edgar, my best friends and supporters; and to my grandparents, Cheo and Pancha, who have been my biggest example of strength, devotion and accomplishment.

ACKNOWLEDGMENTS

I would like to thank Dr. Vicente Fresquet for everything he taught me and for his support throughout my graduate studies. Also, I thank my advisor, Dr. Frank M. Raushel, for his guidance and support and my committee members: Dr. Paul A. Lindahl, Dr. Erik E. Simanek and Dr. Jerry Tsai. Many thanks go to my past and present colleagues from Raushel's laboratory for their friendship and assistance through the years, especially Richard Hall for all the help with the spelling corrections of this dissertation.

TABLE OF CONTENTS

TABLE OF CONTENTS (continued)

LIST OF FIGURES

LIST OF FIGURES (continued)

Page

LIST OF TABLES

Page

CHAPTER I

INTRODUCTION:

THE AMIDOHYDROLASE SUPERFAMILY,

A PARADIGM OF CATALYTIC DIVERSITY

The amidohydrolase superfamily is composed of a group of predominantly hydrolytic enzymes that operate on a wide range of substrates containing amines, imides, amides, phosphotriesters, ureas, carbon and phosphorus centers (*1-3*). The superfamily was first identified in 1997 by Holm and Sander from the three-dimensional structural similarities between urease (URE), phosphotriesterase (PTE), and adenosine deaminase (ADA) (*4*). The landmark for this superfamily is the conservation of a $(\beta/\alpha)_8$-barrel (TIM-barrel) structural fold that binds a mononuclear or binuclear metal center at the C-terminus end of the barrel. In spite of the strongly divergent protein sequences, the conservation of the $(\beta/\alpha)_8$-barrel structural fold has produced a remarkable array of enzymatic activities within the superfamily. This catalytically diverse, yet structurally related group of enzymes suggests that their catalytic transformations may have evolved from an ancestral precursor (*5*). The catalytic diversity extends from the metabolism of purines (*6*) and pyrimidines (*7*) as well as the salvage of amino acid (*8, 9*) to the hydrolysis of organophosphate pesticides (*3, 10*). The amidohydrolase superfamily is one of the thirty one protein superfamilies containing the $(\beta/\alpha)_8$-barrel structural fold

---

This dissertation follows the style of *Biochemistry.*

OMP decarboxylase superfamily (*5, 11-14*), aldolase superfamily (*5, 13*), pyruvate kinase superfamily (*13, 15*), thiyl radical superfamily (*16*), and the crotonase superfamily (*16*).

The divergence of catalytic specificity demonstrated by the amidohydrolase superfamily is represented in Scheme 1.1. The X-ray crystal structures of 19 members of the amidohydrolase superfamily can be obtained from the National Center for Biotechnology Information (NCBI) Protein Data Bank (PDB). From the 19 structures, 12 have known catalytic function. These are urease (URE, PDB entry code 2ubp) (*17*), phosphotriesterase (PTE, PDB entry code 1hzy) (*18*), dihydroorotase (DHO, PDB entry code 1j79) (*19*), D and L-hydantoinases (D-HYD, PDB entry code 1gkp and L-HYD, PDB entry code 1gkr) (*20, 21*), dihydropyrimidinase (DHP, PDB entry code 1k1d) (*22*), renal dipeptidase (RDP, PDB entry code litq) (*23*), *N*-acetyl glucosamine-6-phosphate deacetylase (AGD, PDB entry code 1o12) (*24*), uronate isomerase (URI, PDB entry code 1j5s) (*25*), D-amino acid deacetylase (DAA, PDB entry code 1m7j) (*26*), adenosine deaminase (ADA, PDB entry code 1a4m) (*7*), cytosine deaminase (CDA, PDB entry code 1k6w) (*6*) and β-aspartyl dipeptidase (IAD, PDB entry code 1onw) (*27*). Six of the reported structures remain with unknown biological function, these are the PTE homology protein (PHP, PDB entry code 1bf6) (*28*), three putative DNases from *Escherichia coli* (TatD, YjjV, and YcfH with PDB entry codes 1xwy, 1zzm, and 1yix, respectively) solved by the efforts of the New York Structural Genomics Research Consortium, and two proteins from *Thermotoga maritima* solved by the efforts of the

Joint Center for Structural Genomics, a probable chlorohydrolase (Tm0936, PDB entry code 1j6p) and a tatD related protein (Tm0667, PDB entry code 1j6o).

Scheme 1.1

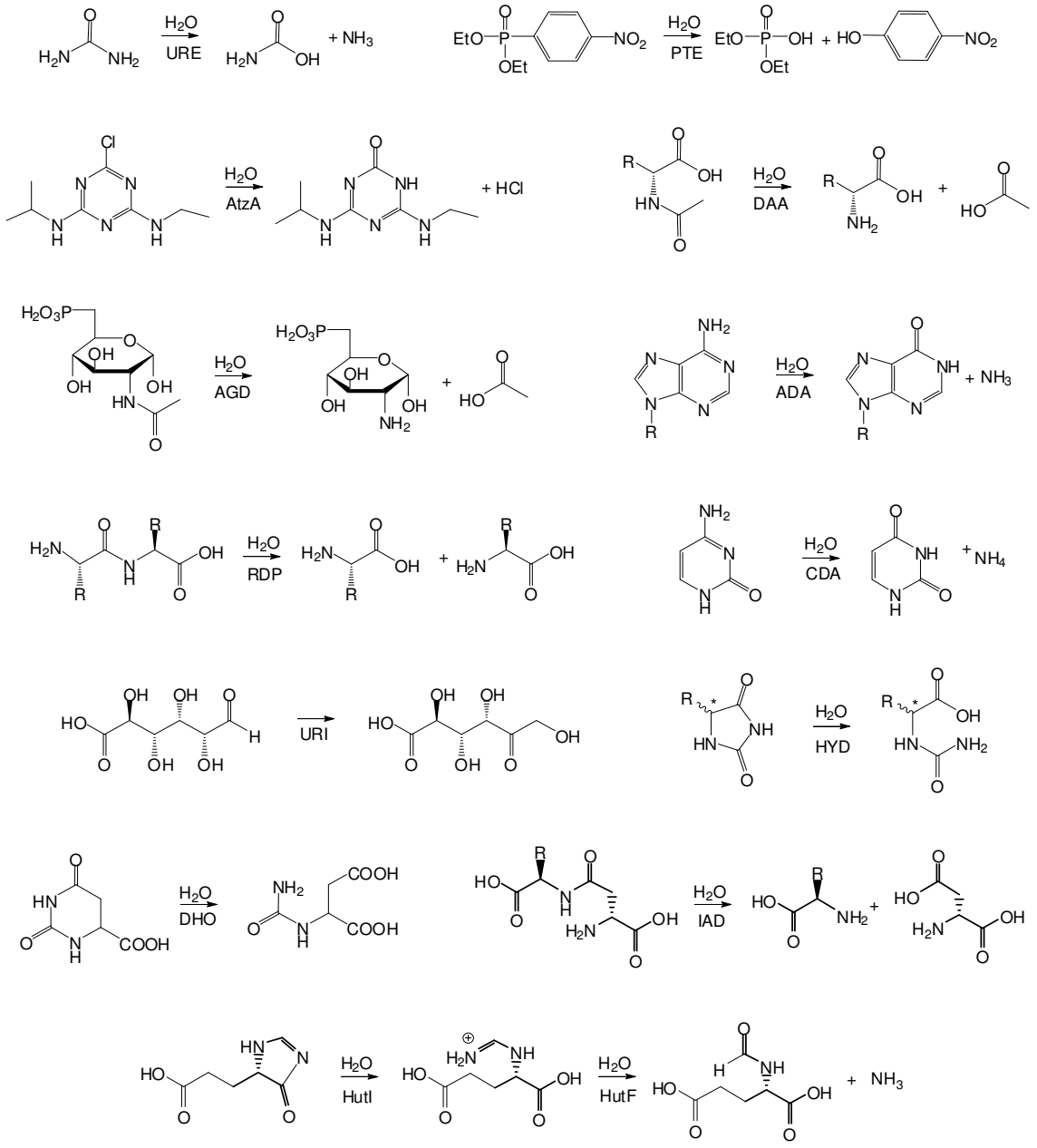

The available X-ray crystal structures for members of the amidohydrolase superfamily have been extensively analyzed (*1, 6, 7, 17-21, 23-28*). Despite the conservation of the $(\beta/\alpha)_8$-barrel structural fold among the superfamily members, evolution has produced similar, yet sufficiently diverse active site architectures to bring out a remarkable array of catalytic activity. The analysis of the X-ray crystal structures of this catalytically diverse group of enzymes has highlighted the existence of at least nine slightly different active sites architectures. This information is expected to widely expand the range of active sites architectures found within the amidohydrolase superfamily members.

The most common of the active sites within the superfamily is the binuclear metal center found in PTE, DHO, IAD, URE, and HYD (Figure 1.1A). A solvent hydroxide and a carboxylated lysine side chain from strand 4 bridge the two divalent metal ions in the active site. The carboxylation of the lysine from strand 4 originates from a post-translational modification (*29*). The more buried metal ion (M_α) is coordinated by the $N^{\varepsilon 2}$ of two histidine residues from strand 1 of the β-barrel and the $O^{\delta 1}$ of the aspartate from strand 8. The more solvent-exposed metal ion or M_β is ligated to the $N^{\delta 1}$ of the imidazole side chain of histidine from strand 5 and the $N^{\varepsilon 2}$ of the imidazole side chain of histidine from strand 6. Some members of the superfamily have virtually the same type of binuclear active site with a slight difference in that the carboxylated lysine is replaced by the carboxylate side chain of a glutamate residue extending from the same strand. An example of this is the PTE homology protein from *Escherichia coli* (*28*) (Figure 1.1A). Another variation in the construction of the

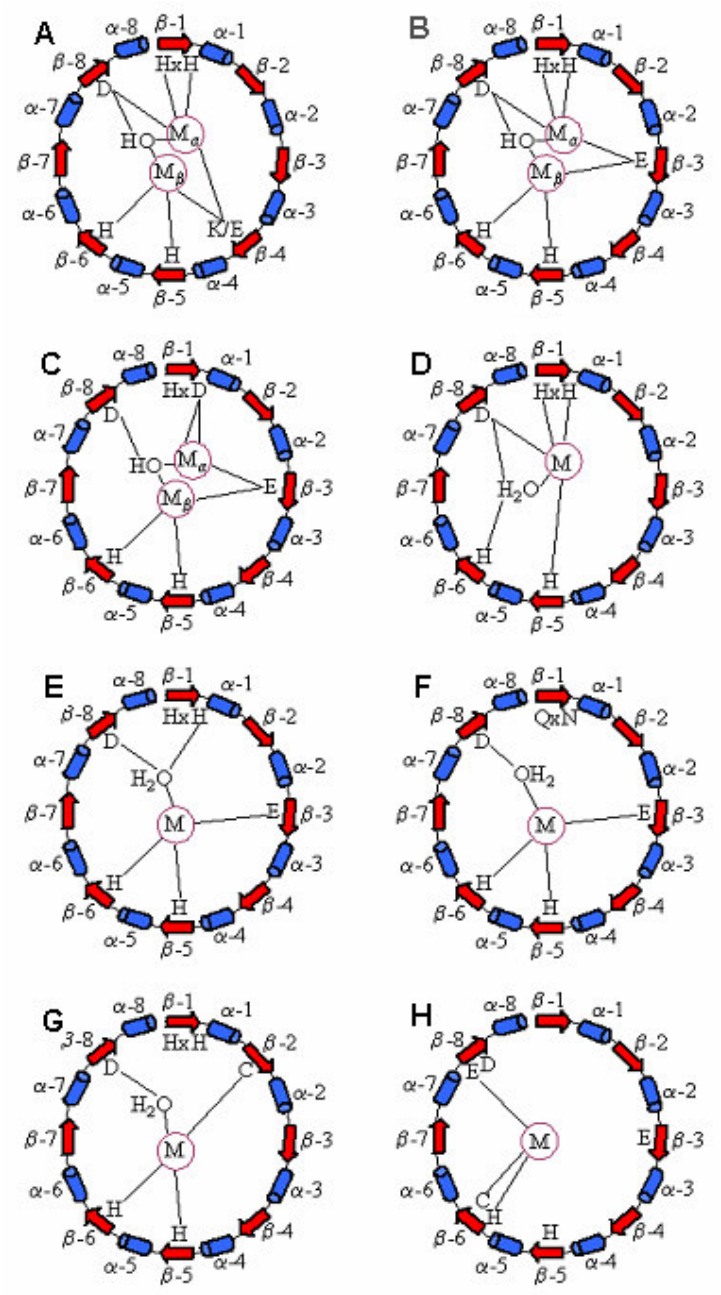

Figure 1.1: Schematic comparison of variations of the mononuclear or binuclear metal centers of enzymes within the amidohydrolase superfamily. The representation of different variations of the active site construction of members of the superfamily are exemplified by PTE (A), AGD from *B. subtilis* (B), RDP (C), ADA (D), AGD from *Thermotoga maritima* (E), AGD from *Escherichia coli* (F), DAA (G), and TatD (H).

binuclear active site is that found in AGD from *Bacillus subtilis* (Figure 1.1B), and consists of an inversion on the orientation of the histidine from strand 5, which ligates M_β with the $N^{\varepsilon 2}$ of the imidazole side chain instead of the $N^{\delta 1}$ and the bridging residue is a glutamate from strand 3 rather than strand 4. The last of the variations, yet found for these types of bimetal active sites is exemplified by RDP from humans. In the RDP active site (Figure 1.1C), the bridging glutamate originates from strand 3, also the second histidine from strand 1 is replaced by an aspartate which coordinates M_α. The aspartate from strand 8 does not appear to ligate to the metal but retains its relative position by ligating the bridging hydroxyl from solvent (*1*).

There are several variations within the active site for those members of the amidohydrolase superfamily that contain a single divalent metal center. In the case of ADA, CDA and related enzymes (Figure 1.1D), the primary metal ligands are the $N^{\varepsilon 2}$ of the two histidines from strand 1, the $N^{\varepsilon 2}$ of the histidine from strand 5, the $O^{\delta 1}$ of the aspartate from strand 8 and a solvent molecule (*6, 7*). The orientation of the single metal ion in the active site is virtually the same as the M_α from the binuclear metal center mentioned above. The metal bridging residue from strand 4 is missing and the histidine from strand 5 shifts toward the lone metal to act as the fourth ligand. The histidine from strand 6 is not coordinated to any metal, but appears to participate in the activation of the hydrolytic water (*7*). The identity of divalent cations required for catalytic activity appears to have inherent flexibility, and may include Cd, Co, Fe, Mn, Ni, and Zn (*6, 7*).

There are three other variations to the mononuclear active sites subgroup. They differ in the orientation of the metal in the active site, which is in the β site rather that the

α site. AGD from *Thermotoga maritima* (Figure 1.1E) is an example in which a single iron ion is coordinated to the $N^{\varepsilon 1}$ of the histidines on strands 5 and 6, the $O^{\gamma 1}$ of a glutamate that originates from strand 3 and two water molecules (*1, 24*). One of the water molecules serves as a bridge between the aspartate from strand 8 and the iron ion. It is also within H-bond distance from the second histidine from strand 1. In this active site variant, the histidines from strand 1 do not interact with the metal, which makes an interesting correlation with its homolog protein in *Escherichia coli*. The AGD in *Escherichia coli* (Figure 1.1F), lacks the two histidines from strand 1. They have been replaced by glutamine and an asparagine residue from the same strand. These types of residues are not usually involved in metal ligation. The rest of the metal ligands remain unchanged.

The last of the variations in the mononuclear metal center group is represented by DAA (Figure 1.1G). The X-ray crystal structure of DAA contains a single zinc ion located at the β site (*26*). The histidines from strand 1 do not interact with the metal. The metal is coordinated by the $N^{\delta 2}$ of the imidazole ring side chain of the histidines on strand 5, the $N^{\varepsilon 2}$ of the imidazole ring side chain of the histidine on strand 6, and an unusual cysteine residue from strand 2. The aspartate from strand 8 is located to act as an activator of the hydrolytic water. It has been demonstrated that a second metal ion can be forced into the active site of DAA by the incubation with high concentrations of the divalent metal (*30*). This presented no effect in catalytic activity.

There are three other very atypical members of the superfamily. URI stands by itself on both active site architecture and the chemical catalysis. The presence of the

metal in the X-ray crystal structure was uncertain because the electron density was not sufficient to differentiate between a metal and a water molecule (*25*). The absence of the divalent metal or metals in the active site may create difficulties in the assignment of the active site residues (*31*). The prediction of the residues in the active site were obtained from structural alignments and suggests the conservation of two histidines from strand 1, a histidine from strand 5, and an aspartate from strand 8. URI lacks a histidine at the end of strand 6, but there are other residues at the end of other strands that may act as potential ligands or catalytic residues (*1*). Another of these atypical members is the recently discovered α-amino-β-carboxymuconic-ε-semialdehyde decarboxylase (ACMSD) (*32*). ACMSD catalyzes the decarboxylation of α-amino-β-carboxymuconic-ε-semialdehyde to α-aminomuconic-ε-semialdehyde (*33*). They are only reported members of the amidohydrolase superfamily that does not catalyze hydrolytic reactions.

One of the most recent X-ray crystal structures of a member of the amidohydrolase superfamily was obtained in 2005 for a putative DNase enzyme from *Escherichia coli* called TatD (Figure 1.1H). This protein is shown to have the lowest identity, in terms of active site composition, to the rest of the proteins mentioned above. In this active site, the mononuclear metal center is ligated by a histidine and a cysteine from strand 6 and a glutamate from strand 8. The conserved glutamate from strand 4, the histidine from strand 5 and the aspartate from strand 8 are present but the absence of biological functional characterization or substrate specificity makes it difficult to define a role for these residues.

The active sites of members of the amidohydrolase superfamily are found at the C-terminal end of the $(\beta/\alpha)_8$-barrel. Immediately after the residues that form the active site are loops that connect the β-strands from the barrel to the subsequent α-helix. These loops vary in length, conformation and amino acid composition. The importance of the loops at the C-terminal end of the $(\beta/\alpha)_8$-barrel on binding and substrate specificity can be inferred from the reported X-ray crystal structures of members of the superfamily (*1*). In the available substrate/inhibitor complexes determined by diffraction, the loops appear to perform several functions. For example, in ADA the loop immediately after strand 2 acts as a gatekeeper, using a hydrophobic tryptophan side chain to shield the catalytic interconversion from the bulk solvent, whilst the loop after strand 1 has a direct interaction with the substrate (*1*). Comparisons between the X-ray crystal structures of the native and complexed proteins have shown that the loops at the end of the C-terminus of the $(\beta/\alpha)_8$-barrel are highly mobile with elevated temperature factors in the absence of the substrate and became organized with much lower temperature factors in the complexed crystal structures (*1, 27*). One of the most interesting contributions of the loops for this superfamily is on the stereoselective hydrolysis of amino acids hydantoins by L-HYD and D-HYD. The X-ray crystal structures for these two enzymes demonstrates how the role of the loops in the orientation of the substrates can discriminate between the enantiomers (*20, 22*). These observations indicate how evolution has conserved the catalytic architecture necessary for the activation and attack of the hydrolytic water of an ancestral precursor, and at the same time enrich its

functionality with a wide variety of active site pockets with high specificity for an extensive assortment of substrates.

The divalent metal ions in the active site play a vital role in the activation of the hydrolytic water and/or the substrate. There are two proposed mechanisms for the hydrolytic transformations performed by the members of the amidohydrolase superfamily. These mechanisms are slightly different depending of the ability of the protein to bind one or two divalent cations to the active site (*1*). The majority of the members of the superfamily that are involved in the elimination of ammonia contain a mononuclear metal center and employ the reaction mechanism illustrated in the Scheme 1.2. Examples of these enzymes are ADA (*34*), CDA (*6*), and guanine deaminase among others (*1*). In this reaction mechanism the water molecule in the active site is coordinated to the single metal ion in the α-position and is H-bonded to the histidine from strand 6 and aspartate from strand 8. After the binding of the substrate, the reaction is initiated by the activation of the water molecule by general base catalysis from the histidine of strand 6. The activated hydroxide attacks the reaction center generating a tetrahedral intermediate and promotes the abstraction of a proton from a conserved glutamate three residues beyond the histidine from strand 5. This HxxE motif is found in most of the enzymes that have a lone metal ion in the α-position (*1*). The collapse of the tetrahedral intermediate is triggered by the general base catalysis of the aspartate by abstracting a proton from the carbinol intermediate, followed by proton donation to the ammonia leaving group by the histidine from strand 6 (*1, 6, 34*).

Scheme 1.2: Proposed reaction mechanisms of hydrolysis of ammonia by members of the superfamily containing mononuclear metal centers. Examples of these enzymes are ADA, CDA, AMP deaminase, guanine deaminase and the proteins annotated as chlorohydrolases.

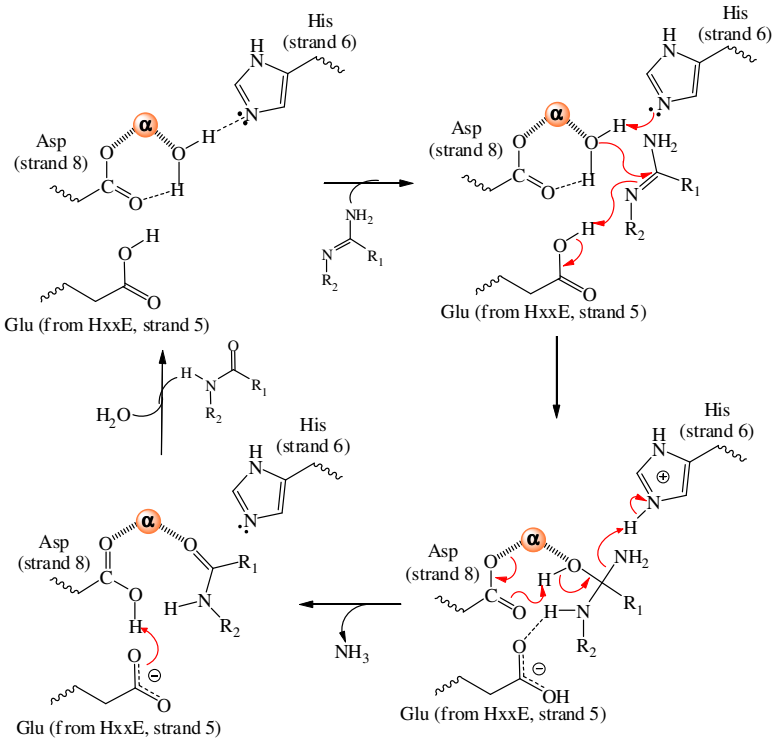

The proposed reaction mechanisms of hydrolysis for members of the superfamily that contain two metal ions in the active site is outlined in Scheme 1.3 and consists of three steps: (*i*) the polarization of the substrate and activation of the bridging solvent molecule, (*ii*) nucleophilic attack by a hydroxide ion, and (*iii*) protonation of the leaving group. The most likely candidate for the nucleophilic attack is the solvent molecule that

bridges the two divalent cations. pH-rate profiles performed on the Zn/Zn species of PTE and DHO demonstrate the loss of catalytic activity at pH values lower than 6 (*35, 36*). This is consistent with the protonation of a single group within the protein because the substrates are not ionizable at that pH. Also it has been shown that the pK_a of a water ligated to Zn^{2+} in an aqueous system is approximately 8.9 (*37*), and for a binuclear Zn^{2+} biomimetic chemical complexed, the pK_a of the bridging hydroxide is 6.8 (*38*). This suggests that the solvent molecule that bridges the metal ions is a hydroxide. In the crystal structures of PTE and DHO, a sp^2 hybridized oxygen of the reaction center of the substrate is complexed to the metal in the β position. This Lewis acid interaction would promote the reduction of electron density at the carbon/phosphorous center and facilitates nucleophilic attack by the bridging hydroxide ion (*17, 35, 36*). The attack of the nucleophilic hydroxide to the electrophilically enhanced reaction center is assisted by basic catalysis of the aspartate from strand 8. The formed tetrahedral intermediate is then stabilized by a bidentate interaction with the α- and β-metals. Subsequently, the tetrahedral intermediate collapses as a results from the donation of a proton by the aspartate from strand 8 (*36*). In the case of PTE, where product release does not require a protonation step, a proton shuttling system is found to regenerate the active site (*35*).

Scheme 1.3: Proposed reaction mechanisms of hydrolysis for members of the superfamily containing binuclear metal centers. Examples of these enzymes are PTE, DHO, IAD, URE, and the three versions of HYD.

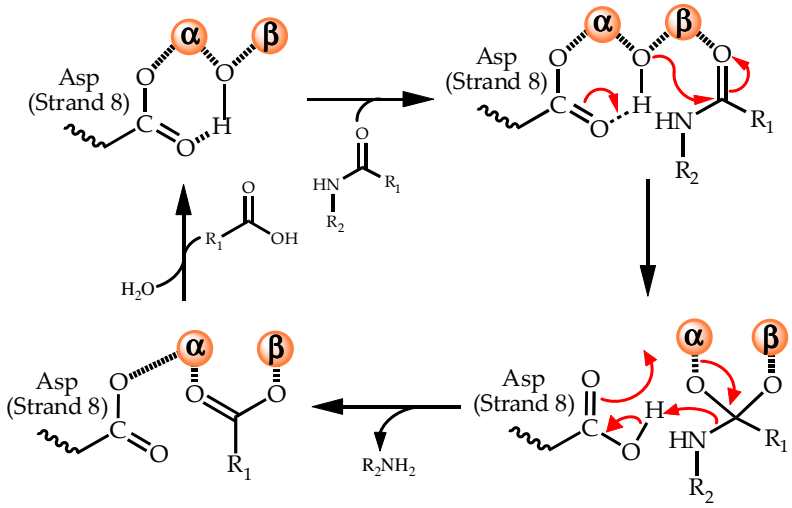

The prediction of these reaction mechanisms has been possible by the integration of the information acquired by several experimental techniques. These techniques include different biochemical procedures, mutagenesis, X-ray crystallography, and a wide variety of computational methodologies. Unfortunately, not always the information obtained from different techniques converges to the same conclusion. Urease is a member of the amidohydrolase superfamily that exhibits this divergence between the biochemical characterization and the computational methodologies. Urease is the only member of the amidohydrolase superfamily that contains a binuclear metal center and is involved in the hydrolysis of ammonia. The hydrolytic decomposition of urea in the active site of urease has been extensively studied (*17, 39-42*). Biochemical and mutagenic characterization, together with several X-ray crystal structures of urease

complexed with various substrate analogs support that hydrolysis of urea occurs by the formation of a tetrahedral intermediate (*17, 39-42*). The creation of a phthalazine-dinickel complexes by Lippard and co-workers (*43*), has opened new theories about what intermediates might be occurring in the active site of urease during catalysis. The decomposition of urea by the phthalazine-dinickel complexes has been proved to occur via formation of a cyanate intermediate (*43, 44*). This mechanism involves the elimination of ammonia to form the cyanate intermediate which is further hydrolyzed to CO_2. The reaction pathway, observed in phthalazine-dinickel urease mimics provides evidence for a possible alternative pathway for the enzymatic hydrolysis of urea (*45*). High-level quantum chemical methodologies were utilized by Merz and coworkers to identify stable intermediates and transition-state structures along several possible reaction mechanisms (*44, 46*). The examination of these mechanisms using computational tools as molecular dynamics (MD) simulations suggests that both, the hydrolytic and the elimination mechanisms are possible (*46*). However, the formation and isolation of a cyanate intermediate in the hydrolysis of urea by urease are yet to be reported.

The purpose of the present study is the characterization of two members of the amidohydrolase superfamily which represent examples of the two types of reaction mechanism described above. Isoaspartyl dipeptidase (IAD) from *Escherichia coli* was first found and characterized by Harvey in 1968 (*8*). IAD catalyzes the hydrolysis of a set of β-aspartyl dipeptides (Scheme 1.1) but does not catalyze the cleavage of the corresponding normal aspartyl dipeptides. β-aspartyl dipeptides can occur through the

post-translational isomerization of aspartyl and asparaginyl residues in proteins (*8*). This nonenzymatic catalyzed process causes L-asparaginyl residues to undergo an intramolecular rearrangement, transferring the peptide backbone from the α-carboxylic group to the β. These rearrangements cause severe alterations in the polypeptide backbone and may generate significant alterations in both structure and function (*47*). In *Escherichia coli* , the Protein-L-isoaspartyl/D-aspartyl *O*-methyltransferase is responsible for the discrimination and restoration of β-aspartyl residues back into α-aspartyl residues and prevents the accumulation of abnormal proteins (*48*). Some limitations to this repair process exist, one limitation is the specificity of the enzyme to a specific subset of β-aspartyl containing impaired proteins; secondly, the accessibility of the protein to buried isomerized residues (*49*). It is suggested that a secondary degradative mechanism is present to prevent the accumulation of β-aspartyl dipeptides after proteolysis (*8*). This enzyme was identified to be isoaspartyl dipeptidase. The characterization of the X-ray crystal structure and the mechanism of the reaction catalyzed by IAD will be described in detail through chapters II, III and IV of this dissertation.

The second protein characterized in this study was found from an extensive list of amidohydrolase superfamily members of unknown function, obtained from genome sequencing projects. As the understanding of the evolutionary divergence of the amidohydrolase superfamily expands, the discovery of the substrate specificity for proteins of unknown function has proved to be rather difficult. Over 2000 sequences from about 200 organisms have been identified as members of this superfamily. In the databases maintained by the NCBI, a significant fraction of these proteins with unknown

function are annotated as probable cytosine deaminases or probable chlorohydrolases. This assignment is based on the sequence similarity of this group of enzymes with enzymes of known function that catalyze the hydrolysis of the carbon-chlorine bonds in atrazine or the hydrolysis of the carbon-nitrogen bond in cytosine (Scheme 1.1) (*2*). The relationship between protein structure and activity is an essential tool for deciphering substrate specificity for these enzymes with unknown function. The chromosomal DNA of *Pseudomonas aeruginosa* PA01 has been sequenced, revealing that the genome contains more than 5,500 proteins (*50*). The protein coding sequence for Pa5106 was annotated as a "probable cytosine deaminase" or a "probable chlorohydrolase". The biochemical characterization of Pa5106 suggests that the function of this gene product is an *N*-formimino-L-glutamate iminohydrolase (HutF) (Scheme 1.1). The discovery of Pa5106 biological function and the characterization of its mechanism of deimination will be addressed in chapters V and VI of this study.

The pathway for the degradation of histidine has been extensively studied (Scheme 1.4). L-Histidine is deaminated to urocanate by histidine ammonia-lyase (HutH); then urocanate is converted to L-5-imidazolone-4-propionate by urocanase (HutU); and afterward, L-5-imidazolone-4-propionate is hydrolyzed to *N*-formimino-L-glutamate by imidazolonepropionate amidohydrolase (HutI). *N*-formimino-L-glutamate can be further degraded to glutamate by three different independent paths. For two of the cases, the conversion of *N*-formimino-L-glutamate to glutamate is a single enzymatic reaction, and the third, is a two step conversion. In mammalian liver, *N*-formimino-L-glutamate can be converted to glutamate by the transfer of the formimino group to

tetrahydrofolic acid through the action of L-glutamate *N*-formimidoyltransferase (*51*). For *Aerobacter aerogenes*, the *N*-formimino-L-glutamate is hydrolyzed to glutamate and formamide (*52*). In *Pseudomonas* sp., *N*-formimino-L-glutamate is deiminated to *N*-formyl-L-glutamate by *N*-formimino-L-glutamate iminohydrolase (HutF) (*53*), then *N*-formimino-L-glutamate is hydrolyzed to formate and L-glutamate by *N*-formyl-L-glutamate deformylase (*54*). Chapter V, of this dissertation, demonstrates that Pa5106 catalyzes the deimination of *N*-formimino-L-glutamate to *N*-formyl-L-glutamate and ammonia, while Pa5091 catalyzes the hydrolysis of *N*-formyl-L-glutamate to formate and L-glutamate. This chapter also reveals the existence of another protein (Pa3175), which is dislocated from the Hut operon, and catalyzes the hydrolysis of *N*-formimino-L-glutamate to formamide and L-glutamate (*2*).

Scheme 1.4

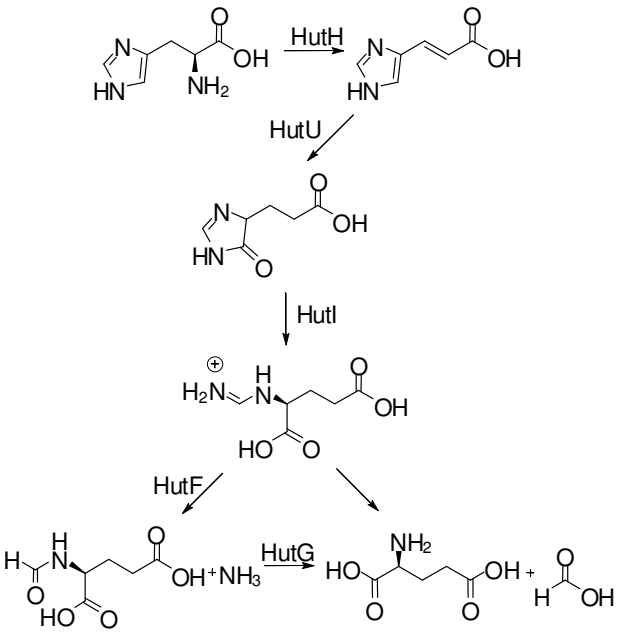

CHAPTER II

HIGH-RESOLUTION X-RAY STRUCTURE OF ISOASPARTYL DIPEPTIDASE FROM *ESCHERICHIA COLI**

Proteins are polypeptides generated with a high level of reliability by the cellular transcriptional and translational machinery. Enzymes are made up of amino acids covalently bonded through amide linkages. In amides, the α-carboxylic group of one amino acid is covalently bound to the amino group of the next amino acid. Proteins are affected by a variety of spontaneous chemical processes such as deamination, racemization and isomerization. Isomerization causes L-asparaginyl residues to undergo nonenzymatic intramolecular rearrangement that transfers the peptide backbone from the α-carboxylic group to the β-carboxylic group (Scheme 2.1) (*47*). The spontaneous post-translational alterations of these residues into β-aspartyl or γ-glutamyl linkages cause an alteration in the polypeptide backbone that may generate a significant alteration in protein structure as well as function (*55*). The repair of damaged protein by converting the L-isoaspartyl residues back into L-aspartyl residues is an efficient way of prevent the accumulation of abnormal proteins in stationary phase (*56*). The protein-L-isoaspartyl/D-aspartyl *O*-methyltransferase is the protein responsible for this activity, but some limitations to this process exist (*55*).

---

*Parts of the data reported in this chapter are reprinted with permission of "High-resolution X-ray structure of isoaspartyl dipeptidase from *Escherichia coli"* by Thoden, J. B., Marti-Arbona, R., Raushel, F. M., and Holden, H. M., 2003. *Biochemistry 42*, 4874-82. Copyright 2003 American Chemical Society.

The specificity of the enzyme for a certain subset of L-isoaspartyl containing damaged proteins is a limitation. Secondly, not all of the damaged residues are exposed on the surface of the protein and accessible for repair (*49*). Finally, protein-L-isoaspartyl/D-aspartyl *O*-methyltransferase has a very poor recognition of L-isoaspartyl residues in small peptides (*56*). The accumulation of unrecognized dipeptides may be toxic to the organism and may result in the depletion of the pool of amino acids necessary for survival in the stationary phase. It has been suggested that in addition to the methyltransferase, there is a secondary catabolic pathway to remove unwanted β-aspartyl linkages (*55*). The identification of an isoaspartyl dipeptidase (IAD) in *Escherichia coli* supports the idea of a secondary degradative pathway (*8*). IAD catalyzes the hydrolysis of β-aspartyl linkages in dipeptides as depicted in Scheme 2.2. Previously, it was determined that not all isoaspartyl dipeptides function as a substrate for IAD (*8*). In addition IAD has low or no activity toward the hydrolysis of tripeptides, γ-glutamyl dipeptides or nonpeptide pyrimidine analogs (*55*). β-Asp-Leu has been shown to be the best substrate for IAD with a K_m of 0.81 mM and specific activity of 13 s^{-1} at pH 7.5 (*8*). Isoaspartyl dipeptidase activity has also been found in plant-type asparaginases from *Synechocystis* sp. PCC 6803, *Anabaena* sp. PCC 7120, *Arabidopsis thaliana*, and *Escherichia coli* (*57*).

Scheme 2.1

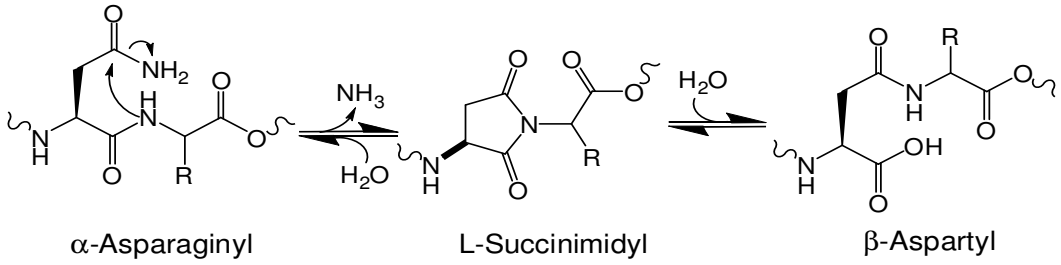

Isoaspartyl dipeptidase is a cytosolic protein located at the 98 min region of the *Escherichia coli* chromosome. IAD is composed of 390 amino acids and has a molecular weight of 41,000 Da. Amino acid sequence alignments reveal no sequence similarity to other peptidases or proteases but there is a significant amino acid sequence similarity to the amidohydrolase superfamily (*55*). These amino acid sequence alignments indicate that IAD most closely resembles dihydroorotase (DHO) and D-hydantoinase (D-HYD) (*4, 56*). DHO and D-HYD are members of the amidohydrolase superfamily and hydrolyze amide bonds with remarkable similarity to the peptide bond of β-aspartyl dipeptides as illustrated in Scheme 2.2 (*19, 22*). The amidohydrolase superfamily catalyzes a diverse set of hydrolytic reactions at carbon and phosphorous centers. This superfamily uses a mononuclear or binuclear metal center to activate a hydrolytic water molecule and to enhance the electrophilic character of the substrate. Other well characterized members of this family of proteins include phosphotriesterase and urease, among others (*39, 58*). The X-ray crystal structures of these proteins reveal that their binuclear metal centers are formed by four histidines, an aspartate and a carboxylated lysine residue (*17-19*). Each of the two metals is ligated to two histidine

residues and one of the metal ions is additionally coordinated to an extra aspartate residue. The two metal ions are bridged by a solvent hydroxide and the carboxylated lysine. The carboxylation of the lysine residue occurs from the post-translational alteration of the ε-amino group (*29*).

Scheme 2.2

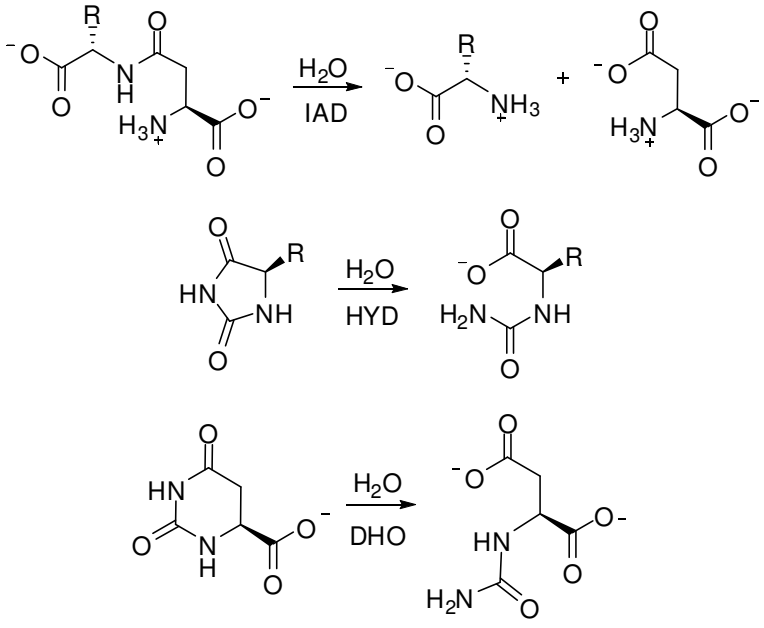

This chapter describes the crystallization and high-resolution X-ray crystallographic analysis of IAD from *Escherichia coli* in both, the native state and complexed with the hydrolysis product, L-aspartate. It also suggests a structural model for the binding of the substrate within the active site of IAD. Gel filtration chromatography and ultracentrifugation experiments suggest that IAD is an octamer. The X-ray crystal structure of IAD reveals that each subunit folds into a $(\beta/\alpha)_8$-barrel motif with a binuclear metal center located at the C-terminal end of the barrel. The

residues forming the binuclear active site of IAD are His-68, His-70, His-201, His-230, Lys-162 and Asp-285. The structural analysis of the quaternary structure and the active site geometry of the enzyme confirm that IAD belongs to the amidohydrolase superfamily (*4, 8*).

MATERIALS AND METHODS

Materials. All chemicals and coupling enzymes were obtained from Sigma-Aldrich, unless otherwise stated. The oligonucleotide synthesis and DNA sequencing reactions were performed by the Gene Technology Laboratory of Texas A&M University. The pET30a(+) expression vector was acquired from Novagen. The T4 DNA ligase and the restriction enzymes, *Nde*I and *Hind*III, were purchased from New England Biolabs. The Platinum *Pfx* DNA polymerase and the Wizard® Plus SV Mini-Prep DNA purification kit were obtained from Invitrogen and Promega, respectively.

Cloning and Protein Purification. The *iad*A gene from *Escherichia coli* was amplified by PCR with two primers, 5'-GGAATTCCATATGATTGATTATACCGC-AGCCGG-3' and 5'-GGCGAATTCTCATCATCATCATTAAGCCG-3', containing *Nde*I and *EcoR*I sites, respectively. The resulting fragment was ligated into the *Nde*I and *EcoR*I sites of a pET30a(+) plasmid. The protein was expressed in the strain BL21(DE3)star (Novagen). Cultures were grown in Luria-Bertani medium at 37 °C with a rotatory shaker until an A_{600} of ~0.5-0.7 was reached. Induction was initiated by the addition of 1.0 mM isopropyl-β-D-thiogalactoside (IPTG), and the culture was further incubated overnight at 37 °C. The bacterial cells were isolated by centrifugation at 4500 × *g* for 15 min at 4 °C, re-suspendedin 5.0 mL of 50 mM Tris-

HCl buffer, pH 8.1 (buffer A), 5 μg/mL of RNAse containing DNAse, and 0.1 mg/mL of the protease inhibitor (PMSF) per gram of cells and disrupted by sonication. The soluble protein was separated from the lysed cells by centrifugation at 12,000 × *g* for 15 min at 4 °C. The protein solution was fractionated between 20% and 50% saturation of ammonium sulfate. The precipitated protein was re-suspended in a minimum quantity of buffer A and loaded onto a ACA gel filtration column using 20 mM Tris, pH 8.1 (buffer B) as the elution buffer. Fractions containing IAD were pooled and loaded onto a Resource Q ion exchange column and eluted with a gradient of NaCl in buffer B. The final step in the purification was accomplished with a High Load 16/60 Superdex 200 prep grade filtration column buffer A as the eluant. The purity of IAD during the isolation procedure was monitored by SDS-PAGE. The concentration of the enzyme was determined by measuring the absorbance at 280 nm using an extinction coefficient of 18307 M^{-1} cm^{-1}.

Enzyme Assays. The activity of IAD toward the hydrolysis of the substrates, β-Asp-Leu and β-Asp-Gly was followed by a coupled assay that monitors the production of aspartate through conversion to oxaloacetate and malate by the action of aspartate aminotransferase and malate dehydrogenase (*57*). The assay mixtures contained 100 mM HEPES pH 8.0, 100 mM KCl, 3.7 mM α-ketoglutarate, 0.4 mM NADH, 0.36 units malate dehydrogenase, 6 units aspartate aminotransferase, the appropriate β-aspartyl dipeptide, and IAD in a final volume of 250 μL. The oxidation of NADH at 30 °C was followed spectrophotometrically at 340 nm with a SPECTRAmax-340 microplate reader (Molecular Devices Inc.).

Molecular Weight Determination. The molecular weight of IAD was estimated using a calibrated gel filtration column. A HiLoad 16/60 Superdex 200 column (GE Health Care) was calibrated with six standard molecular weight markers (MW-GF-1000 from Sigma). IAD was applied to the column and eluted with buffer A at a flow rate of 1.0 mL per minute. The quaternary structure of IAD was confirmed by sedimentation velocity experiments. The sedimentation velocity experiments were also performed on a 2.0 mg/mL sample of IAD in 50 mM Tris-Cl buffer at pH 8.1 using a Beckman Optima XL-A centrifuge and an An 60 Ti rotor at 25 °C. The 12 mm double sector charcoal filled Epson centerpieces had a sample capacity of 300 μL, and experiments were conducted at a rotor speed of 42000 rpm with scans at 4 min intervals. The sedimentation of IAD was monitored by the absorption of light at 280 nm. The sedimentation data were analyzed with the program SVEDBERG. These experiments were performed with the help of Dr. Jungwook Kim.

Crystallization of IAD. The crystal structure of IAD was solved in collaboration with James B. Thoden and Hazel M. Holden at the Department of Biochemistry, University of Wisconsin, at Madison, Wisconsin. The crystal structure coordinates were deposited in the Research Collaboratory for Structural Bioinformatics, Rutgers University, at New Brunswick, New Jersey. The PDB entry codes are 1onw for the native form and 1onx for the complexed form of IAD with the product of hydrolysis, L-aspartate.

RESULTS

Expression and Purification of Isoaspartyl Dipeptidase. The protein IAD was overexpressed after the transformation of the pET30a(+) plasmid containing the *iad*A gene into BL21(DE3)star cells. The protein was purified to homogeneity and found to contain 2.0 equiv of Zn^{2+} per subunit. IAD elutes as a symmetric peak during chromatography and migrates as a single band on SDS-PAGE with an electrophoretic mobility of ~41 kDa, which agrees with the previously reported value of 41,084 Da (*8, 56*). The identity of the purified protein was confirmed by measurement of the N-terminal amino acid sequence (Protein Chemistry Laboratory, Texas A&M University). Two sequences, M-I-D-Y-T (95%) and I-D-Y-T (5%), were found, which correspond with the predicted sequence for the first five amino acids of IAD, although a small fraction of the isolated enzyme remains with an unprocessed methionine.

Kinetic Parameters of IAD. The kinetic parameters for the catalytic hydrolysis of β-aspartyl-L-leucine were obtained by coupling the formation of aspartate to the oxidation of NADH. IAD hydrolyzed β-aspartyl-L-leucine with a specific activity of (104 ± 3) s^{-1} and a K_m of (1.02 ± 0.09) mM. This present a ~10 fold increase in catalytic activity for the purified IAD over the previously reported for IAD was 13 s^{-1} with a K_m of 0.8 mM (*8, 55, 56*).

Tertiary Structure of the IAD Subunit. The crystals contained two subunits per asymmetric unit, these subunits were practically identical such that their back bone and side chains superimpose with root-mean-square deviations of 0.26 and 0.51 Å, respectively. Each subunit is divided in two domains, as shown in Figure 2.1. The first

domain or the N-terminal domain is composed of eight strands of mixed β-sheets formed by the residues Met-1 to Gly-63 and Gly-346 to Thr-389, followed the second domain, which is composed of the residues Phe-64 to Lys-345 folding into a $(\beta/\alpha)_8$ TIM-barrel motif. The β-strands forming the barrel motif are connected to each other by ten α-helices and a variety of protein loops.

Figure 2.1: X-ray crystal structure ribbon representation of a single subunit of IAD from *Escherichia coli*. The N-terminal domain is colored green and the C-terminal domain is colored blue. The conserved residues forming the active site are highlighted in orange and the two zinc metal ions in yellow. The image was drawn with the program WebLab Viewer Pro using the coordinates from PDB file 1onw (*27*).

Quaternary Structure of IAD. The oligomeric conformation of IAD was determined from the elution profile from a calibration of the gel filtration column and sedimentation experiments. Previously, it was reported that IAD from *Escherichia coli* has a molecular weight of 120 kDa (*8*). The elution volume obtained from the loading of

IAD to a previously calibrated of a HiLoad 16/60 Superdex 200 prep grade gel filtration column with six standard molecular weight markers was representative of a protein with a molecular weight of ~320 kDa. IAD eluted between β-amylase (MW = 200 kDa) and apoferritin (MW = 443 kDa), and the calculated molecular weight was calculated to be 316 kDa. Sedimentation velocity experiments gave a $s_{20,w}$ = 12.9 S and a calculated molecular weight of around 320 kDa. With these experiments and since the monomeric molecular weight of IAD is 41.1 kDa, the protein apparently exist as an octamer in solution. The eight asymmetric subunits are organized in four groups of two, or a tetramer of dimers. Examination of the molecular packing arrangement within the crystalline lattice reveals that the octamer is situated along the crystallographic 4-fold rotational axis, thus resulting in only two subunits per asymmetric unit (Figure 2.2) (*27*).

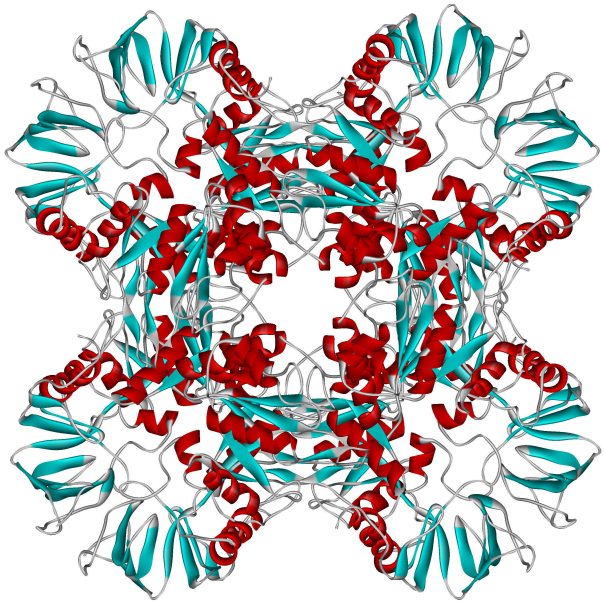

Figure 2.2: Octamer quaternary structure of IAD. The octamer is situated along the crystallographic 4-fold rotational axis, these organizes the eight asymmetric subunits in a tetramer of dimers.

The Active Site. A close look at the active site of the native form of IAD is illustrated in Figure 2.3. The two zinc cations are separated by 3.4 Å and are bridged by a hydroxide ion and carboxylated site chain of a lysine residue (Lys-162). The more buried zinc ion, referred to as the α-metal, is coordinated by $N^{\varepsilon 2}$ of the imidazole ring side chain of His-68 and His-70, the $O^{\delta 1}$ of the carboxylate side chain of Asp-285, the O^{2} of Lys-162, and the bridging hydroxide ion in a distorted trigonal bipyramidal arrangement. The second zinc ion, depicted here as the β-metal, of the binuclear center is ligated by the $N^{\delta 1}$ of the imidazole ring side chain of His-201, the $N^{\varepsilon 2}$ of the imidazole ring side chain of His-230, the O^{1} of a carboxylated site chain of Lys-162, and the bridging hydroxide ion in a distorted tetrahedral arrangement. The O^{η} of the phenolic side chain of tyrosine residue (Tyr-137) is located at 3.4 Å from the β-metal and in proper position to serve as a fifth metal ligand. This creates a trigonal bipyramidal coordination sphere for the β-metal.

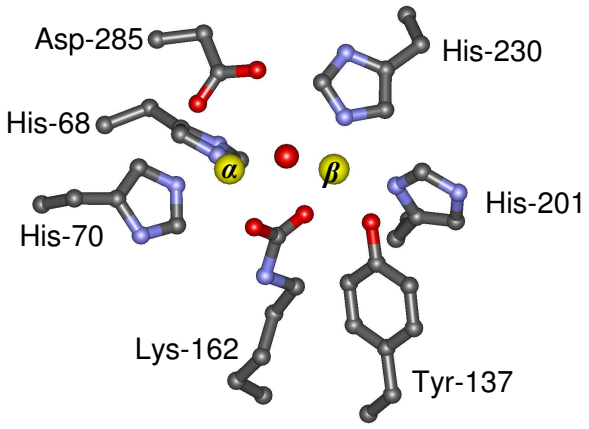

Figure 2.3: Close-up view of the binuclear metal center of IAD. The yellow spheres represent the zinc ions and red sphere the metal bridging solvent molecule. The image was drawn with the program WebLab Viewer Pro using the coordinates from PDB file 1onw (*27*).

Structure of IAD with Bound Aspartate. The overall molecular fold of IAD with bound aspartate is essentially identical to that of the resting enzyme with the exception of the loop defined by Phe-292 to His-301, in which electron density was too weak to model in the crystal structure of the unbound form of IAD. The crystal structure of the bound aspartate suggests that the hydrogen bond interaction between the hydroxyl side chain of Ser-289 and the α-amino group on the aspartate helps the residues in the loop to become more ordered upon substrate binding. The α-carbon of Ser-289 moves approximately 1.7 Å towards the active site when the aspartate is bound. The only significant differences between the unbound and bound forms of IAD are limited to this loop region.

A close-up view of the active site of IAD with the bound aspartate is depicted in Figure 2.4. The carboxylate side chain of aspartate bridges the binuclear metal center with oxygen/α-metal and oxygen/β-metal distances of 2.9 and 2.0 Å, respectively. The oxygen that is coordinated to the β-metal is also located within 2.4 Å of O^{η} of Tyr-137. The α-carboxylate group of aspartate forms additional hydrogen bonding interactions with a water molecule and the peptidic amides of Thr-106 and Gly-75. Figure 2.4 illustrates these interactions as well as the interaction between the α-amino group of the complexed aspartate with the side chains of Ser-289 and Glu-77 and the backbone carbonyl oxygen of Ser-289.

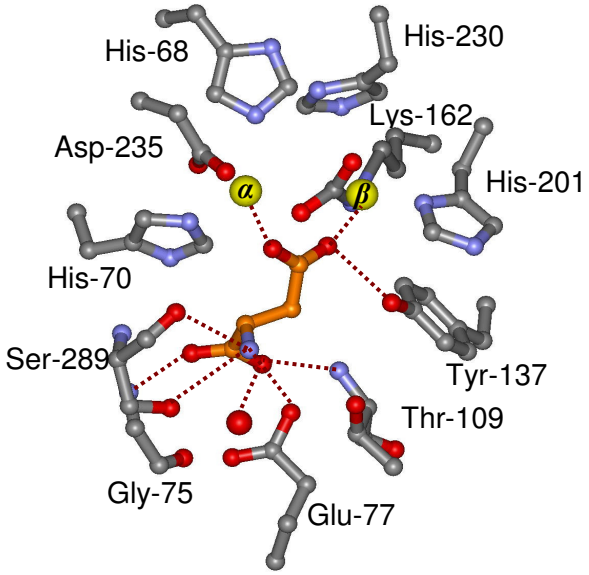

Figure 2.4: Close-up view of the active site of IAD with the complexed aspartate. The potential hydrogen bonding interactions are indicated by the dashed lines.

Substrate Binding Model. In addition to the amino acid sequence alignments, the three-dimensional structure of IAD is very similar to that of DHO, phosphotriesterase, and urease, among others (*19, 39, 58*). In all four enzymes, the binuclear metal center architectures are similar with respect to distances, angles, and coordination geometries. The orientation of the aspartate product in IAD active site is analogous to that observed for *N*-carbamoyl aspartate in DHO. In both structures, the side chain carboxylate groups interact with the metals, displacing the bridging hydroxide. In the structure of DHO complexed with dihydroorotate, the bridging hydroxide is present, and O4 of dihydroorotate is located within 2.9 Å of the β-metal (*19*). The structures of DHO and the model of IAD with bound product, allow us to speculate on how isoaspartyl dipeptides might be lodged within the active site of IAD. A model of β-Asp-Leu built

into the active site of IAD (Figure 2.5) was accomplished by positioning the α-carboxylate of the aspartate side chain moiety of the substrate in the same orientation as that observed for L-aspartate moiety of the *N*-carbamoyl-L-aspartate bounded to the active site of DHO (*19*). The carbonyl oxygen of the peptide bond was positioned into IAD with the same orientation of dihydroorotate in the crystal structure of DHO (*19*). The modeling of the β-aspartyl dipeptide into the active site of IAD resulted in the Leu moiety of the substrate being oriented toward the opening of the TIM-barrel. This positioned two arginine residues, Arg-169 and Arg-233, into an orientation capable of interacting with the carboxylate group of the Leu moiety.

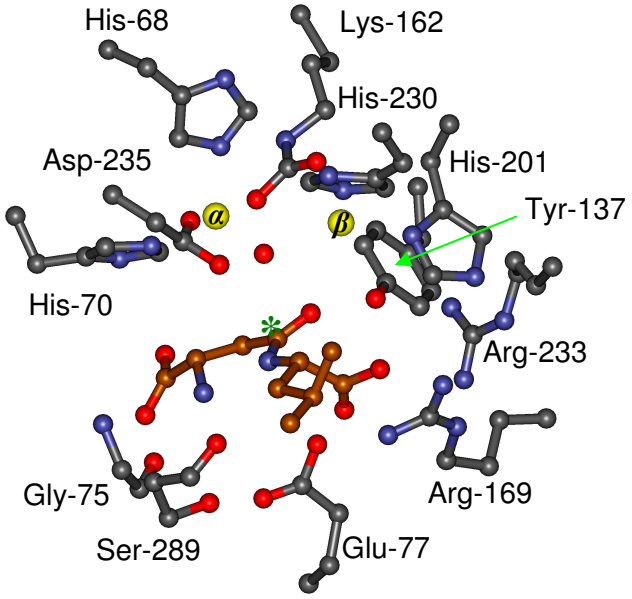

Figure 2.5: Possible model for the binding of β-Asp-Leu binding in the active site of IAD. The β-aspartyl dipeptide is highlighted in brown bonds. The position of the reaction center attacked during catalysis is indicated by the green asterisk.

DISCUSSION

Since the discovery of the amidohydrolase superfamily by Holm and Sander in 1997, the three-dimensional structural similarities among this group of proteins have been a key tool in the identification and classification of the members of the superfamily. Similarities are also observed for their amino acid sequence, substrate structures and mechanisms of hydrolysis. The active sites of members of the amidohydrolase superfamily that contain a binuclear metal center are very similar and share most of their characteristics. An overlay of the active site residues of IAD, DHO, and PTE is presented in Figure 2.6. IAD most closely resembles DHO and D-HYD, likewise, they catalyze the hydrolysis of analogous amide bonds in substrates with remarkable structural resemblance, as shown in Scheme 2.2 (*19, 22*).

The X-ray crystal structures of the native and product bound IAD and its similarities with DHO have allowed the projection of various key points of information in the characterization of IAD. The construction of a model of the bound substrate in the active site of IAD (Figure 2.5) has produce a more clear view of possible hydrogen bond interaction between the protein and the substrate and the identification of residues that might be important in catalysis.

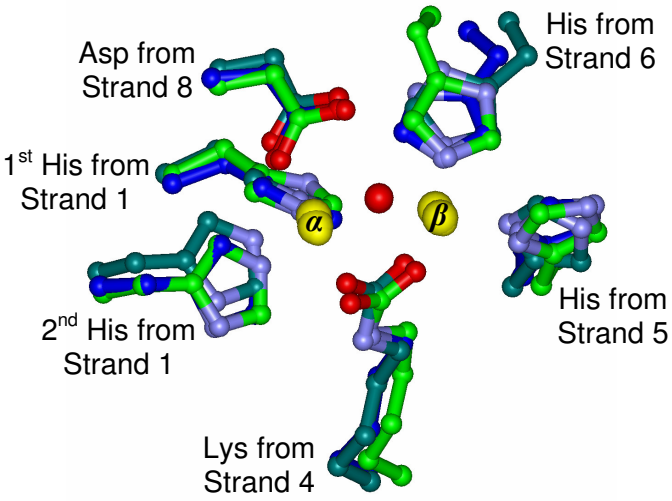

Figure 2.6: Superposition of the active site region for the resting forms of the wild-type IAD, DHO, and PTE. The PDB entry codes for IAD, DHO and PTE are 1onw, 1j79, and 1hzy, respectively. The side chains of the IAD, DHO, and PTE are depicted with dark cyan, green, and blue bonds, respectively. The zinc ions for all of the structures are in a similar position and are presented as yellow spheres. The solvent molecule that bridges the binuclear metal centers is drawn as a red sphere. The image was drawn with the program WebLab viewer Pro.

Based on the careful inspection of the X-ray crystal structures of the native IAD, the product bound to the active site, the enzyme/substrate model and observations of DHO crystal structures with the substrate and product bound, a reaction mechanism for the hydrolysis of β-aspartyl dipeptides by IAD can be proposed (Scheme 2.3). Upon the binding of the substrate to the active site, the carbonyl oxygen of the peptide bond coordinates to the β-metal. This interaction enhances the electrophilic character of the reaction center. The bridging hydroxide ion then attacks the *re* face of the peptide bond and is assisted by general base catalysis via Asp-285. This leads to the formation of a

tetrahedral intermediate which is stabilized by bidentate interactions with the α- and β-metals. The newly protonated Asp-285 donates a proton to the peptidic nitrogen of the substrate, resulting in the collapse of the intermediate and cleavage of the peptide bond. The other possible candidates for proton donation to the leaving group, include Glu-77, Tyr-137, and the α-amino group of the isoaspartyl moiety. A more clear view of this proposal can be obtained from a more thorough biochemical characterization of the wild type and mutant enzymes, in addition to the analysis of the structure of the enzyme in the presence of the appropriate substrate analogues.

Scheme 2.3

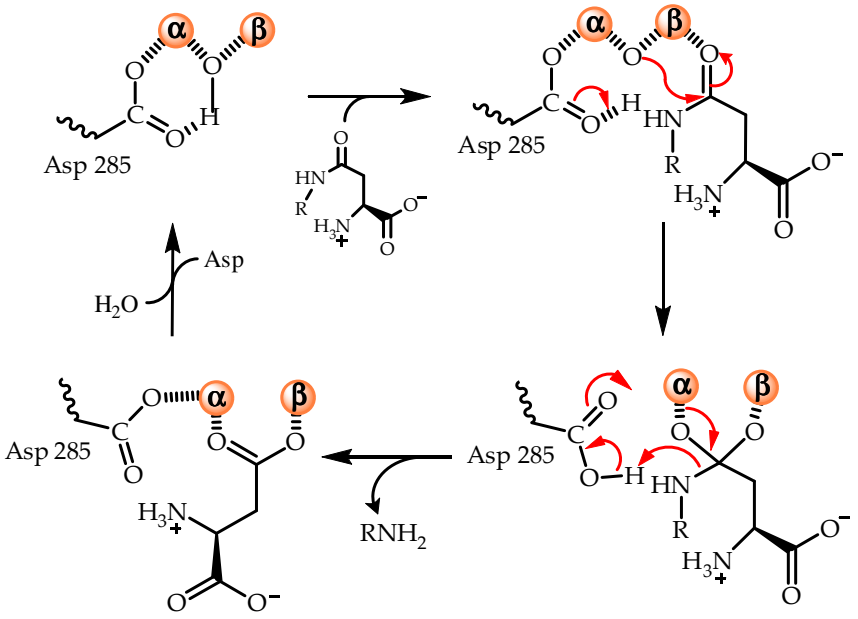

CHAPTER III

MECHANISM OF THE REACTION CATALYZED BY ISOASPARTYL DIPEPTIDASE FROM *ESCHERICHIA COLI**

Isoaspartyl dipeptidase (IAD) from *Escherichia coli* catalyzes the hydrolysis of β-aspartyl dipeptides (*8*). Isoaspartyl dipeptides are formed via an intramolecular rearrangement of the polypeptide backbone of proteins. This isomerization process causes L-asparaginyl or L-glutaminyl residues to undergo a nonenzymatic intramolecular rearrangement transferring the peptide backbone from the α-carboxylate to the β- or γ-carboxylate, respectively (*56*). These abnormal peptidic bonds are resistant to proteolysis and may accumulate, reaching toxic levels for the cells if they are not efficiently depleted (*8*). The apparent physiological role of IAD in *Escherichia coli* is to prevent the accumulation of β-aspartyl dipeptides after proteolysis of these modified proteins. IAD has low or no activity toward the hydrolysis of tripeptides, γ-glutamyl dipeptides or nonpeptide pyrimidine analogs (*55*). IAD has been shown to hydrolyze β-aspartyl dipeptides with different side chains at their C-terminal end (*8*). The general reaction catalyzed by IAD is presented in Scheme 3.1. Isoaspartyl dipeptidase activity has also been found in plant-type asparaginases from *Synechocystis* sp. PCC 6803, *Anabaena* sp. PCC 7120, *Arabidopsis thaliana*, and *Escherichia coli* (*57*).

---

*Parts of the data reported in this chapter are reprinted with permission of "Mechanism of the reaction catalyzed by isoaspartyl dipeptidase from *Escherichia coli*" by Marti-Arbona, R., Fresquet, V., Thoden, J. B., Davis, M. L., Holden, H. M., and Raushel, F. M., 2005. *Biochemistry 44*, 7115-24.

Scheme 3.1

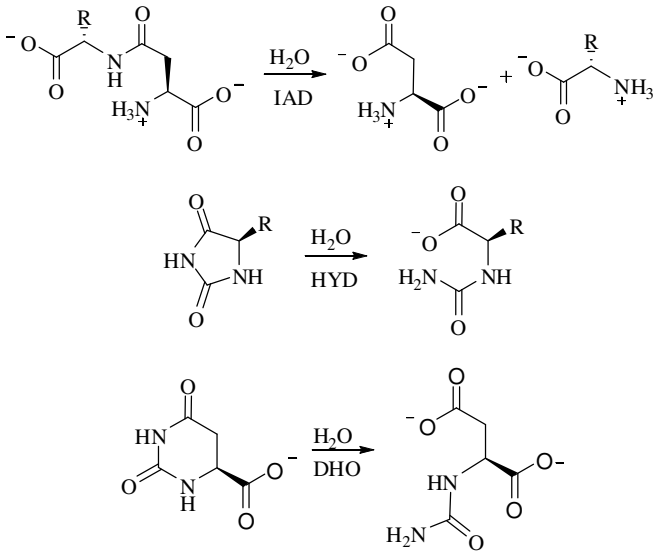

Amino acid sequence alignments with members of the amidohydrolase superfamily suggests that the closest relatives are dihydroorotase (DHO) and D-hydantoinase (D-HYD) (*4, 56*). These enzymes also catalyze the hydrolysis of amide bonds as shown in Scheme 3.1. The hallmark for proteins in this superfamily is their folding into a $(\beta/\alpha)_8$-barrel domain with a mononuclear or binuclear metal center embedded at the C-terminal end of the barrel (*4*). The X-ray crystal structure of IAD from *Escherichia coli* was determined in collaboration with the Holden group at University of Wisconsin, Madison, Wisconsin. The crystal structures for the native enzyme and the protein complexed with the hydrolysis product, L-aspartate, were solved with a resolution of 1.65 Å and 2.1 Å, respectively. IAD was shown to be an octamer with each subunit folding into two domains, the first composed of eight strands of mixed β-sheets, followed by a $(\beta/\alpha)_8$-barrel motif as illustrated in Figure 3.1. The coordination core for the α-metal of the binuclear metal center is composed of His-68, His-70, Lys-

162, Asp-285, and the bridging solvent, whereas the metal in the β-position is ligated by a tetrahedral arrangement of residues Lys-162, His-201, His-230, and the bridging solvent. The post-translational modification of the ε-amino group of Lys-162 to a carboxylate allows it to act as a bridging ligand between the two metal ions.

Figure 3.1: X-ray crystal structure of IAD from *Escherichia coli*. The N-terminal domain is colored green and the C-terminal domain is colored blue. The conserved residues forming the active site are highlighted in orange and the two zinc metal ions in yellow. The image was drawn with the program WebLab Viewer Pro using the coordinates from PDB file 1onw.

Significant insights into the composition and geometry of the residues forming the active site of IAD were obtained from the X-ray structure of the product complexed to IAD and substrate model presented in the previous chapter (Chapter II). Tyr-137 sits about 3.4 Å from the β-metal ion, while Glu-77 was in position to hydrogen bond to the

α-amino group of a dipeptide substrate. The structure of IAD complexed with hydrolysis product, L-aspartate, demonstrates that the carboxylate side chain of the aspartate product displaces the bridging solvent molecule. The binding of the aspartate induces the displacement of the loop composed of residues between Phe-292 and His-301, toward the active site. This movement results in the formation of a hydrogen bond between O^{γ} of the side chain of Ser-289 and the α-amino moiety of the aspartate ligand. Figure 3.2 presents the bonding interactions of the aspartate ligand and the active site of IAD.

There are many unsolved questions regarding the mechanism of reaction by which IAD hydrolyzes β-aspartyl dipeptides. It is unclear how the hydrolytic water molecule is activated or how the β-aspartyl peptide bond is polarized for nucleophilic attack. In addition, the structural determinants to the substrate specificity have not been elucidated. It is also uncertain how the catalytic mechanism of this protein might differ from those of other homologous enzymes within the amidohydrolase superfamily. In the current investigation, reconstitution of IAD with a variety of divalent cations will help to understand the pathway for the activation of the hydrolytic water molecule. Several dipeptides, substrate analogs and inhibitors were used to explore their effects on the substrate specificity and catalysis. Also, a series of active site mutants have been constructed to study their role on substrate binding and catalysis. This chapter presents the X-ray crystal structure of the D285N mutant complexed with the substrate β-Asp-L-His. This crystal structure and the previously described experiments provided invaluable

insights toward elucidation of the mechanism of hydrolysis of β-aspartyl dipeptides by isoaspartyl dipeptidase.

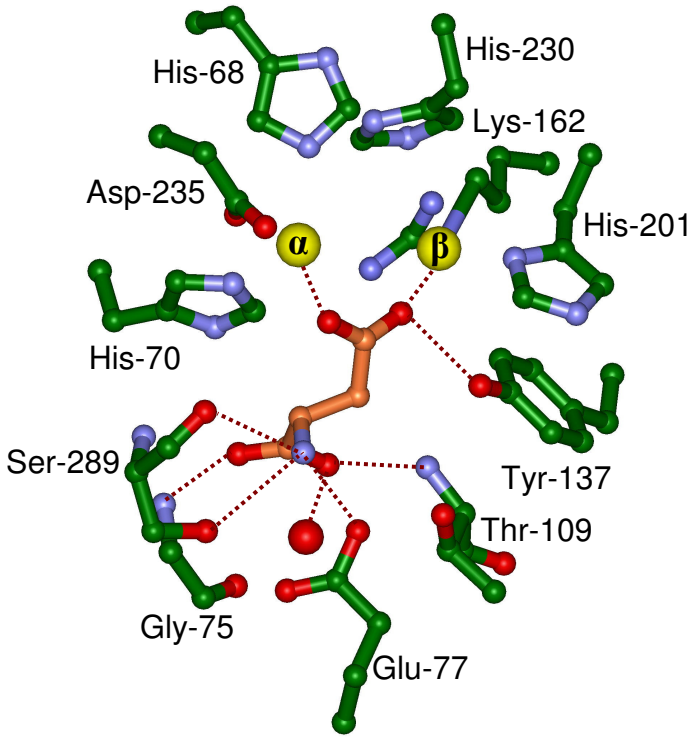

Figure 3.2: Close-up view of the active site of IAD with the complexed aspartate. The potential hydrogen bonding interactions between the aspartate ligand and the active site residues are indicated by the dashed magenta lines. Coordinates were taken from the Protein Data Bank (1onx).

MATERIALS AND METHODS

Materials. All chemicals, dipeptides, substrate analogs, and coupling enzymes were obtained from Sigma/Aldrich, unless otherwise stated. The dipeptides β-Asp-Leu (**I**), α-Asp-Leu (**II**), β-Asp-Lys, β-Glu-Leu, and β-Asp-Ala were purchased from

Bachem. The structures for some of the substrates and inhibitors are presented in Scheme 3.2.

Scheme 3.2

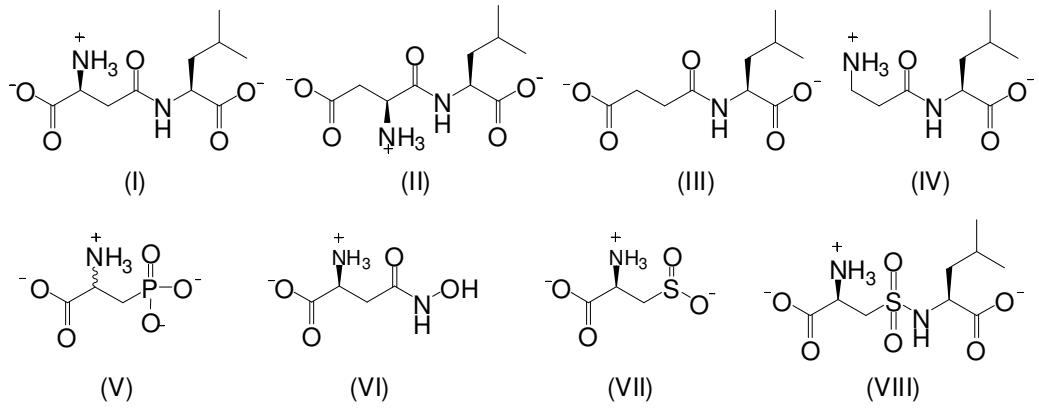

Cloning and Site-Directed Mutagenesis. The *iad*A gene was cloned from the XL1Blue strain of *Escherichia coli* into a pET30a(+) expression vector (Stratagene). Site-directed mutagenesis of IAD at residues Glu-77, Tyr-137, Arg-169, Arg-233, Asp-285, and Ser-289 was accomplished using the Quick Change site-directed mutagenesis kit from Stratagene. For expression of the IAD mutants, JDG 11000 cells (Δ*iad*A) were lysogenized using the λDE3 lysogenization kit from Novagen. The *Escherichia coli* strain JDG 11000 (Δ*iad*A) that lacks a functional *iad*A gene was kindly provided by Professor Steven Clarke at UCLA (*59*). The plasmids containing the desired IAD mutation were then transformed in JDG 11000 (λDE3) competent cells.

Protein Purification. JDG 11000 (λDE3) cells were transformed by the pET30a(+) plasmid encoding IAD. Cultures were grown in Luria-Bertani medium at

37 °C, induced by the addition of 1.0 mM isopropyl-β-thiogalactoside (IPTG) after an A_{600} of 0.6 OD was reached and then incubated overnight. Cells from the late logarithmic-phase culture were pelleted and re-suspended in 50 mM *N*-(2-hydroxyethyl)piperazine-*N*'-2-ethanesulfonic acid (HEPES) buffer at pH 8.1 (buffer A), 5 µg/mL RNAse and 0.1 mg/mL phenylmethylsulfonyl fluoride (PMSF). The cells were disrupted by sonication. The soluble protein was isolated from the lysed cells by centrifugation at 12,000 × *g* for 15 min at 4 °C and fractioned between 20% and 50% saturation ammonium sulfate in buffer A. The precipitated protein from the 50% saturation pellet was re-suspended in a minimum quantity of buffer A and loaded onto a High Load 16/60 Superdex 200 prep grade gel filtration column (GE Health Care) and eluted with buffer A. The fractions containing IAD were pooled and loaded onto a Resource Q ionic exchange column (GE Health Care) and eluted with a gradient of NaCl in buffer A. The pooled fractions were then precipitated with 80% ammonium sulfate saturation, re-suspended, and loaded into a High Load 16/60 Superdex 200 prep grade gel filtration column and eluted with buffer A. The presence and purity of IAD in the fractions was confirmed by SDS–PAGE. The purified enzyme was pooled and stored at -20°C.

*Synthesis of Succinyl-L-Leucine (**III**).* L-Leucine benzyl ester (1.84 g, 8.3 mmol) was added to a solution of succinic anhydride (1.0 g, 10 mmol) and 4-dimethyaminopyridine (1.02 g, 8.3 mmol) in CH_2Cl_2 (300 mL). After stirring at room temperature for 5 hours, the reaction mixture was extracted 3 times with 300 mL of a 5% solution of sodium bicarbonate. The aqueous phase was acidified with 6 N HCl and the

product was extracted with ethyl acetate. The ethyl acetate layer was washed with brine, dried over sodium sulfate and concentrated to dryness under vacuum. The succinyl-L-leucine benzyl ester was obtained as a colorless syrup (1.50 g) with a 56% yield. ESI-MS *m/z* 320.2 [M-H], 356.0 [M+Cl]. ^{1}H NMR ($CDCl_3$): 7.36 ppm (s, 5H), 5.85 (d, J = 12 Hz, 1H), 5.12 ppm (d, J = 18 Hz, 2H), 4.68 ppm (q, J = 12 Hz, 1H), 3.92 ppm (m, 4H), 3.04 ppm (m, 1H), 2.97 ppm (m, 2H), 2.30 ppm (d, J = 6.5, 3H), 2.26 ppm (d, J = 6.5, 3H). ^{13}C NMR ($CDCl_3$): 176.74 ppm, 172.94 ppm, 171.66 ppm, 135.16 ppm, 128.59 ppm, 128.45 ppm, 128.22 ppm, 67.20 ppm, 50.95 ppm, 41.48 ppm, 30.48 ppm, 29.64 ppm, 29.37 ppm, 24.77 ppm, 22.71 ppm and 21.87 ppm.

The unprotected succinyl-leucine was prepared by hydrogenation of the succinyl-L-leucine benzyl ester (0.80 g, 3.5 mmol) using 50 mg of Pd/C in 30 mL of methanol and H_2 with constant stirring. After 5 hours the Pd/C was removed by filtration and the sample taken to dryness under vacuum. The succinyl-leucine was obtained as a colorless syrup (0.68 g) with an 85% yield. ESI-MS *m/z* 230.1 [M-H]. ^{1}H NMR (methanol): 4.68 ppm (q, J = 12 Hz, 1H), 3.92 ppm (m, 4H), 3.09 ppm (m, 1H), 2.99 ppm (m, 2H), 2.33 ppm (d, J = 6.5, 3H), 2.29 ppm (d, J = 6.5, 3H). ^{13}C NMR (methanol): 52.38 ppm, 49.86 ppm, 49.57 ppm, 49.22 ppm, 49.00 ppm, 48.72 ppm, 49.44 ppm, 48.15 ppm, 41.70 ppm, 31.35 ppm, 30.23 ppm, 25.99 ppm, 23.40 ppm and 21.78 ppm.

*Synthesis of 3-Sulfo-L-Alanine-S-L-Leucine (**VIII**).* L-Leucine benzyl ester (0.55 g, 1.4 mmol) and 0.42 µL (1.4 mmol) of Et_3N were dissolved in 10 mL of chloroform at 4 °C under constant stirring. *N*-carbobenzoxy-3-(sulfonylchloro)-L-alanine benzyl ester

(0.39 g, 0.95 mmol) dissolved in 10 mL of chloroform was added slowly (*60*). The reaction was allowed to reach room temperature and stirred for 3 hours. The reaction mixture was taken to dryness under vacuum. The colorless syrup was re-suspended in a minimal amount of mixed hexanes and loaded onto a silica column and eluted with 5:1 hexanes:ethyl acetate. The product was taken to dryness and crystallized from 5:1 hexanes:ethyl acetate to obtain 0.13 g of *N*-carbobenzoxy-3-sulfo-L-alanine-*S*-L-leucine dibenzyl ester (24 % yield). ESI-MS *m/z* 597.2 [M+H]. ^{1}H NMR ($CDCl_3$): 7.37 ppm (br. s, 10H), 6.08 ppm (d, J = 6.6, 1H), 5.17 ppm (d, J = 18 Hz, 2H), 5.13 ppm (d, J = 18 Hz, 2H), 5.02 ppm (d, J = 6.6 Hz, 1H) 4.82 ppm (q, J = 12 Hz, 1H), 4.16 ppm (m, 1H), 3.47 ppm (m, 1H), 1.87 ppm (m, 2H), 1.50 ppm (d, J = 6.5, 3H), 0.90 ppm (d, J = 6.5 Hz, 3H), 0.877 ppm (d, J = 6.5 Hz, 3H). ^{13}C NMR ($CDCl_3$): 172.95 ppm, 171.67 ppm, 170.12 ppm, 168.68 ppm, 128.95 ppm, 128.78 ppm, 128.42 ppm, 68.92 ppm, 67.65 ppm, 65.29 ppm, 50.99 ppm, 41.48 ppm, 30.49 ppm, 29.64 ppm, 29.38 ppm, 24.78 ppm, 22.71 ppm and 21.87 ppm.

The unprotected product was prepared by mixing *N*-carbobenzoxy-3-sulfo-L-alanine-*S*-L-leucine dibenzyl ester (0.134 g, 0.5 mmol) with 50 mg of Pd/C in 15 mL of methanol and H_2 was bubbled with constant stirring. After 4 hours the Pd/C was filtered and the solvent was removed under vacuum. The 3-sulfo-L-alanine-*S*-L-leucine was obtained as a colorless syrup (46 mg) with a 72 % yield. ESI-MS *m/z* 283.09 [M+H]. ^{1}H NMR (D_2O): 4.03 ppm (d, J = 9.3 Hz, 2H), 3.62 ppm (m, 1H), 3.69 ppm (m, 1H), 3.46 ppm (m, 2H), 1.57 ppm (m, 2H), 1.46 ppm (d, J = 6.5 Hz, 3H), 0.761 ppm (d, J = 6.5 Hz, 3H), 0.742 ppm (d, J = 6.5 Hz, 3H). ^{13}C NMR ($CDCl_3$): 170.13 ppm, 168.67

ppm, 68.92 ppm, 65.28 ppm, 50.98 ppm, 41.48 ppm, 30.49 ppm, 29.63 ppm, 29.37 ppm, 24.76 ppm, 22.70 ppm and 21.87 ppm.

Substrate Activity. The compounds β-Asp-Leu (**I**), α-Asp-Leu (**II**), succinyl-Leu (**III**), β-Ala-Ala (**IV**), β-Asp-Ala, β-Asp-Gly, β-Asp-His, β-Asp-Lys, β-Asp-Phe, and γ-Glu-Leu were tested as substrates for IAD. The specific activity of IAD toward the hydrolysis of isoaspartyl (β-aspartyl) dipeptides was followed by the coupling the formation of aspartate to the oxidation of NADH (*57*). The decrease of NADH concentration was measured spectrophotometrically at 340 nm using a SPECTRAmax-340 microplate spectrophotometer (Molecular Devices Inc.). The standard assay contained 100 mM HEPES at pH 8.1, 100 mM KCl, 3.7 mM α-ketoglutarate, 0.4 mM NADH, 0.64 units of malate dehydrogenase, 6 units of aspartate aminotransferase, the appropriate isoaspartyl dipeptide and IAD to a final volume of 250 μL at 30 °C.

The capacity of IAD to hydrolyze γ-Glu-L-Leu was determinate by the use of a system that couples the formation of glutamate to the reduction of 3-acetylpyridine adenine dinucleotide (APAD) (13). The 200 μL assay was composed of 100 mM HEPES at pH 8.1, 100 mM KCl, 11 μg IAD and γ-Glu-L-Leu (from 0 to 44 mM). The reaction mixture was incubated at 30 °C for 30 min. and stopped by the addition of 75 μL of 10% trichloroacetic acid (TCA) and incubated at 4 °C for 20 min. The mixture was neutralized with 14 μL of 3.0 M Tris-Cl at pH 8.1, then 800 μL of a solution containing 100 mM HEPES at pH 6.8, 1.0 mM 3-acetylpyridine adenine dinucleotide (APAD), and 10 units of glutamate dehydrogenase was added and incubated at 30°C

for 2 hours. The reaction mixture was then centrifuged and the absorbance measured at 363 nm.

The ability of IAD to hydrolyze Succ-L-Leu (**III**) was assayed by amino acid analysis determination performed by Dr. Lawrence J. Dangott in the Department of Biochemistry and Biophysics of the Texas A&M University, College Station, TX. Reaction mixtures contains 100 mM HEPES pH 8.1, 100 mM KCl, 41.4 mM Succ-L-Leu or 2.0 mM β-Asp-L-Leu (control) and 3.05 μg of IAD. The reaction mixture was incubated for one hour and the reaction was stopped by filtering the protein with a Micron Centrifugal Filter Device (Millipore). The filtrate was analyzed for the content of free leucine in solution.

In the case of β-Ala-Ala (**IV**) and β-Asp-Ala the hydrolytic activity of IAD was analyzed by coupling the formation of L-alanine to the transformation of iodonitrotetrazolium (INT) to INT-formazan by diaphorase. The reaction was monitored at 500 nm and contained 100 mM Hepes, pH 8.1, 1.5 mM *p*-iodonitrotetrazolium violet, 1.5 mM NAD^+, 2.0 units of diaphorase, 7.0 units of L-alanine dehydrogenase, the appropriate substrate or inhibitor and 64 ng of IAD in a final volume of 250 µL at 30 °C (*61*).

Inhibition by Substrate Analogs. Substrate and product analogs were tested as inhibitors of the IAD reaction. Succinyl-Leu (**III**), 3-sulfo-L-Ala-*S*-L-Leu (**VIII**), and β-Ala-Ala (**IV**), were tested as inhibitors using the assay that monitors the formation of aspartate with β-Asp-Leu as the substrate. 3-Phosphono-D,L-Ala (**V**), β-Asp-hydroxamate (**VI**) , L-cysteine sulfinic acid (**VII**), and β-methyl-aspartate were tested as

inhibitors using the assay that monitors the formation of alanine with β-Asp-Ala as the substrate.

Metal Analysis. The role of the metals in the IAD active site was addressed by the preparation and reconstitution of apo-IAD. Purified IAD was treated with 3 mM dipicolinate at 4 °C and pH 5.6 for 72 hours. The chelator was removed by loading the protein onto a PD10 column (GE Health Care) and eluting with metal-free buffer A. The metal-free buffer A was prepared by passing it through a Chelex 100 resin. The apo-IAD was reconstituted with 45 equivalents of the desired metal (Zn, Co, Ni, Cd and Mn), 50 μM $NaHCO_3$ and 100 mM HEPES at pH 7.5. The metal content of the apo-IAD and reconstituted enzyme was verified using a Perkin-Elmer AAnalyst 700 atomic absorption spectrometer.

pH Profiles. The pH dependence of the kinetic parameters were determined for the Zn/Zn, Co/Co, Cd/Cd, and Ni/Ni forms of the wild type IAD and the Zn/Zn IAD mutants E77Q, Y137A and Y137F using β-Asp-Leu as the substrate. The pH range was assayed between 5.0 and 10.0 with 0.2 pH unit increments. Different buffers at 100 mM were used at different pH: MES (5.0-6.6), PIPES (6.6-7.2), HEPES (7.2-8.2), TAPS (8.2-8.8), and CHES (8.8-10.0) were used at a concentration of 100 mM. The pH was measured after the reaction was completed in order to confirm the pH to be the expected.

Data Analysis. The kinetic parameters, were determined by fitting the initial velocity data to the equation 3.1 (*62*), where v is the initial velocity, E_T is the enzyme

concentration, k_{cat} is the turnover number, S is the substrate concentration, and K_m is the Michaelis constant.

$$v / E_T = \frac{k_{cat} S}{K_m + S} \qquad 3.1$$

The pK values were calculated by fitting the k_{cat} or k_{cat}/K_m values (y) to equation 3.2 (*62*), where c is the pH independent value of y, K_a and K_b are the dissociation constants of the groups that ionize and H is the hydrogen ion concentration.

$$\log y = \log\left(\frac{c}{1 + \frac{H}{K_a} + \frac{K_b}{H}}\right) \qquad 3.2$$

Competitive inhibition patterns were fitted to the equation 3.3 (*62*) were v is the initial velocity, V_{max} is the maximal velocity, S is the substrate concentration, and K_m is the Michaelis constant, I is the inhibitor concentration and K_i is the slope inhibition constant.

$$v = \frac{V_{max} S}{K_m\left(\frac{1 + I}{K_i}\right) + S} \qquad 3.3$$

Structural Analysis. The crystal structure for the IAD D285N mutant protein was solved in collaboration with James B. Thoden and Hazel M. Holden at the Department of Biochemistry, University of Wisconsin, at Madison, Wisconsin. The crystal structure coordinates were deposited in the Research Collaboratory for Structural Bioinformatics,

Rutgers University, at New Brunswick, New Jersey. The PDB entry codes are 1onx and 1ybq for the complexed form of IAD with the product of hydrolysis, L-aspartate, and the substrate, β-Asp-His, respectively.

RESULTS

Specific Activity Determination. The compounds tested as substrates for IAD (Zn/Zn) at pH 8.1 and their kinetic constants are presented in Table 3.1. In accordance with previous publications (*8, 55, 56*), β-Asp-Leu (**I**) is the best substrate with a K_m of 1.0 mM and a k_{cat}/K_m 1.0 x 10^5 $M^{-1}s^{-1}$ (*56*). Despite the high preference for β-aspartyl dipeptides, IAD was able to hydrolyze α-Asp-Leu (**II**), with a K_m of 5.0 mM and a k_{cat}/K_m 3.1 x 10^3 $M^{-1}s^{-1}$. β-Asp-Gly is a slow substrate with a K_m of 18 mM and a k_{cat} of 0.94 s^{-1}. Although β-Asp-Ala has the higher specific activity, the K_m is elevated, making the k_{cat}/K_m to be low relative to other substrates. β-Asp-Phe has the lowest K_m but at the same time a relatively low turnover. No activity was detected with succinyl-Leu (**III**), β-Ala-Ala (**IV**) and β-Glu-Leu.

Inhibitors. Different compounds were tested as suitable inhibitors of IAD. No inhibition could be detected with β-Ala-Ala (**IV**) with concentrations up to 29 mM. The compound, β-Ala-Ala lacks the α-carboxy group on the aspartate moiety of the substrate. Another derivative of the substrate, which lacks the free α-amino group, succinyl-L-Leu (**III**), is a weak competitive inhibitor with a K_i of 130 ± 30 mM. The analog of β-Asp-Leu that resembles the putative transition state intermediate, 3-sulfo-L-Ala-S-L-Leu (**VIII**), did not inhibit at concentrations up to 26 mM. Three aspartate analogs, 3-phosphono-D,L-Ala (**V**), β-Asp-hydroxamate (**VI**), and L-cysteine sulfinic acid (**VII**)

were tested for inhibition of the hydrolysis of β-Asp-Ala. All were found to act as competitive inhibitors with K_i values of 1.5 ± 0.2 mM, 4.7± 0.6 mM and 77 ± 9 mM, respectively. The kinetic constants for the competitive inhibition of IAD were obtained from fits of the data to equation 3.3.

Metal Analysis. The role of the metals in the active site of IAD was probed by formation of apo-IAD and reconstitution with Zn^{2+}, Co^{2+}, Cd^{2+}, Ni^{2+}, or Mn^{2+}. The specific activity of apo-IAD was calculated to be lower than 1 % and the metal content to be about 0.07 equivalents of zinc per active site. The reconstitution of apo-IAD with different divalent metals, results in a 100% recovery of activity for Zn/Zn, 54% for Co/Co, 32% for Cd/Cd, and 10% for Ni/Ni (Table 3.2). The recovery of activity after the reconstitution with Mn^{2+} was not different from the apo-IAD, which suggests no incorporation. After incubation, the metal content of IAD was lower than 0.04 equivalents of Mn and 0.07 equivalents of Zn. The reconstitution of apo-IAD with zinc was relatively fast achieving maximal activity in 2 hours. The reconstitution of apo-IAD with cadmium, nickel, and cobalt achieved maximal activity in 15 hours, 50 hours, and 75 hours, respectively. The average metal content per subunit of the reconstituted proteins was 2.0, 2.7, 2.9, and 1.4 for the Zn-, Co-, Cd, and Ni-substituted forms of IAD, respectively. IAD (Zn/Zn) has the higher k_{cat} and K_m with 104 s^{-1} and 1.02 mM respectively. IAD Ni/Ni presents the lower k_{cat} and K_m (Table 3.2). Remarkably, as the K_m values decrease with the different metal substitution, the k_{cat} decreases accordingly.

Table 3.1: Kinetic Parameters for IAD with Different Substrates[a]

substrate	K_m (mM)	k_{cat} (s^{-1})	k_{cat}/K_m ($M^{-1}s^{-1}$)
β-Asp-Leu	1.0 ± 0.1	104 ± 3	(102 ± 9) x 10^3
β-Asp-Phe	0.23 ± 0.02	17 ± 1	(73 ± 7) x 10^3
β-Asp-Lys	0.91 ± 0.07	58 ± 1	(63 ± 5) x 10^3
β-Asp-Ala	3.7 ± 0.2	213 ± 5	(58 ± 3) x 10^3
β-Asp-His	3.7 ± 0.2	20.8 ± 0.7	(5.6 ± 0.7) x 10^3
β-Asp-Gly	18 ± 1	0.93 ± 0.05	51 ± 1
α-Asp-Leu	5.0 ± 0.2	15.7 ± 0.2	(3.1 ± 0.1) x 10^3
γ-Glu-Leu	-	-	< 7.8 x 10^{-3}
Succ-Leu	-	-	< 7.9 x 10^{-6}
β-Ala-Ala	-	-	< 3.6 x 10^{-2}

[a]The kinetic parameters were obtained at pH 8.1 and 30 °C from fits to eq 3.1.

Table 3.2: Kinetic Parameters for Different Metal Reconstituted IAD and Mutants[a]

IAD	K_m (mM)	k_{cat} (s^{-1})	k_{cat}/K_m ($M^{-1}s^{-1}$)
WT (Zn/Zn)	1.02 ± 0.09	104 ± 3	(1.0 ± 0.1) x 10^5
WT (Co/Co)	0.62 ± 0.03	34.0 ± 0.4	(5.5 ± 0.3) x 10^4
WT (Cd/Cd)	0.38 ± 0.05	11.9 ± 0.4	(3.3 ± 0.4) x 10^4
WT (Ni/Ni)	0.09 ± 0.01	9.3 ± 0.2	(1.0 ± 0.1) x 10^5
E77D	6.9 ± 0.9	(5.1 ± 0.3) x 10^{-3}	(7.4 ± 0.1) x 10^{-1}
E77Q	1.0 ± 0.1	(4.3 ± 0.1) x 10^{-3}	4.3 ± 0.1
Y137A	2.5 ± 0.2	(3.2 ± 0.1) x 10^{-1}	(1.3 ± 0.1) x 10^1
Y137F	0.97 ± 0.07	(3.1 ± 0.1) x 10^{-1}	(3.16 ± 0.1) x 10^2
R169K	27 ± 2	4.5 ± 0.2	(1.7 ± 0.1) x 10^2
R169M	> 58	-	(1.4 ± 0.1) x 10^{-2}
R233K	26 ± 4	28 ± 3	(1.1 ± .2) x 10^3
R233M	27 ± 3	2.7 ± 0.2	(1.0 ± 0.1) x 10^2
D285A	-	-	<(2.0 ± 0.7) x 10^{-4}
D285N	0.95 ± 0.08	(1.2 ± 0.1) x 10^{-3}	1.3 ± 0.1
S289A	3.0 ± 0.2	3.2 ± 0.1	(1.1 ± 0.1) x 10^3

[a]The mutants were reconstituted with zinc. The kinetic constants were determined with β-Asp-Leu as the substrate and fits to eq 3.1.

pH Profiles. The effect of pH on the kinetic constants, k_{cat} and k_{cat}/K_m, was determined for the Zn, Co, Cd, and Ni substituted forms of IAD using β-Asp-Leu as the substrate. The pH-rate profiles for wild type IAD with different metal substitutions present a loss in activity at low and high pH, as presented in Figure 3.3. Table 3.3 illustrates how the kinetic parameters, the pK_a and the pK_b values, are affected by the metal content of IAD active site. The kinetic and ionization constants were obtained from fits to equations 3.1 and 3.2, respectively. The pH-rate profiles indicate that the maximal activity of the enzyme requires that one group must be unprotonated while another group must be protonated. Variations in the metal substitution of the binuclear metal center demonstrates that the group that must be unprotonated for activity is very much dependent on the specific metal ion that is bound to the active site, whilst the pK_b is not significantly affected.

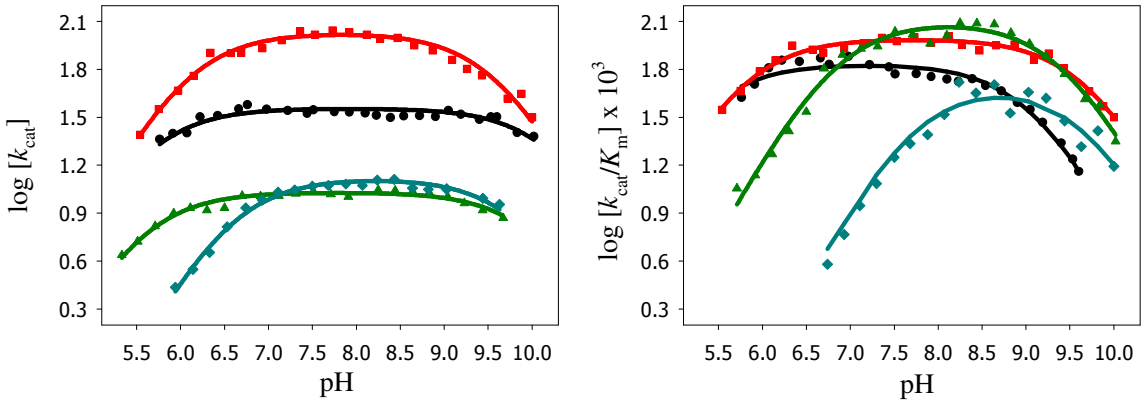

Figure 3.3: pH-rate profiles of k_{cat} and k_{cat}/K_m for different metal reconstituted IAD WT (■ Zn, ● Co, ▲ Ni and ♦ Cd). The kinetic constants were obtained for Zn, Co, Ni, and Cd. The data obtained using β-Asp-Leu as the substrate was fit to equation 3.2. Additional details are provided in the text and in Table 3.3.

Table 3.3: Ionization Constants for Metal-Substituted IAD from pH-Rate Profiles[a].

IAD	log k_{cat} vs. pH		log k_{cat}/K_m vs. pH	
	pK_a	pK_b	pK_a	pK_b
WT (Zn/Zn)	6.1 ± 0.1	9.6 ± 0.1	5.8 ± 0.1	9.7 ± 0.1
WT (Co/Co)	5.1 ± 0.2	9.8 ± 0.1	5.5 ± 0.1	9.2 ± 0.1
WT (Cd/Cd)	6.1 ± 0.1	10.5 ± 0.4	7.7 ± 0.1	9.7 ± 0.7
WT (Ni/Ni)	5.5 ± 0.1	10.5 ± 0.1	6.7 ± 0.1	9.4 ± 0.1

[a]The kinetic constants were determined with β-Asp-Leu as the substrate and fits of the data to eq 3.2

Active Site Directed Mutants of IAD. The roles of Glu-77, Tyr-137, Arg-169, Arg-233, Asp-285, and Ser-289 on the substrate binding and catalytic activity of IAD were studied by site-directed mutations to these amino acids. The mutant proteins were purified to homogeneity and the zinc content varied from 1.3 to 2.0 per subunit. The crystal structure of IAD suggests that Asp-285 is in the proper position to serve as a metal ligand and to form a hydrogen bond with the solvent molecule that bridges the two metals. There is a substantial decrease in activity when Asp-285 is mutated to alanine or asparagine. A similar effect is also found in other members of the amidohydrolase superfamily when the aspartate from the strand 8 is mutated (*35, 36*). The largest decrease in catalytic activity, relative to the wild-type enzyme, was obtained from the mutations at positions Glu-77, Arg-169, and Asp-285. The kinetic constants for the zinc containing mutants were determined from fits to equation 3.1 and the results are presented in Table 3.3.

X-Ray Crystal Structure of the D285N Mutant Complexed with β-Asp-His. The structure of the D285N mutant complexed with β-Asp-His was determined to 2.0 Å resolution. The mutation of Asp-285 to asparagine reduces the occupancy for the zinc ions. Other than reducing the metal content of the enzyme, the mutation of the Asp-285 to an asparagine resulted in little overall structural perturbation. In one subunit of the asymmetric unit, Lys-162 does not appear to be carboxylated. The electron density for Lys-162 in the second subunit of the asymmetric unit is consistent with a carboxyl group attached to the ε-nitrogen of its side chain. The substrate, β-Asp-His, is bound to both subunits. The reduction in metal content and the decarboxylation of the modified Lys-162 in one subunit for the D285N mutant are probably caused by minor structural perturbations due to the loss of a direct metal ligand at the α-position. The overview of the active site of IAD complexed with the substrate and the possible hydrogen bonding interactions with the substrate ligands are shown in Figure 3.4. As predicted in the previous chapter (Chapter II), the side chain of Glu-77 interacts with the α-amino group of the β-Asp-His, while the backbone amide groups of Gly-75, Thr-106, and Ser-289 interact with the α-carboxylate group of the ligand. The carbonyl moiety of β-Asp-His is positioned 2.4 Å from O^{η} of Tyr-137 and 2.4 Å from the β-metal. The guanidinium side chains of Arg-169 and Arg-233 interact with the carboxylate group of the histidine moiety. There are no interactions between the protein and the imidazole side chain of the β-Asp-His ligand. The side chain of the histidine moiety of the substrate is orientated toward the opening of the active site.

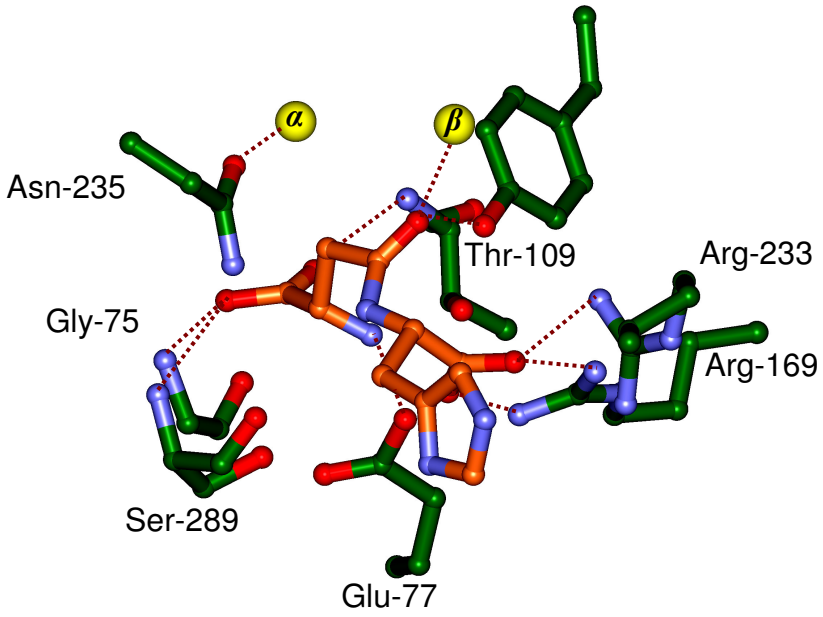

Figure 3.4: Close-up view and potential hydrogen bonding interactions between β-Asp-His and the D285N mutant. The potential protein-ligand interactions are represented by the dashed magenta lines. The image was drawn with the program WebLab Viewer Pro using the coordinates from PDB file 1ybq.

DISCUSSION

Isoaspartyl dipeptidase catalyzes the hydrolysis of dipeptides formed from the β-carboxylate group of aspartic acid (*8*). IAD has shown high specificity toward the hydrolysis of dipeptides containing aspartate at the N-terminus of the dipeptide but has relatively lower specificity for the amino acid occupying the C-terminal position. The analysis of the amino acid sequence and the X-ray crystal structure of this enzyme have confirmed that IAD is a member of the amidohydrolase superfamily (*4*). This catalytically diverse group of metalloproteins act on the hydrolysis of amides and esters at carbon and phosphorus centers (*4, 5*). The active sites of proteins within this superfamily contain either mononuclear or binuclear metal centers at the C-terminal

end of the $(\beta/\alpha)_8$-barrel (*4*). IAD contains a binuclear metal center and is similar to that previously described for phosphotriesterase (*18*), dihydroorotase (*19*), and urease (*39*), among others. The analysis of the mechanistic investigations of the reactions catalyzed by these enzymes has demonstrated that their binuclear metal centers are responsible for the activation of the nucleophilic water molecule and enhancement of the electrophilic character of the bond to be cleaved (*35, 36*).

Substrate Specificity. A set of substrates including, β-Asp-Leu (**I**), β-Asp-Ala, β-Asp-Gly, β-Asp-His, β-Asp-Lys, and β-Asp-Phe were tested for substrate turnover with IAD from *Escherichia coli*. All were found to be substrates with k_{cat} values that ranged from 1 to 200 s^{-1}. The best substrate was β-Asp-Leu with a k_{cat}/K_m of ~1.0 x 10^5 M^{-1} s^{-1}, whereas the highest turnover number was found for β-Asp-Ala. These substrates contained side chains with aromatic, hydrophilic, and hydrophobic substituents at the C-terminus of the dipeptide. Due to the variety of properties of the side chains of the C-terminus residue of the dipeptide, the environment for the active site that accommodates this part of the substrate cannot be very specific. The X-ray structure of β-Asp-His bound to the D285N mutant demonstrates that the imidazole side chain of the histidine moiety of the substrate is not within 3.5 Å of any protein group and is orientated toward the active site opening. This provides the ambiguity necessary for the nonspecific binding of a variety of side chains at C-terminus of the dipeptide.

The structure of the wild-type IAD bound to a phosphonate analogue of α-Asp-Leu (Asp-$\Psi[PO_2CH_2]$-LeuOH) (*63*), positioned the α-amino group of the inhibitor in

a similar orientation to that found for the β-Asp-His substrate bound to the D285N mutant. The purified IAD was able to hydrolyze the peptidic bond of α-Asp-Leu (**II**) with a k_{cat}/K_m of ~10^3 M^{-1} s^{-1}. This result demonstrates that the positioning of the α-amino group of the substrate on C_2 instead of C_3 of the aspartate moiety is important but not vital for the catalytic activity. The X-ray structure of the bound β-Asp-His complexed to the D285N mutant demonstrates that the α-amino group of this substrate is ion-paired with the side chain carboxylate of Glu-77 (Figure 3.4). Since succinyl-Leu (**III**) is not a substrate, but a relatively poor inhibitor of IAD, it can be suggested that the α-amino group of the aspartate moiety is required for substrate turnover. Furthermore, the α-carboxylate of a β-aspartyl dipeptide is also required for catalytic activity since β-Ala-Ala (**IV**) is not a substrate for the enzyme.

There are two guanidinium side chains from arginines 169 and 233 involved in the positioning of the α-carboxylate group from the amino acid at the C-terminus of a dipeptide substrate (Figure 3.4). When either of these arginines are mutated to a lysine residue, the K_m value is substantially elevated and k_{cat} is reduced accordingly. However, the reduction in catalytic proficiency is larger with mutations to Arg-169 than to Arg-233. When Arg-169 is mutated to a methionine residue, the value of k_{cat}/K_m is reduced by more than 6 orders of magnitude relative to that of the wild-type, while the methionine mutation of Arg-233 remains significantly more active (Table 3.3).

Activation of Water. The crystal structure of the wild-type enzyme shows a single solvent molecule bridging the metal ions in the active site. In the structure of

the enzyme bound to the hydrolysis product, the β-carboxylate group of the aspartate is ligated between the two metal ions as shown in Figure 3.2. Taken together, these two structures demonstrate that the hydrolytic nucleophile most likely originates from the hydroxide or water that bridges the two metal ions. These results also indicate that the β-carboxylate group of the aspartate product acts as a bridging ligand between the two divalent cations at the conclusion of the enzymatic reaction. This is also observed in the crystal structure of DHO (PDB entry 1j79), where in one subunit is the substrate, L-dihydroorotate, coordinated to the β-metal and the bridging solvent molecule bridging the two metals. In the other subunit, the β-carboxylate of the aspartate moiety of the product of the reaction, *N*-carbamoyl-L-aspartate, is found to bridge the two metal ions (*19*).

pH-rate profiles were used to address the identity of the molecule that bridges the two divalent metals. For the wild-type enzyme, the pH-rate profiles for either k_{cat} or k_{cat}/K_m show that one group must be protonated and another group must be unprotonated for maximal catalytic activity. The loss of catalytic activity at low pH is consistent with the protonation of a bridging hydroxide to water. When the zinc metal is replaced with cadmium, the pK_a for k_{cat}/K_m increases by 1.9 pH units (from 5.8 to 7.7). Since the kinetic pK_a obtained from the pH-rate profiles is a function of the specific metal ion bound to the active site, the ionization at low pH should represent the protonation of a metal bridging hydroxide. This protonation will decrease the nucleophilic character of the metal bridging hydroxyl molecule, whilst diminishing the catalytic proficiency. In aqueous systems, the pK_a of water bound to Zn^{2+} is 8.9,

whereas it is 10.1 for Cd^{2+} (*37*). In addition, studies of a biomimetic chemical analogue of a binuclear Zn^{2+} complex demonstrate that the pK_a of the bridging hydroxide was 6.8 (*38*). This kinetic pK_a dependence on the identity of the metal ion binuclear metal center is also found for phosphotriesterase (*35*) and dihydroorotase (*36*).

The kinetic pK_a for the group that must be protonated for maximal activity remains relatively unaffected with changes in the divalent cation. The average value for this ionization at high pH is 9.5 ± 0.2. The loss of catalytic activity at high pH is most likely to originate from the ionization of the α-amino group of the dipeptide substrate. The ionizations of the free α-amino groups of single amino acids have been reported to vary from 9.2 to 9.7 (*64*). The inability of IAD to catalyze the hydrolysis of succinyl-leucine (**III**) supports this conclusion. More evidence can be derived from the ion-pair interaction between the α-amino group of the substrate and the side chain carboxylate of Glu-77 in the X-ray structure of the D285N mutant. Mutations of the glutamate side chain to aspartate and glutamine reduce the values of k_{cat} and k_{cat}/K_m by approximately 4 orders of magnitude. Another important interaction of the α-amino group of the aspartate moiety in the wild-type-product complex and the D285N mutant-substrate complex is the hydrogen bonding with the backbone carbonyl and side chain hydroxyl of Ser-289 (Figure 3.2 and Figure 3.4). When Ser-289 is mutated to alanine, the catalytic activity diminishes by ~2 orders of magnitude suggesting that the interaction of Ser-289 is important but not vital for catalysis and substrate binding.

Activation of the Substrate. The coordination of the carbonyl group of the substrate peptide bond to the β-metal can activate it for nucleophilic attack. This interaction polarizes the carbonyl group of the peptidic bond and enhances the electrophilic character of the carbonyl carbon. The X-ray structure of the complexed β-Asp-His substrate to the metal center of the D285N mutant, demonstrates that the carbonyl oxygen of the scissile bond is coordinated to the β-metal ion at a distance of 2.4 Å. Similar enzyme-ligand interactions of bound substrates and/or inhibitors have been previously observed for phosphotriesterase (*65*), dihydroorotase (*19*), and urease (*17, 39*). In all four enzymes, the conserved function for the β-metal ion within the binuclear metal center is the polarization of the carbonyl or phosphoryl bond via Lewis acid catalysis.

Activation of the Leaving Group. The hydrolysis of the peptide bond requires that the amide nitrogen of the leaving group must be protonated. In the case of dihydroorotase (DHO), the residue responsible for protonation of the leaving group is the Asp-250, which coordinates the α-metal and is hydrogen bound to the hydroxide nucleophile (*64*). The homologous residue in IAD is Asp-285. The X-ray structure of the native form of IAD, shows the side chain carboxylate of Asp-285 hydrogen bonded to the hydroxide molecule that bridges the two divalent cations. The importance of this residue can be derived from the site-directed mutagenesis of Asp-285, to alanine or asparagine. These mutations result in a catalytically deficient form of IAD, and confirm its critical function. The crystal structure of the substrate trapped in the active site of the mutant IAD was possible due to the catalytic deficiency of the

D285N mutant (Figure 3.4). The binding of the substrate in this inactive complex orients the carbonyl oxygen of the scissile bond in position to be attacked by the bridging hydroxide. It is proposed that this reaction is facilitated by the abstraction of the proton from the hydroxide by the side chain carboxylate from Asp-285. The protonated carboxylate from Asp-285 is positioned to donate the proton to the leaving group amine and promote the cleavage of the amide bond of the dipeptide substrate.

Mechanism of Action. A self consistent mechanism of reaction for the hydrolysis of β-aspartyl dipeptides can be formulated from observations made with the various X-ray structures and the catalytic properties of the wild-type and mutant forms of IAD. In the resting state of the enzyme, the two divalent cations are bridged by a hydroxide molecule and the Asp-285 is ligated to the α-metal and hydrogen bonded to the metal bridging hydroxide. The substrate is bound to the active site in an orientation that positions the carbonyl oxygen of the scissile bond adjacent to the β-metal ion. This interaction polarizes the carbonyl group and enhances the electrophilic character of the carbon to be attacked. The ion pair interaction between the side chain carboxylate of Glu-77 and the α-amino group of the substrate facilitates the binding of β-aspartyl dipeptides to the active site. Additional ion pair interactions between the α-carboxylate of the leaving group product and the guanidinium groups of Arg-169 and Arg-233 help the orientation of the substrate in the active site. Upon binding of the β-aspartyl dipeptide, the enzymatic reaction is initiated by the nucleophilic attack at the *re* face of the amide bond concomitant with proton transfer from the hydroxide to the side chain carboxylate of Asp-285, forming a tetrahedral intermediate. The lately

protonated Asp-285 transfers the proton to the α-amino group of the departing amino acid causing the collapse of the tetrahedral intermediate and the cleavage of the peptide bond. The reaction finalizes with the newly formed carboxylate at the side chain of aspartate product, coordinated to the binuclear metal center, as observed in the X-ray structure of the complexed product. The products depart the active site, and the binuclear metal center is regenerated with a new hydroxide molecule via a mechanism that has not been addressed in this investigation. This mechanism of reaction is analogous to that previously established for phosphotriesterase (*35*) and dihydroorotase (*19, 36*). Scheme 3.3 outlines the proposed reaction mechanism for the hydrolysis of β-aspartyl dipeptides by isoaspartyl dipeptidase.

Scheme 3.3:

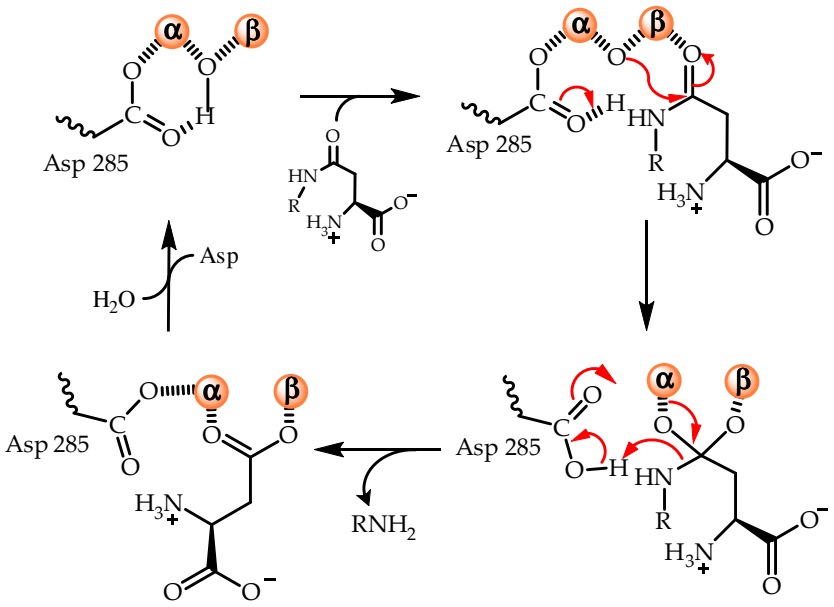

CHAPTER IV

FUNCTIONAL SIGNIFICANCE OF GLU-77 AND TYR-137 WITHIN THE ACTIVE SITE OF ISOASPARTYL DIPEPTIDASE*

Isoaspartyl dipeptidase (IAD) is responsible for the hydrolytic cleavage of β-aspartyl dipeptides (Scheme 4.1) (*8, 55, 56*). The best substrate found for IAD is β-Asp-Leu with a k_{cat}/K_m of 10^5 $M^{-1}s^{-1}$. IAD displays little or no activity toward the hydrolysis of tripeptides or γ-glutamyl dipeptides. IAD is a member of the amidohydrolase superfamily and most closely resembles dihydroorotase (DHO) and D-hydantoinase (D-HYD) (*27, 59*). Several X-ray crystal structures of IAD have been solved to high resolution (*27, 63, 66*). The resting enzyme, the bound substrate (β-Asp-His), the bound hydrolysis product (aspartate) and the phosphonate inhibitor have been solved to 1.65 Å, 2.0 Å, 2.1 Å and 3.3 Å, respectively (*27, 63, 66*). The folded protein is divided into two domains, one composed of eight strands of mixed β-strands forming the N-terminus and the other by an $(\beta/\alpha)_8$-barrel forming the C-terminus. The binuclear metal active site is found at the end of the $(\beta/\alpha)_8$-barrel and is composed of four histidines, an aspartic acid and a carboxylated lysine that bridges the two metal ions. The α-metal is coordinated by His-68, His-70 and Asp-285. The β-metal is coordinated by His-201 and His-230 as primary ligands. The metals are bridged by the carboxylated Lys-162 and a solvent

---

*Parts of the data reported in this chapter are reprinted with permission of "Functional significance of Glu-77 and Tyr-137 within the active site of isoaspartyl dipeptidase" by Marti-Arbona, R., Thoden, J. B., Holden, H. M., and Raushel, F. M., 2005. *Bioorganic Chemistry 33,* 448-458. Copyright 2005 Elsevier.

molecule. The carboxylation of the lysine residue occurs from the post-translational alteration of the ε-amino group (*29*). The α-metal is buried inside the protein, while the β-metal is more exposed to the solvent. The crystal structure of the substrate complexed to the D285N mutant shows that Tyr-137 is within 2.4 Å and in the correct orientation to interact as a fifth ligand for the β-metal and also to hydrogen bond to the carbonyl oxygen of the peptide bond of the substrate (Figure 4.1). The crystal structure of the wild-type IAD complexed to hydrolysis product reveals that the side chain carboxylate of the aspartate product displaces the bridging solvent molecule as it binds to the active site (*27*). It also suggests that the loop defined by Phe-292 to His-301 moves toward the active site, bringing Ser-289 within hydrogen bond distance to the α-amino group of the aspartate ligand (Figure 4.1).

Scheme 4.1

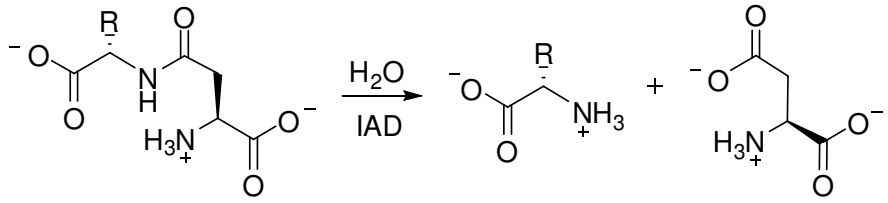

The mechanism of hydrolysis of β-aspartyl dipeptides by IAD have been suggested to begin with the nucleophilic attack of the metal bridging hydroxyl to the *re* face of the amide bond and a simultaneous proton transfer from the hydroxide to the side chain carboxylate of Asp-285. This forms a tetrahedral intermediate that collapses by the donation of a proton to the α-nitrogen of the leaving group, promoting the cleavage of the peptide bond (Scheme 4.2) (*27, 66*).

Scheme 4.2

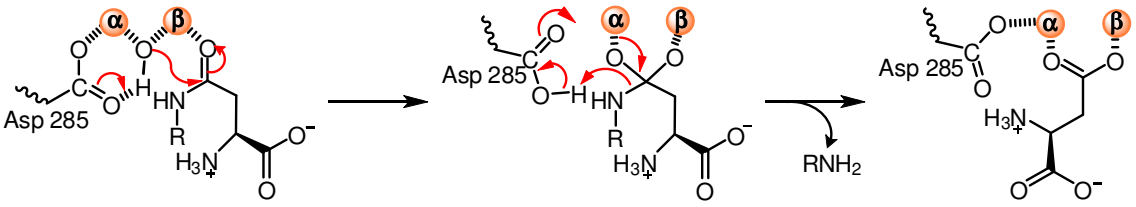

The pH-rate profile for the hydrolysis of β-aspartyl-leucine by wild-type IAD displays a bell-shaped pH dependence (*66*). The decrease in the catalytic activity at low pH suggests the protonation of a single group. The kinetic pK_a obtained from the pH-rate profiles with different metal substituted IAD (Zn, Co, Cd, and Ni), demonstrate that the pK_a for the ionization at low pH is dependent of the identity of metal ions in the binuclear active site (*66*). This is consistent with the protonation of a metal bridging hydroxide (*35, 67*). The kinetic pK_a for the group that needs to be protonated for catalytic activity remains relatively unchanged with variations on the specific metal forming the binuclear active site. This ionization has been suggested to be related to the deprotonation of the α-amino group of the aspartate moiety of the substrate (*66*).

In addition to the conserved residues that form the binuclear metal center in the active site of IAD, there are two other highly conserved residues within the active site proximity that may contribute to the overall rate enhancement for this enzyme. The X-ray crystal structure of IAD D285N complexed to the substrate, β-Asp-His, shows that the phenolic side chain of Tyr-137 is 2.4 Å from the β-metal and in the proper orientation to function as a fifth metal ligand. The residue may serve as a Lewis acid catalyst for the polarization of the carbonyl oxygen of the scissile amide bond. The

carboxylate side chain of Glu-77 also appears to form an ion pair with the free α-amino group of the substrate or, alternatively, as part of a proton shuttle mechanism. The relative orientation of these two residues within the active site of IAD is presented in Figure 4.1. Site-directed mutagenesis of the residues Glu-77 and Tyr-137 cause significant decrease in catalytic activity. The effect of these mutations on the pH dependence of the catalytic activity has not been previously addressed. This investigation clarifies the involvement of these two residues in the catalytic activity of IAD by measuring the kinetic constants and through the analysis of the X-ray crystal structures of the site directed mutants, E77Q and Y137F.

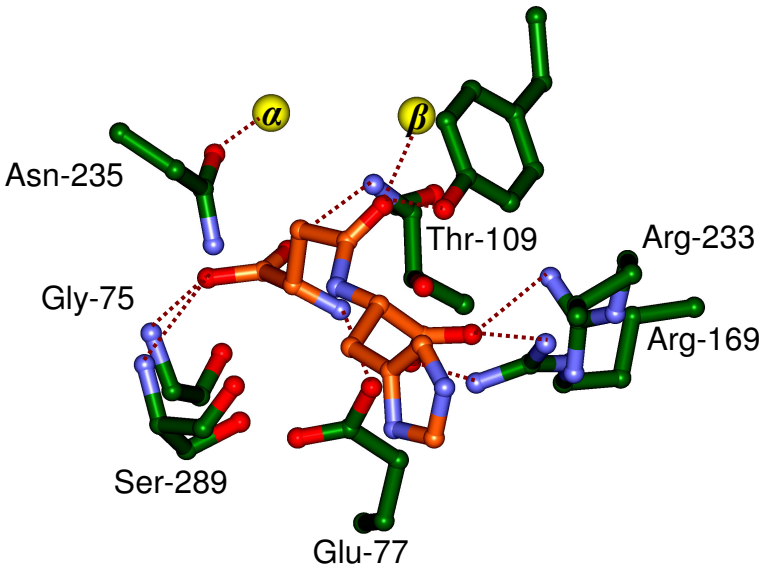

Figure 4.1: A close-up view of the active site of the D285N mutant with bound β-Asp-His, highlighted in gold bonds. Potential hydrogen bonding interactions are represented by the magenta dashed lines. The image was drawn with the program WebLab Viewer Pro using the coordinates from PDB file 1ybq.

MATERIALS AND METHODS

Materials. All chemicals, substrates, and coupling enzymes were obtained from Sigma-Aldrich. The *iad*A gene was cloned from the *Escherichia coli* XL1Blue strain into a pET30a(+) expression vector (Stratagene) (*27*). Site-directed mutants of IAD at residues Glu-77 and Tyr-137 were accomplished using the Quick Change site-directed mutagenesis kit (Stratagene).

Protein Purification. The pET30a(+) plasmids encoding the wild-type and mutant IAD were transformed in JDG 1000 (λDE3). IAD was purified according to published procedures (*66*). Cultures were grown in Luria-Bertani medium at 37 °C until an absorbance at 600 nm reached ~0.6 OD. The expression of IAD was induced by the addition of 1.0 mM isopropyl-β-thiogalactoside and incubated overnight at 37 °C. Cells were collected by centrifugation and re-suspended in 50 mM HEPES buffer at pH 8.1 (buffer A) containing 5 μg/mL RNAse and 0.1 mg/mL phenylmethylsulfonyl fluoride. The cells were disrupted by sonication and the insoluble cell debris was removed by centrifugation. The soluble protein was then fractionated between 20% and 50% saturation of ammonium sulfate in buffer A. The precipitated protein from the 20-50% ammonium sulfate pellet was re-suspended and loaded onto a High Load 26/60 Superdex 200 prep grade gel filtration column (GE Health Care). The active fractions were pooled and loaded onto a Resource Q ionic exchange column (GE Health Care) and eluted with a gradient of NaCl in buffer A. The purification was finalized by pooling and precipitating the fractions that contained IAD with ammonium sulfate. The pellet was re-suspended and reloaded onto the High Load 26/60 Superdex 200 prep

grade gel filtration column and eluted with buffer A. The chromatographic profiles for wild-type and mutant IAD were identical. The presence and purity of IAD in the different purification steps were confirmed by SDS–PAGE. The purified enzyme was stored at -20 °C.

Kinetic Measurements and Data Analysis. The catalytic constants of IAD were determined by coupling the formation of aspartate to the oxidation of NADH (*57*). The oxidation of NADH at 30 °C was followed spectrophotometrically at 340 nm with a SPECTRAmax-340 microplate reader (Molecular Devices Inc.). The assay reactions were composed of 100 mM HEPES, 100 mM KCl, 3.7 mM α-ketoglutarate, 0.4 mM NADH, 0.64 units of malate dehydrogenase, 6 units of aspartate aminotransferase, and variable amounts of β-Asp-Leu and IAD in a final volume of 250 μL. The kinetic constants were determined by fitting the initial velocity data to equation 4.1. In equation 4.1, v is the initial velocity, E_T is the enzyme concentration, k_{cat} is the turnover number, S is the substrate concentration, and K_m is the Michaelis constant (*62*).

$$v / E_T = \frac{k_{cat} S}{K_m + S} \qquad 4.1$$

The pH dependence of the kinetic parameters was determined for the zinc substituted forms of the wild-type and mutant forms of IAD using β-Asp-Leu as the substrate. The pH range was assayed between 5.0 and 10.0 in 0.2 pH unit increments. The buffers MES (5.0-6.6), PIPES (6.6-7.2), HEPES (7.2-8.2), TAPS (8.2-8.8), and CHES (8.8-10.0) were used at a concentration of 100 mM and the pH of each solution was measured after the reaction was finalized. Equation 4.2 was utilized to calculate the

ionization constants when the activity diminishes at both low and high pH (*62*). The p*K* values were calculated by fitting the values of k_{cat} or k_{cat}/K_m (y) to equation 4.2, where c is the pH independent value of y, K_a and K_b are the dissociation constants of the groups that ionize and H is the hydrogen ion concentration.

$$\log y = \log\left(\frac{c}{1+\frac{H}{K_a}+\frac{K_b}{H}}\right) \qquad 4.2$$

Structural Analysis. The X-ray crystal structure for E77Q (PDB entry code 2aqo) and Y137F (PDB entry code 2aqv) mutants were solved in collaboration with James B. Thoden and Hazel M. Holden at the Department of Biochemistry, University of Wisconsin, at Madison, Wisconsin. The crystal structure coordinates were deposited in the Research Collaboratory for Structural Bioinformatics, Rutgers University, at New Brunswick, New Jersey.

RESULTS

Kinetic Parameters Determination. The kinetic parameters for the zinc species of the wild-type and mutant IAD at pH 8.1 with β-Asp-Leu as the variable substrate are shown in Table 4.1. Wild-type IAD has a K_m of 1.0 mM and a k_{cat}/K_m of 10^5 $M^{-1}s^{-1}$ for the catalytic hydrolysis of β-Asp-Leu (*66*). The crystal structure of the β-Asp-His ligand complexed to the D285N mutant suggests that residues Glu-77 and Tyr-137 are in direct proximity of the active site (Figure 4.1). The carboxylate side chain of Glu-77 is in the proper position for ion-pairing with the α-amino group of the dipeptide. Mutations at Glu-77 cause a remarkable decrease in specific activity by

reducing the k_{cat} by about 5 orders of magnitude. When Glu-77 is mutated to aspartate, the K_m is increased 7 fold, but there is no significant effect on the Michaelis constant for the glutamine mutant. The O^{η} of the phenolic side chain of Tyr-137 is positioned 2.4 Å from the carbonyl oxygen of the peptide bond of β-Asp-His and 2.4 Å from the β-metal. Site directed mutagenesis of Tyr-137 to alanine elevated the K_m 2.5 fold, but no significant effect was observed for the phenylalanine mutant. Both mutants of Tyr-137 diminished the value of k_{cat} by about 3 orders of magnitude.

pH-Rate Profiles. The ionization constants were determined for the pH dependence of the kinetic parameters for the wild-type IAD, E77Q, and Y137F. The pH-rate profiles for wild type IAD and the mutants are bell-shaped as shown in Figure 4.2. This indicates that one group must be unprotonated while another group must be protonated for maximum catalytic activity. Table 4.2 illustrates the pK values for wild-type IAD and mutants obtained from fits to equation 4.2 using β-Asp-Leu. For E77Q and Y137F mutants, the pK values obtained from k_{cat} and k_{cat}/K_m do not differ from the ones observed for the wild type IAD.

Table 4.1: Kinetic Parameters for Different Species of Isoaspartyl Dipeptidase[a]

IAD	K_m (mM)	k_{cat} (s^{-1})	k_{cat}/K_m ($M^{-1}s^{-1}$)
WT	1.0 ± 0.1	$(1.04 \pm 0.03) \times 10^{2}$	$(1.0 \pm 0.1) \times 10^{5}$
E77D	6.9 ± 0.9	$(5.1 \pm 0.3) \times 10^{-3}$	$(7.4 \pm 0.1) \times 10^{-1}$
E77Q	0.8 ± 0.1	$(5.6 \pm 0.1) \times 10^{-3}$	7 ± 1
Y137A	2.5 ± 0.2	$(3.2 \pm 0.1) \times 10^{-1}$	$(1.26 \pm 0.01) \times 10^{1}$
Y137F	0.97 ± 0.07	$(3.1 \pm 0.1) \times 10^{-1}$	$(3.16 \pm 0.1) \times 10^{1}$

[a]The kinetic constants were determined with β-Asp-Leu at pH 8.1 and fits to eq 1.

Table 4.2: p*K* Values for Wild-Type and Mutant IAD from pH-Rate Profiles[a].

IAD	log k_{cat} vs. pH		log k_{cat}/K_m vs. pH	
	pK_a	pK_b	pK_a	pK_b
WT	6.1 ± 0.4	9.6 ± 0.1	5.8 ± 0.4	9.6 ± 0.1
E77Q	5.2 ± 0.1	9.7 ± 0.1	< 5.0	9.1 ± 0.1
Y137F	5.6 ± 0.1	9.6 ± 0.1	5.3 ± 0.1	9.1 ± 0.1

[a]The kinetic constants were determined with β-Asp-Leu as the variable substrate and fits of the data to eq 4.2.

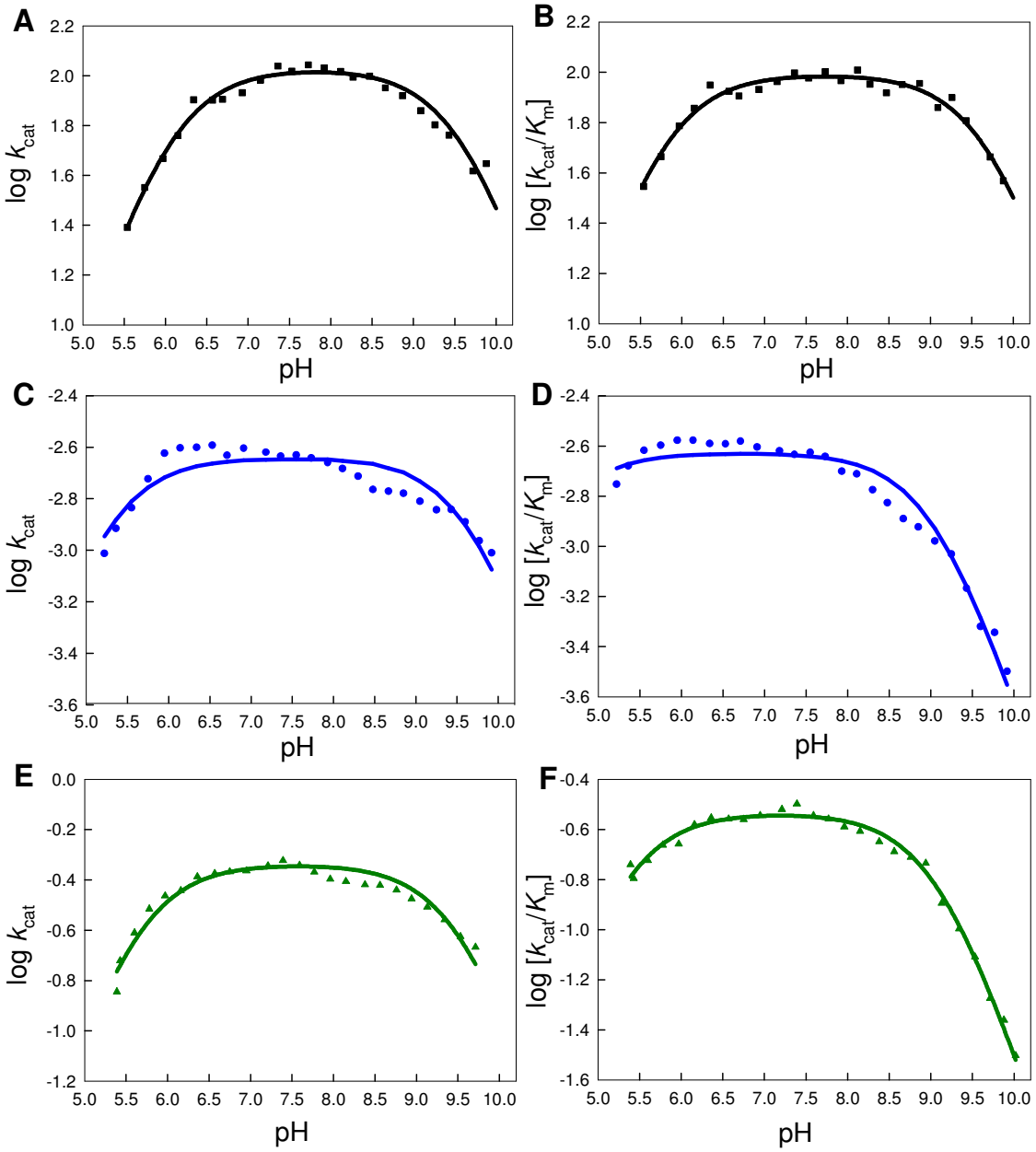

Figure 4.2: The pH-rate profiles of k_{cat} and k_{cat}/K_m for wild-type (■), E77Q (●) and Y137F mutant enzyme (▲). The pH-rate profiles for the wild type enzyme are presented in panels A and B. The pH-rate profiles for the mutant E77Q are shown in panels C and D, and ones for the mutant Y137F are shown in panels E and F. The data were fit to equation 4.2 using β-Asp-Leu. Additional details are provided in the text and in Table 4.2.

Structure of E77Q and Y137F Mutant Proteins. The X-ray crystal structures of the E77Q and Y137F mutant proteins were determined to a resolution of 1.95 Å with R-factors of 18.0 % and 18.5 %, respectively. The mutations of these two residues within the active site of IAD did not affect the relative occupancies of the zinc ions in the binuclear metal center. The overall molecular folds of the mutant proteins are basically identical to that found for the wild-type IAD. For both mutants, the electron density of Lys 162 in both of the asymmetric subunits is consistent with the carboxylation of the ε-amino group. Interestingly, the orientation of the Gln-77 in the resting state X-ray crystal structure of the E77Q mutant resembles the crystal structures of the aspartate complexed wild-type IAD and the β-Asp-His bound D285N mutant rather than of the apo-form of IAD (Figure 4.3). However, the γ-carbonyl oxygen of the side chain of Gln 77 in the E77Q mutant remains virtually in the same position as one of the oxygens of the γ-carboxylate of Glu-77.

The crystal structure of β-Asp-His complexed to the D285N mutant active site, shows that the O^{η} of the side chain of Tyr-137 is situated 2.4 Å from the β-metal and also 2.4 Å from the carbonyl oxygen of the peptidic bond of the substrate. The superposition of the active site residues for the resting state of IAD and the Y137F mutant is presented in Figure 4.4. The replacement of the Tyr-137 for phenylalanine did not generate any significant perturbation of the aromatic ring orientation relative to the corresponding side chain on the resting state of the wild-type IAD.

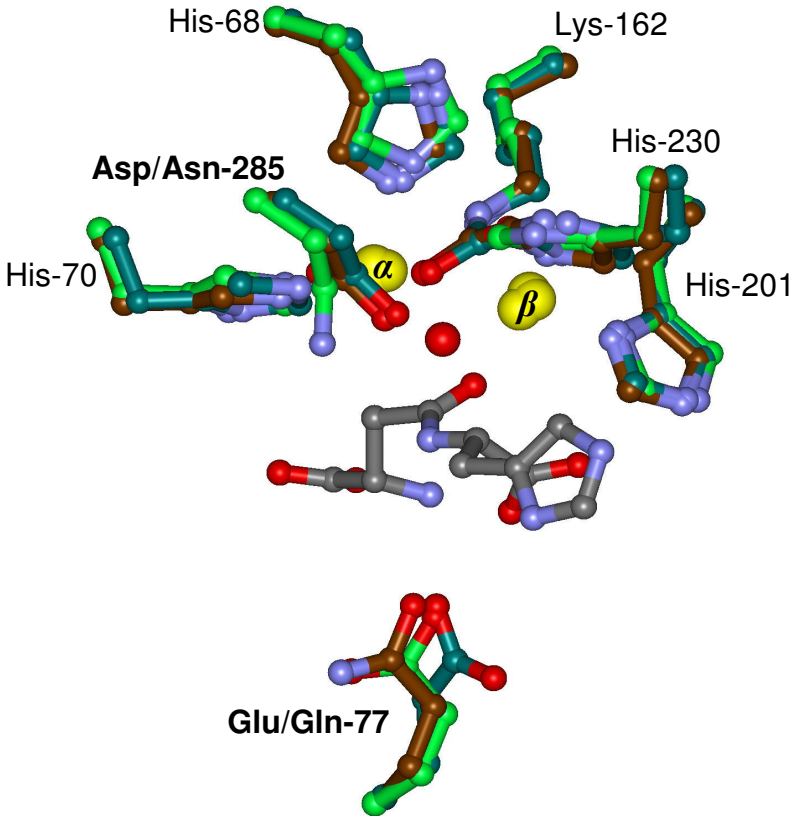

Figure 4.3: Superposition of the active site region for the resting forms of wild-type IAD, the mutant E77Q, and the substrate bound complex of the mutant D285N. The PDB entry codes for wild-type IAD, the mutant E77Q and the substrate bound complex of the mutant D285N are 1onw, 2aqo, and 1ybq, respectively. The side chains of the wild-type IAD are depicted with dark cyan bonds, the E77Q mutant side chains are represented in brown, and the side chains of the substrate bound complex of the D285N mutant are displayed in green. The zinc ions for all of the structures are in a similar position and are presented as yellow spheres. The solvent molecule that bridges the binuclear metal center of the wild-type IAD is drawn as a red sphere. The substrate β-Asp-His is presented with grey bonds. The image was drawn with the program WebLab viewer Pro.

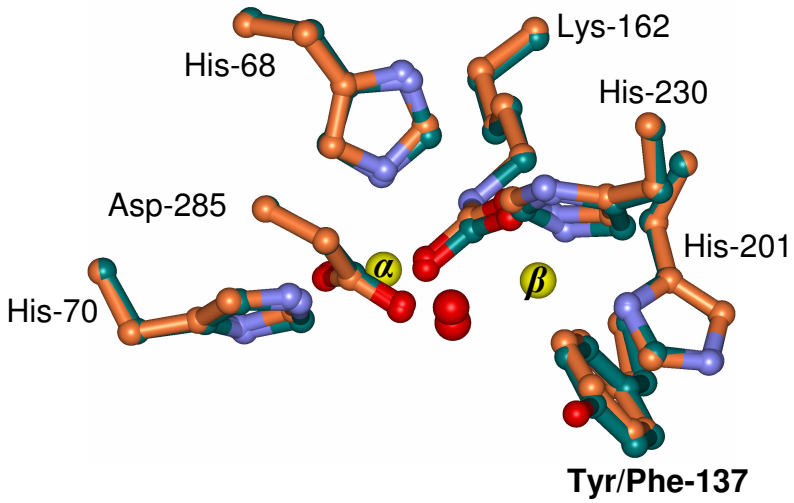

Figure 4.4: Superposition of the wild type IAD and the mutant Y137F. The PDB entry codes for wild-type IAD and the mutant Y137F are 1onw and 2aqv, respectively. The side chains corresponding to the wild type enzyme are depicted in the dark cyan bonds while those of the Y137F mutant protein are displayed in orange bonds. The positions of the zinc ions from both structures are essentially the same and are indicated by yellow spheres. The metal bridging solvent molecules are represented by red spheres. The image was created with the program WebLab Viewer Pro.

DISCUSSION

Isoaspartyl dipeptidase is a member of the amidohydrolase superfamily and catalyzes the hydrolysis of β-aspartyl dipeptides (*8, 27, 55*). This superfamily catalyzes the hydrolysis of amides and esters at carbon and phosphorus centers (*4, 5*). The binuclear metal center of IAD is similar to that found for phosphotriesterase (*68*), dihydroorotase (*19*), and urease (*39*). Mechanistic investigations of the reactions catalyzed by these enzymes have demonstrated that the binuclear metal center is

responsible for the activation of the nucleophilic water molecule and enhancement of the electrophilic character of the bond to be cleaved. The three-dimensional X-ray structures of the different species of IAD and the kinetic experiments have laid the groundwork for the reaction mechanism (Scheme 4.2).

The mechanism for the hydrolysis of β-aspartyl dipeptides by IAD hypothesizes that Asp-285 is involved in the activation of the solvent molecule between the two metals via proton transfer to the carboxylate group. The pH-rate profiles for IAD display a significant decrease in catalytic activity at pH values lower than 6 and higher than 9. The loss of catalytic activity at pH lower than 6 suggests the protonation of a single group with a pK_a of ~6. The dependence of this kinetic pK_a on the identity of the metal forming the binuclear center is consistent with the protonation of the bridging hydroxide (*35, 36, 66*). In contrast, the kinetic pK_a for the group that must be protonated for catalytic activity appears to be independent of the specific metal ion bound to the active site. The previous chapter proposed that the deprotonation of the α-amino group of the aspartate moiety of the substrate is consistent with decrease in the catalytic activity at pH higher than 9 (*66*).

The amino acid sequence alignments and the analysis of various X-ray crystal structures have demonstrated that in addition to the metal ligands, there are two other highly conserved residues within the active site that may be implicated with the catalytic efficiency of the enzyme. The γ-carboxylate of Glu-77 is in the right location to interact as a proton shuttle or to ion pair to the α-amino group of the substrate. Tyr-137 is positioned to function as a fifth ligand to the β-metal and/or participate in the

polarization of the peptidic carbonyl via Lewis acid catalysis. The pK_a for the loss of the catalytic activity at low pH for the Tyr-137 mutant is similar for that found in the wild-type IAD. This suggests that the alteration of the coordination sphere of the β-metal does not cause major changes on the pK_a of the bridging hydroxide molecule. Although, perturbation of the charges in the active site created by the E77Q mutation causes the pK_a at low pH, obtained from the log k_{cat}/K_m vs. pH, to shift to a pK_a lower than 5. The pK_a for the loss of the catalytic activity at high pH is around 9 for both IAD mutants. Consequently, it is unlikely for these residues to be responsible for the loss of catalytic activity at high pH. However, the significant drop in catalytic activity for the E77Q and Y137F mutants (Table 4.1) suggest a critical role for the γ-carboxylate side chain of Glu-77 and the phenolic hydroxyl group of Tyr-137.

The x-ray structure of the Y137F mutant reported in this chapter shows that the aromatic ring of the phenylalanine is precisely in the same orientation as the aromatic ring of the tyrosine found in the structure of the wild type enzyme (Figure 4.4). A comparison between the x-ray crystal structures of the E77Q mutant and the D285N mutant complexed to the bound substrate demonstrates that the loss in catalytic activity is not due to any apparent conformational differences between the wild type and mutant enzyme. Figure 4.3 demonstrates that the carbonyl of the side chain of Gln-77 is in position to help orient the α-amino group of the aspartate moiety of the substrate within the active site. This interaction is be important since the removal of the α-amino group from the substrates results in the total loss of catalytic activity (*66*). This observation rules out the possibility that a conformational difference between the

mutant enzymes and the wild type is the root cause for the attenuation of the catalytic activity.

The X-ray crystal structure of D285N mutant bound with the substrate demonstrates that the O^{η} of the phenolic side chain of Tyr-137 lies within 2.4 Å of the carbonyl oxygen of the reaction center and about 2.4 Å from the β-metal. This distance is consistent with a partial proton sharing between the tyrosine and the tetrahedral intermediate during hydrolysis of the peptide bond. This Lewis acid interaction would help in the stabilization of the tetrahedral intermediate in the active site. However, residues with similar function have not been detected within the active sites of other members of the amidohydrolase superfamily.

This chapter explored the role of two highly conserved residues within the active site of isoaspartyl dipeptidase. The side chain carboxylate of Glu-77 forms a critical ion-pair interaction with the free α-amino group of dipeptide substrates. Perturbations to this interaction, either by changes in the protein or the substrate, result in a significant decrease in activity. The phenolic hydroxyl of the side chain of Tyr-137 serves as a Lewis acid catalyst via stabilization of the tetrahedral adduct formed upon nucleophilic attack by the bridging hydroxide within the binuclear metal center. Other very important residues are the highly conserved Arg-169 and Arg-233, which ion pair with the terminal carboxylate of the substrate. These molecular interactions are summarized in Scheme 4.3.

Scheme 4.3

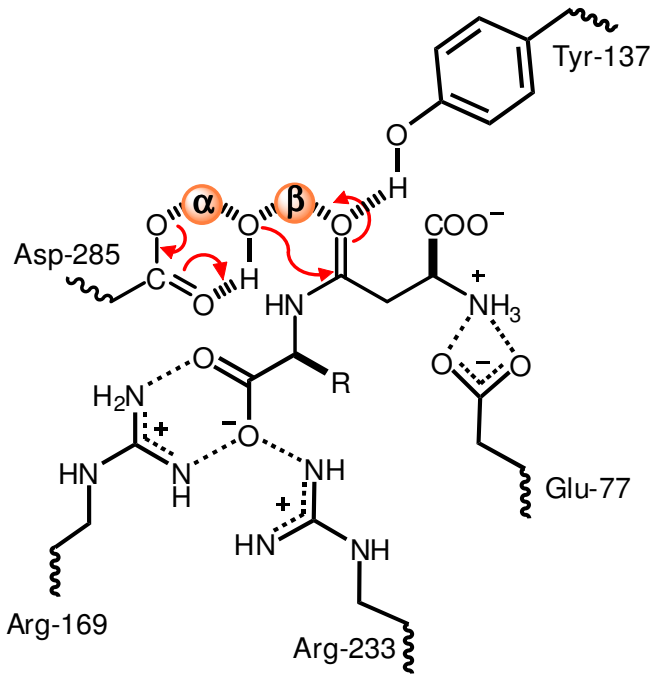

CHAPTER V

ANNOTATING ENZYMES OF UNKNOWN FUNCTION: *N*-FORMIMINO-L-GLUTAMATE DEIMINASE IS A MEMBER OF THE AMIDOHYDROLASE SUPERFAMILY*

As the understanding of the evolutionary development of the amidohydrolase superfamily is unraveled, the discovery of the substrate specificity for proteins of unknown function has become quite challenging. The pace by which the whole genomic DNA sequence of an organism can be determined is rapidly accelerating. This explosion in the total number of available gene sequences has dramatically unveiled the evolutionary relationships within broadly dispersed enzyme superfamilies (*16, 69*). Over 2000 sequences from about 200 organisms have been identified as members of the amidohydrolase superfamily. However, the functional annotation for many of these genes is uncertain, unknown or incorrect (*70-73*). Nevertheless, the knowledge obtained from the substrate and reaction diversity within the amidohydrolase superfamily can provide considerable information for the assignment of function for those enzymes with unknown substrates.

The amidohydrolase superfamily is a functionally diverse group of enzymes, and members of this superfamily are found in every organism sequenced to date (*1, 74*).

---

*Parts of the data reported in this chapter are reprinted with permission of "Annotating enzymes of unknown function: *N*-formimino-L-glutamate deiminase is a member of the amidohydrolase superfamily" by Martí-Arbona, R., Xu, C., Steele, S., Weeks, A., Kuty, G. F., Seibert, C. M., and Raushel, F. M., 2006. *Biochemistry 45, 1997-2005.* Copyright 2006 American Chemical Society.

The structural landmark for this superfamily is a mononuclear or binuclear metal center embedded within an $(\beta/\alpha)_8$-barrel structural fold (*4*). Enzymes within the amidohydrolase superfamily catalyze the hydrolysis of ester or amide bonds at carbon or phosphorous centers. Catalysis within the superfamily occurs by the activation of the scissile bond of the substrate for bond cleavage, and the enhancement of nucleophilic attack by the water molecule. Some of the best studied members of the amidohydrolase superfamily include urease (*39*), phosphotriesterase (*18*), adenosine deaminase (*7*), and dihydroorotase (*19*). The relationship between protein structure and activity can be a useful tool for deciphering substrate specificity for proteins of unknown fuction. Over 30 different enzymatic reactions have been established for members of this superfamily, and it has been suggested that as many as other 100 reactions remain to be determined (*1, 4*).

A significant fraction of the members of the amidohydrolase superfamily with unknown function have been annotated as *probable chlorohydrolases* or *probable cytosine deaminases*. This functional assignment is based upon the apparent sequence similarity of these unknown proteins to enzymes that catalyze the hydrolysis of the carbon-chlorine bond in atrazine or the carbon-nitrogen bond in cytosine as illustrated in the reactions presented in Scheme 5.1. The chromosomal DNA of *Pseudomonas aeruginosa* PA01 contains more than 5,500 protein coding gene sequences (*50*). One of these genes (Pa5106; gi:15600299) was annotated as a "probable cytosine deaminase" and "probable chlorohydrolase". The amino acid sequence alignment against the

sequenced microbial genomes available in the data bases maintained by the NCBI identified at least 38 other genes with an overall sequence identity greater than 40%. An examination of the genomic context of the organisms containing this group of amidohydrolases revealed that in nearly every instance these genes are found to be adjacent or in within a cluster of genes involved in the histidine degradation pathway. This suggests that this subgroup of amidohydrolase superfamily enzymes may be involved in the degradation of histidine.

Scheme 5.1

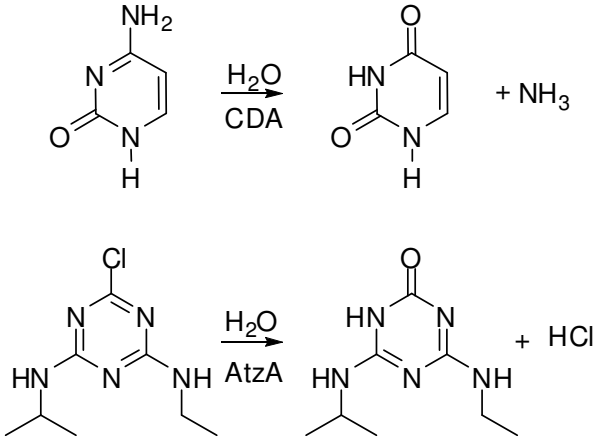

The pathway for the degradation of histidine has been extensively studied (*9*). The first three steps of the degradation of histidine are similar in most organisms. L-Histidine is deaminated to urocanate by histidine ammonia-lyase (HutH); then urocanate is converted to L-5-imidazolone-4-propionate by urocanase (HutU); and afterward, L-5-imidazolone-4-propionate is hydrolyzed to *N*-formimino-L-glutamate by imidazolonepropionate amidohydrolase (HutI). In all cases, *N*-formimino-L-glutamate is

further degraded to glutamate. The degradation of *N*-formimino-L-glutamate can occur by three different paths totally independent of each other (*52*). For two of the cases, the conversion of *N*-formimino-L-glutamate to glutamate is a single enzymatic reaction, and the third, is a two step conversion. In animal liver, *N*-formimino-L-glutamate can be converted to glutamate by the transfer of the formimino group to tetrahydrofolic acid by the action of L-glutamate *N*-formimidoyltransferase (*51*). For *Aerobacter aerogenes*, the *N*-formimino-L-glutamate is hydrolyzed to glutamate and formamide (*52*). In *Pseudomonas*, *N*-formimino-L-glutamate is deiminated to *N*-formyl-L-glutamate by *N*-formimino-L-glutamate iminohydrolase (HutF) (*53*) (Scheme 5.2). *N*-formyl-L-glutamate is then hydrolyzed to formate and L-glutamate by *N*-formyl-L-glutamate deformylase (HutG) (*54*).

Scheme 5.2

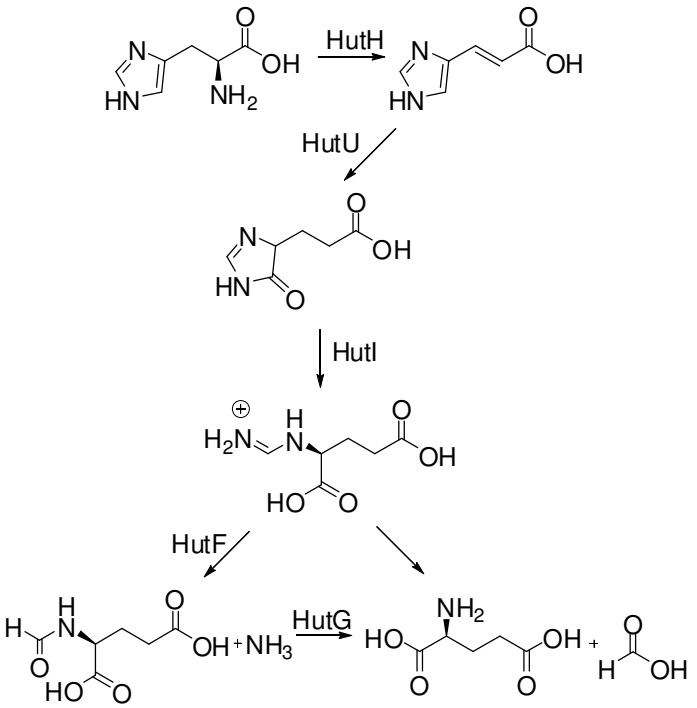

This chapter reports the cloning, expression and characterization of three proteins from *Pseudomonas aeruginosa* . These proteins are Pa5106, Pa5091 and Pa3175. The protein Pa5106 is shown to catalyze the hydrolysis of N-formimino-L-glutamate to ammonia and N-formyl-L-glutamate, while Pa5091 catalyzes the hydrolysis of N-formyl-L-glutamate to formate and L-glutamate. The protein Pa3175 catalyzes the hydrolysis of N-formimino-L-glutamate to formamide and L-glutamate, this protein is found about two million bases away from the Hut operon in the *Pseudomonas aeruginosa* genome.

MATERIALS AND METHODS

Materials. All chemicals and coupling enzymes were obtained from Sigma-Aldrich, unless otherwise stated. The genomic DNA from *Pseudomonas aeruginosa* was purchased from the American Type Culture Collection (ATCC). The oligonucleotide synthesis and DNA sequencing reactions were performed by the Gene Technology Laboratory of Texas A&M University. The pET30a(+) expression vector was acquired from Novagen. The T4 DNA ligase and the restriction enzymes, *Nde*I and *Hind*III, were purchased from New England Biolabs. The Platinum *Pfx* DNA polymerase and the Wizard® Plus SV Mini-Prep DNA purification kit were obtained from Invitrogen and Promega, respectively.

Cloning and Sequencing. The genes encoding Pa5106, Pa5091, and Pa3175 from *Pseudomonas aeruginosa* were amplified from the genomic DNA by standard PCR methods, stipulated in the manufacturer's instructions, using the oligonucleotide primers

listed in Table 5.1. These primers contain *Nde*I and *Hind*III restriction sites at either end. The PCR products were purified, digested with *Nde*I and *Hind*III, ligated with T4 DNA ligase to the expression vector pET30a(+) containing the respective restriction sites and then transformed into XL1Gold cells. Individual colonies were selected from LB/Agar plates containing 50 μg/mL kanamycin and were then used to inoculate 5 mL cultures of LB with 50 μg/mL kanamycin. The entire coding region of the plasmids containing the genes for Pa5106, Pa5091 and Pa3175 were sequenced with the T7 promoter and terminator primers in order to confirm the fidelity of the PCR amplification.

Table 5.1: Oligonucleotide Primers for the Cloning of the *Pseudomonas aeruginosa* Genes.

Gene	*Nde*I	*Hind*III
Pa5106	5'-GGGATTACCATATGTCC GCAATTTTCGCTGAACG-3'	5'-CCCAAGCTTTCATCAGT CGAGCAGTTCCCCCAGC-3'
Pa5091	5'-GGGAATTCCATATGGATG AAGTCCTGAGTTTCAAGCG-3'	5'-CCGGAATTCTCATCAGG CGTAGCGCTCGCGACC- 3'
Pa3175	5'-GGGAATTCCATATGTACC CCGCCCCCGACATGAGCC-3'	5'-CCGGAATTCTCATCAGTTG ACCAGGCTGTCGACCAGG-3'

Purification of Pa3175, Pa5091, and Pa5106. Cells harboring the expression plasmid for Pa5106 were grown overnight and a single colony was used to inoculate 50 mL of LB media containing 50 μM kanamycin which was subsequently used to inoculate 4 L of the same medium. Cell cultures were grown at 37 °C with a rotatory shaker until an A_{600} of ~0.5-0.7 was reached. Induction was initiated by the addition of 1.0 mM isopropyl-thiogalactoside (IPTG), and the culture was further incubated

overnight at 37 °C. The cells were isolated by centrifugation at 6,500 × *g* for 15 min at 4 °C. The pellet was re-suspended in 50 mM Hepes buffer at pH 7.5 (buffer A) containing 0.1 mg/mL of the protease inhibitor (PMSF) per gram of wet cells and then disrupted by sonication. The soluble protein was separated from the lysed cells by centrifugation at 12,000 × *g* for 15 min at 4 °C. Nucleic acids were precipitated by the addition of 1.5% (w/v) protamine sulfate. The remaining soluble proteins were fractionated between 40% and 60% saturation of ammonium sulfate. The precipitated protein from the 40-60% fractionation was re-suspended in a minimal quantity of buffer A and loaded onto a High Load 26/60 Superdex 200 prep grade gel filtration column (GE Health Care) and eluted with buffer A. Fractions that contained Pa5106 were identified by SDS-PAGE, pooled and loaded onto a 6 mL Resource Q anion ion exchange column (GE Health Care) and eluted with a gradient of NaCl in 20 mM Hepes at pH 7.5 (buffer B). The fractions containing Pa5106 were pooled, reprecipitated by saturation with 65% ammonium sulfate, centrifuged at 12,000 × *g* for 15 min at 4 °C, and re-suspended in a minimum amount of buffer A. The final step in the purification was accomplished by chromatography on a High Load 26/60 Superdex 200 prep grade gel filtration column. The purity of the protein during the isolation process was monitored by SDS-PAGE. The purification of Pa3175 and Pa5091 was performed as described above with minimal modifications. In the case of Pa5091, buffer A was supplemented with 5 mM dithiothreitol (DTT) and the ammonium sulfate fractionation was accomplished between 20% and 60% of saturation. For Pa3175, the cell pellet was re-suspended in buffer A supplemented with 50 μM $MnCl_2$ and 2.5 mM glutathione at pH 8.5.

Molecular Weight Determination. A HiLoad 16/60 Superdex 200 column (GE Health Care) was calibrated with six standard molecular weight markers (MW-GF-1000 from Sigma). Pa5106, Pa5091 and Pa3175 were applied to the column in sequential runs and eluted with buffer A at a flow rate of 1.0 mL per minute. The elution volume for each of the proteins was used to calculate the apparent molecular weight of the protein in solution.

Metal Analysis and Amino Acid Sequence Verification. The purified Pa5106 was subjected to N-terminal amino acid sequence analysis by the Protein Chemistry Laboratory at Texas A&M University. The first six amino acids were M-S-A-I-F-A which agrees with the reported DNA sequence for Pa5106. The N-terminal amino acid sequence analysis for the first five amino acids of purified Pa5091 gave the sequence as M-Y-P-A-P-D which corresponds to the reported DNA sequence. In the case of Pa3175, the amino acid sequence obtained for the first six amino acids was M-D-E-V-L-S that matches the reported DNA sequence.

The protein concentration was determined spectrophotometrically at 280 nm using a SPECTRAmax-340 microplate reader (Molecular Devices Inc.). The extinction coefficients used for these measurements were 66,810 $M^{-1}cm^{-1}$ for Pa5106, 40,800 $M^{-1}cm^{-1}$ for Pa5091 and 45,080 $M^{-1}cm^{-1}$ for Pa3175. These extinction coefficients were obtained based upon the derived protein sequence. The metal content of the purified proteins was determined with a Perkin-Elmer AAnalyst 700 atomic absorption spectrometer and by Inductively Coupled Plasma Emission-Mass Spectrometry (ICP-MS). The protein Pa5106 contained 1.2 equivalents of Zn^{2+} per subunit, Pa5091

contained 1.1 equivalents of Zn^{2+}. The metal content of Pa3175 was found to be 0.2 equivalents of Mn^{2+} and 0.4 equivalents of Zn^{2+}. The metal was removed from Pa5106 by treating the protein with 3 mM dipicolinate at 4 °C at pH 5.6 for 48 hours. The dipicolinate chelator was removed by loading the chelator/protein mixture onto a PD10 column (GE Health Care) and eluting with metal-free buffer A. Metal-free buffer A was prepared by passage through a column of Chelex 100 resin. The apo-Pa5106 was reconstituted with the addition of 1 equivalent of the desired metal (Zn^{2+}, Co^{2+}, Ni^{2+}, Cd^{2+} and Mn^{2+}) in 50 mM HEPES at pH 7.5. The metal content of the reconstituted proteins was verified using by atomic absorption spectrometer and ICP-MS.

*Synthesis of N-Formimino-L-glutamate (**I**).* The synthesis of *N*-formimino-L-glutamate was performed by Dr. Chengfu Xu. L-glutamic acid (1.47 g, 10 mmol), formamidine hydrochloride (1.61 g, 20 mmol), silver carbonate (3.03 g, 11 mmol) and formamide (8 mL) were added to a 100 mL flask and stirred at room temperature for 36 h (*75*). After the reaction was complete, the excess ammonia and carbon dioxide were removed under reduced pressure for a period of 30 min. At this time, 150 mL of 0.06 N HCl were added and the pH was adjusted to between 4 and 6. The mixture was filtered and the carbon dioxide was removed under vacuum. The solution was applied to a column of Dowex-1-acetate, washed with water (150 mL) and then eluted with 0.5 M acetic acid. The *N*-formimino-L-glutamate compound was isolated with an overall yield of 40% (0.70 g). ^{1}H NMR (300 MHz, D_2O): 7.60 ppm (1H, s, C<u>H</u>=NH), 4.02 ppm (1H, t, J = 5.7 Hz, C<u>H</u>NH), 3.92 ppm, (1H, t, J = 5.7 Hz, C<u>H</u>NH), 2.26 ppm (2H, t, J = 7.2 Hz, C<u>H$_2$</u>CO), 2.12-1.89 ppm (2H, m, CHC<u>H$_2$</u>). ^{13}C NMR (75.4 MHz, D_2O): 177.43, 177.36,

175.66, 174.33, 157.14, 153.90, 60.58, 55.38, 30.30, 30.08, 27.65, and 26.14 ppm. Mass spectrometry (ESI negative mode); observed: 173.03 $(M–H)^-$, expected: 173.06 $(M–H)^-$. The rest of the *N*-formimino amino acid derivatives were synthesized using a similar protocol.

*Synthesis of N-Formyl-L-glutamate (**II**).* The synthesis of *N*-formyl-L-glutamate was performed by Dr. Chengfu Xu. Acetic anhydride (8 mL) was added dropwise to a 100 mL flask containing L-glutamic acid (4.41 g, 30 mmol) and formic acid (50 mL) (*76*). After stirring for 30 min, the reaction was quenched by the addition of 2 mL of water and the solvent removed by rotary evaporation. The compound was purified by chromatography on a silica gel column using a 6/1 mixture of chloroform and methanol (v/v) as the eluant. The solvent was removed, and then the solid material washed with ethyl acetate and ether and then dried to obtain 2.11 g of material with an overall yield of 40%. ^{1}H NMR (300MHz, DMSO): 12.42 ppm (1H, s, COO<u>H</u>), 8.37 ppm (1H, d, J = 7.2Hz, N<u>H</u>), 8.03 ppm (1H, s, C<u>H</u>O), 4.32-4.24 ppm (1H, m, C<u>H</u>NH), 2.28-2.23 ppm (2H, m, $CHCH_2C\underline{H}_2$), 2.02-1.91 ppm (1H, m, $CHC\underline{H}_2CH_2$), 1.83-1.68 ppm (1H, m, $CHC\underline{H}_2CH_2$). Mass spectrometry (ESI negative mode): observed: 174.2 $(M–H)^-$, expected: 174.05 $(M–H)^-$. The rest of the *N*-formyl amino acid derivatives were synthesized using a similar protocol.

Assay for Deimination of N-Formimino Amino Acids. The measurement of the enzymatic activity for the deimination of *N*-formimino amino acids was conducted by coupling the production of ammonia to the oxidation of NADH with glutamate dehydrogenase. The decrease in the concentration of NADH was followed

spectrophotometrically at 340 nm using a SPECTRAmax-340 microplate reader. The standard assay was modified from that reported by Muszbek *et al.* (*77*) and contained 100 mM Hepes at pH 8.0, 100 mM KCl, 7.4 mM α-ketoglutarate, 0.4 mM NADH, 6 units of glutamate dehydrogenase, and the appropriate *N*-formimino amino acid in a final volume of 250 μL at 30 °C. The following compounds were tested for enzymatic activity at a concentration of 10 mM using this protocol: *N*-formimino-L-glutamate (**I**), *N*-formimino-D-glutamate (**VIII**), *N*-guanidino-L-glutamate (**V**), *N*-formimino-α-aminobutyric acid (**VI**), *N*-formimino-γ-aminobutyric acid (**VII**), *N*-formimino-L-alanine, *N*-formimino-L-aspartate (**IX**), *N*-formimino-glycine, *N*-formimino-L-isoleucine, *N*-formimino-L-leucine, *N*-formimino-L-methionine, *N*-formimino-L-phenylalanine, *N*-formimino-L-tyrosine, and *N*-formimino-L-valine.

Assay for Hydrolysis of N-Formyl Amino Acids. The enzymatic deformylation of N-formyl amino acids was monitored by following the production of formate with formate dehydrogenase. The increase in the concentration of NADH was measured spectrophotometrically at 340 nm using a SPECTRAmax-340 microplate spectrophotometer. The protocol was modified from the reported assay of Nanba *et al.* (*78*) and contained 100 mM Hepes at a pH of 7.5, 100 mM KCl, 5 mM DTT, 5 mM NAD^+, and the appropriate amount of an *N*-formyl amino acid in a final volume of 250 μL at 30 ^oC. The following *N*-formyl amino acids were tested as substrates for this activity at a concentration of 10 mM: *N*-formyl-L-glutamate (**II**), *N*-formyl-D-glutamate, *N*-formyl-L-alanine, *N*-formyl-L-aspartate, *N*-formyl-glycine, *N*-formyl-L-

isoleucine, *N*-formyl-L-leucine, *N*-formyl-L-methionine, *N*-formyl-L-phenylalanine, *N*-formyl-L-tyrosine, and *N*-formyl-L-valine.

Assay for Hydrolysis of N-Acyl Amino Acids. The enzymatic hydrolysis of *N*-acyl-L-glutamate was followed by coupling the production of L-glutamate to the reduction of NAD^+ by glutamate dehydrogenase and the subsequent transformation of iodonitrotetrazolium (INT) to INT-formazan by diaphorase. The formation of INT-formazan was monitored at 500 nm. The standard assay was modified from the protocol reported by Beutler (*79*) and contained 100 mM Hepes at pH of 8.5, 1.5 mM NAD^+, 1.5 mM *p*-iodonitrotetrazolium violet, 2.0 units of diaphorase, 6 units of glutamate dehydrogenase and the appropriate amount of the *N*-acyl-L-glutamate in a final volume of 250 μL at 30 ^oC. Several *N*-acyl amino acids were tested for activity with this assay: *N*-formimino-L-glutamate (**I**), *N*-guanidino-L-glutamate (**V**), *N*-carbamoyl-L-glutamate (**IV**), *N*-acetyl-L-glutamate (**III**), and *N*-formyl-L-glutamate (**II**). The assay described above was modified to monitor the formation of L-alanine by substitution of 7 units of alanine dehydrogenase for glutamate dehydrogenase. The following compounds were assayed for the formation of L-alanine at a concentration of 10 mM: *N*-formimino-L-alanine, *N*-carbamoyl-L-alanine, *N*-acetyl-L-alanine, and *N*-formyl-L-alanine.

The deacylation of *N*-acyl-L-aspartate derivatives was monitored by following the production of aspartate spectrophotometrically at 340 nm using the combined enzymatic activities of malate dehydrogenase and aspartate aminotransferase. The standard assay contained 100 mM Hepes (pH 8.1), 100 mM KCl, 3.7 mM α-

ketoglutarate, 0.4 mM NADH, 0.64 units of malate dehydrogenase, 6 units of aspartate aminotransferase, and the *N*-acyl-L-aspartate derivative in a final volume of 250 μL at 30 °C. The following compounds were tested for enzymatic activity at a concentration of 10 mM: *N*-formimino-L-aspartate (**IX**), *N*-carbamoyl-L-aspartate, *N*-acetyl-L-aspartate, and *N*-formyl-L-aspartate.

Inhibition of Pa5106 by N-Acyl-L-Glutamate Analogs. The inhibition of the enzymatic deimination of *N*-formimino-L-glutamate (**I**) by Pa5106 was studied. *N*-acetyl-L-glutamate (**III**), *N*-carbamyl-L-glutamate (**IV**), *N*-formimino-L-aspartate (**IX**), *N*-formimino-α-aminobutyric acid (**VI**), *N*-formimino-γ-aminobutyric acid (**VII**), *N*-formyl-L-glutamate (**II**), *N*-guanidino-L-glutamate (**V**), and *N*-succinyl-L-glutamate were tested as inhibitors using the assay that monitors formation of ammonia with *N*-formimino-L-glutamate (**I**) as the substrate.

Scheme 5.3

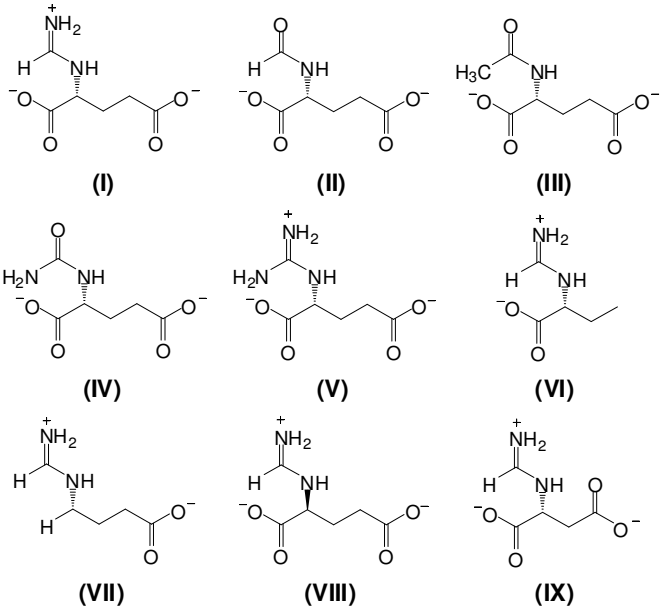

Data Analysis. The kinetic parameters, k_{cat} and k_{cat}/K_m, were determined by fitting the initial velocity data to the equation 5.1, where v is the initial velocity, E_T is the enzyme concentration, k_{cat} is the turnover number, S is the substrate concentration, and K_m is the Michaelis constant (*62*). Competitive inhibition patterns were fitted to equation 5.2 where I is the inhibitor concentration and K_i is the inhibition constant (*62*).

$$v / E_T = \frac{k_{cat} S}{K_m + S} \tag{5.1}$$

$$v = \frac{V_{max} S}{K_m \left(\frac{1 + I}{K_i} \right) + S} \tag{5.2}$$

RESULTS

Purification and Properties of Pa5106. The protein Pa5106 was overexpressed in BL21(DE3)star cells by the use of the modified pET30a(+) plasmid. The pure protein contained 1.2 equivalents of Zn^{2+} per subunit. A single band corresponding to an apparent molecular weight of 49 kDa was obtained for the isolated protein using SDS-PAGE analysis. This agrees with the molecular weight calculated from the reported DNA sequence. The molecular weight of the native protein in solution was calculated from the elution volume of the enzyme from a calibrated gel filtration column. It was found to have an apparent molecular weight of 100 kDa. Since the monomeric molecular weight is 49 kDa, Pa5106 is a dimer in solution.

The localization of the gene that encodes the protein sequence for Pa5106 in the genome of *Pseudomonas aeruginosa* suggests that this enzyme may be involved in the metabolism of histidine, via the hydrolysis of *N*-formimino-L-glutamate. NMR spectroscopy was used to monitor the reaction catalyzed by Pa5106. The incubation of *N*-formimino-L-glutamate (**I**) with Pa5106 at pH 8.0 causes the proton resonances for the hydrogen attached to the carbon of the formimino group to shift from 7.68 and 7.66 ppm to 7.95 and 7.81 ppm. These new resonances are coincident with the proton attached to the formyl group of *N*-formyl-L-glutamate and suggest that Pa5106 catalyzes the deamination of *N*-formimino-L-glutamate to *N*-formyl-L-glutamate and ammonia. The measurement of the NMR spectra for the products was performed by Ms. LaKenya Williams. The measurement of the kinetic parameters for PA5106 was accomplished by monitoring the formation of ammonia with glutamate dehydrogenase. The turnover number of the purified protein for the deimination of *N*-formimino-L-glutamate (**I**) at pH 8.0 is $13.2 \pm 0.4\ s^{-1}$ with a Michaelis constant of 0.22 ± 0.03 mM.

The metal requirement of Pa5106 was determined by preparation of the apo-enzyme via the removal of the metal with chelators, revealing that the protein contained a single zinc ion. The apo-Pa5106 exhibited less than 1% of the specific activity of the holo-enzyme. The metal center in the apo-enzyme was reconstituted with 1 equivalent of the other divalent cations in approximately 10 minutes, resulting in catalytically active enzyme in the presence of Cd^{2+}, Ni^{2+}, Zn^{2+}, or Cu^{2+}. No reconstitution was obtained with Co^{2+} or Mn^{2+} under the conditions used for this investigation. The Table 5.2 presents the kinetic parameters for the metal reconstituted forms of Pa5106.

Table 5.2: Kinetic Parameters for Metal-Reconstituted Form of Pa5106[a]

HutF	K_m (mM)	k_{cat} (s^{-1})	k_{cat}/K_m ($M^{-1}s^{-1}$)
WT (Zn)	0.22 ± 0.03	13.2 ± 0.4	(6.0 ± 0.8) x 10^4
WT (Ni)	2.7 ± 0.1	21.3 ± 0.3	(8.0 ± 0.3) x 10^3
WT (Cd)	2.1 ± 0.3	31.0 ± 0.1	(1.5 ± 0.2) x 10^4
WT (Cu)	1.2 ± 0.1	8.5 ± 0.1	(7.3 ± 0.6) x 10^3

[a]The kinetic parameters were determined with *N*-formimino-L-glutamate as the substrate at pH 8.0, 30 °C from a fit of the data to eq 5.1.

Substrate Specificity of Pa5106. A variety of *N*-acyl-D/L amino acids were tested as potential substrates for Pa5106. These compounds included, *N*-formimino-D/L-amino acids like: *N*-formimino-L-alanine, *N*-formimino-L-aspartate (**IX**), *N*-formimino-glycine, *N*-formimino-L-glutamate (**I**), *N*-formimino-D-glutamate (**II**), *N*-formimino-L-isoleucine, *N*-formimino-L-leucine, *N*-formimino-L-methionine, *N*-formimino-L-phenylalanine, *N*-formimino-L-tyrosine, and *N*-formimino-L-valine. *N*-formimino-L-amino acids derivatives were also tested, such as: *N*-formimino-α-aminobutyric acid (**VI**), and *N*-formimino-*γ*-aminobutyric acid (**VII**). *N*-acyl substituted forms of glutamate were additionally tested: *N*-guanidino-L-glutamate, *N*-acetyl-L-glutamate (**III**), *N*-carbamoyl-L-glutamate (**IV**), and *N*-formyl-L-glutamate (**II**). Some of the structures of these compounds are illustrated in Scheme 5.3. The best substrate found for Pa5106 was *N*-formimino-L-glutamate (**I**) with K_m of 220 μM and a k_{cat} of 13 s^{-1}. At a concentration of 10 mM, *N*-formimino-D-glutamate (**VIII**) showed a much lower activity with 5.0 x 10^{-2} s^{-1}. The compounds, *N*-formimino-L-isoleucine and *N*-formimino-L-methionine were

deiminated at a rate less than or equal to 1.9 x 10^{-2} s^{-1} and 1.0 x 10^{-2} s^{-1}, respectively, at a concentration of 10 mM. The remaining *N*-formimino-L amino acids and other *N*-acyl substituted forms of glutamate tested as substrates for this enzyme were found to have specific activities lower than 1.0 x 10^{-3} s^{-1}. The high specificity of Pa5106 toward the hydrolysis of *N*-formimino-L-glutamate demonstrates it is an *N*-formimino-L-glutamate deiminase, as suggested by its location in the genome of *Pseudomonas aeruginosa*.

Inhibition of Pa5106 by N-Acyl-L-Glutamate analogs. Several *N*-acyl-L-glutamate analogs were tested as inhibitors for the deimination of *N*-formimino-L-glutamate (**I**) by Pa5106. These compounds included *N*-acetyl-L-glutamate (**III**), *N*-carbamoyl-L-glutamate (**IV**), *N*-formimino-L-aspartate (**IX**), *N*-formimino-α-aminobutyric acid (**VI**), *N*-formimino-γ-aminobutyric acid (**VII**), *N*-formyl-L-glutamate (**II**), *N*-guanidino-L-glutamate (**V**), and *N*-succinyl-L-glutamate. At concentrations up to 10 mM, no inhibition was detected using *N*-acetyl-L-glutamate (**III**), *N*-carbamoyl-L-glutamate (**IV**), and N-formyl-L-glutamate (**II**) as inhibitors. The substrate analogues *N*-formimino-α-aminobutyric acid (**VI**) and *N*-formimino-γ-aminobutyric acid (**VI**) which lack the carboxylate group at the α or γ positions, did not exhibit any inhibition at concentrations up to 10 mM. *N*-guanidino-L-glutamate (**V**) and *N*-formimino-L-aspartate (**IX**) showed to be competitive inhibitors with K_i values of 890 μM and 30 μM, respectively.

Purification and Properties of Pa5091. The protein Pa5091 was overexpressed in BL21(DE3)star cells. The protein was isolated by standard methods described above containing 1.1 equivalents of Zn^{2+} per subunit and the molecular weight was judged by

SDS-PAGE to be ~30 kDa. The predicted size of the protein based upon the DNA sequence was 29,824 Da. The molecular weight of the protein in solution was estimated from the elution volume of a calibrated gel filtration column to be 28 kDa, and thus Pa5091 is a monomer. Pa5091 was expected to hydrolyze N-formyl-L-glutamate to formate and L-glutamate, based upon its location in the genome of *Pseudomonas aeruginosa*. The reaction catalyzed by Pa5091 was determined by NMR spectroscopy. Incubation of Pa5091 with *N*-formimino-L-glutamate (**1**) at pH 8.0 results a shift in the proton resonance for the hydrogen attached to the carbon of the formyl group. This shift is from 7.95 ppm for the hydrogen attached to the formyl group to 8.32 ppm for hydrogen attached to the carbonyl carbon in formate. The measurement of the NMR spectra for the products was performed by Ms. LaKenya Williams. The formation of formate was confirmed and quantified by monitoring the reaction spectrophotometrically with formate dehydrogenase.

Substrate Specificity of Pa5091. Pa5091 was tested for turnover with several *N*-substituted amino acids at pH 7.5. These compounds were *N*-formyl-L-alanine, *N*-formyl-L-aspartate, *N*-formyl-D-glutamate, *N*-formyl-L-glutamate, *N*-formyl-L-glutamine (**II**), *N*-formyl-glycine, *N*-formyl-L-isoleucine, *N*-formyl-L-leucine, *N*-formyl-L-methionine, *N*-formyl-L-phenylalanine, *N*-formyl-L-tyrosine, *N*-formyl-L-valine, *N*-acetyl-L-glutamate (**III**), *N*-carbamoyl-L-glutamate (**IV**), and *N*-formimino-L-glutamate (**I**). From these compounds, only *N*-formyl-L-glutamate (**II**) and *N*-formyl-L-glutamine were hydrolyzed by Pa5091. The best substrate found for Pa5091 was *N*-formyl-L-glutamate with a k_{cat}/K_m is 306 M^{-1} s^{-1}. In the case of *N*-formyl-L-glutamine, saturation

could not be achieved within the solubility limits of the compound, thus the value for k_{cat}/K_m was calculated to be 14.9 $M^{-1}s^{-1}$. At a concentration of 10 mM, the turnover number obtained for the hydrolysis of *N*-formyl-L-lysine, *N*-formyl-L-histidine, and *N*-formyl-L-arginine was 2.6 x 10^{-2} s^{-1}. All other compounds were tested at 10 mM concentration, and showed specific activities less than 1.0 x 10^{-3} s^{-1}. The specificity of Pa5091 toward the hydrolysis of *N*-formyl-L-glutamate demonstrates that is a *N*-formyl-L-glutamate deformylase as suggested by the gene location in the genome of *Pseudomonas aeruginosa*.

Purification and Properties of Pa3175. The protein Pa3175 was overexpressed and purified in *Escherichia coli*. The purified protein had 0.2 equivalents of Mn^{2+} and 0.4 equivalents of Zn^{2+} per subunit. The SDS-PAGE analysis of the purified protein showed a single band with an apparent molecular weight of 34 kDa. The theoretical molecular weight calculated from the reported DNA sequence was 34,230 Da. The oligomeric molecular weight obtained after the elution from a calibrated gel filtration column suggested that Pa3175 migrated with a molecular weight of 69 kDa. Therefore, Pa3175 is a dimer in solution. The activity of Pa3175 towards the hydrolysis of *N*-formimino-L-glutamate (**I**) to formamide and L-glutamate was confirmed by the appearance of a new proton resonance at 7.93 ppm and the disappearance of the resonance peaks at 7.68 and 7.66 ppm. This is consistent with the disappearance of the resonance peaks for the hydrogen attached to the carbon of the formimino group and the appearance of the resonance peak for the aldehyde proton of formamide. The measurement of the NMR spectra for the products was performed by Ms. LaKenya

Williams. The hydrolysis of *N*-formimino-L-glutamate (**I**) to formamide and L-glutamate was confirmed spectrophotometrically using glutamate dehydrogenase.

Substrate Specificity of Pa3175. A variety of *N*-acyl-L amino acids were tested as potential substrates for Pa3175. The compounds, *N*-formimino-L-glutamate (**I**), *N*-acetyl-L-glutamate (**III**), *N*-carbamoyl-L-glutamate (**IV**), *N*-formyl-L-glutamate (**II**), *N*-formimino-L-aspartate (**IX**), *N*-acetyl-L-aspartate, *N*-formyl-L-aspartate, *N*-formimino-L-alanine, *N*-acetyl-L-alanine, and *N*-formyl-L-alanine were screened for turnover. The sole compound hydrolyzed by Pa3175 was *N*-formimino-L-glutamate (**I**) with a k_{cat} of 73 ± 4 s^{-1} and a K_m of 4.3 ± 0.6 mM. Therefore, the value of k_{cat}/K_m was (1.72 x 0.03) x 10^4 $M^{-1}s^{-1}$. All of the other compounds tested, presented no turnover with specific activities lower than 1.0 x 10^{-3} s^{-1}. These results corroborate that Pa3175 catalyzes the hydrolysis of *N*-formimino-L-glutamate to L-glutamate and formamide with a high level of specificity.

DISCUSSION

The amidohydrolase superfamily is a functionally diverse group of enzymes, of which members are found in every organism sequenced to date (*1, 74*). Over 2000 gene sequences have been identified as members of this superfamily among the partially and completely sequenced bacterial genomes. Enzymes within this protein superfamily catalyze the hydrolysis of C-N or P-O bonds in a vast variety of substrates including amino acids, carbohydrates, pesticides, and nucleic acids. There are 18 members of the superfamily found within the genome of *Escherichia coli* K12. From these, eleven

enzymes perform known chemical transformations, but for the other seven, no substrates or chemical reactions have been identified. These circumstances found for *Escherichia coli* are not unique for this organism. Due to the substrate and reaction diversity of the amidohydrolase superfamily, a significant fraction of the recently identified members remain with unknown function. A considerable portion of those genes with unknown or ambiguous function have been annotated as probable chlorohydrolases or cytosine deaminase-like proteins. A subgroup of 39 proteins annotated as probable chlorohydrolases or cytosine deaminase-like share an overall sequence identity of 40% to one another as presented in the dendrogram that appears in Figure 5.1. Within this subgroup is the protein Pa5106 from *Pseudomonas aeruginosa*. An examination of the genomic DNA of the organisms containing these proteins showed that in each and every case, they are localized within genes that are involved in the histidine degradation pathway. This suggests that the enzymes within this subgroup, including Pa5106, may be from the part of the operon that is responsible for the catabolism of histidine.

The chemistry involved in the degradation of histidine to glutamate is presented in Scheme 5.2. The genes involved in these chemical transformations are clearly identified within the genome of *Pseudomonas aeruginosa* as HutH (histidine ammonia lyase; Pa5098), HutU (urocanase; Pa5100), HutI (imidazolone propionate amidohydrolase; Pa5092), and HutG (*N*-formyl-L-glutamate deformylase; Pa5091). If the degradation of histidine in *Pseudomonas aeruginosa* follows the same path previously reported for *Pseudomonas fluorescens* (*76*) and *Pseudomonas putida* (*80*),

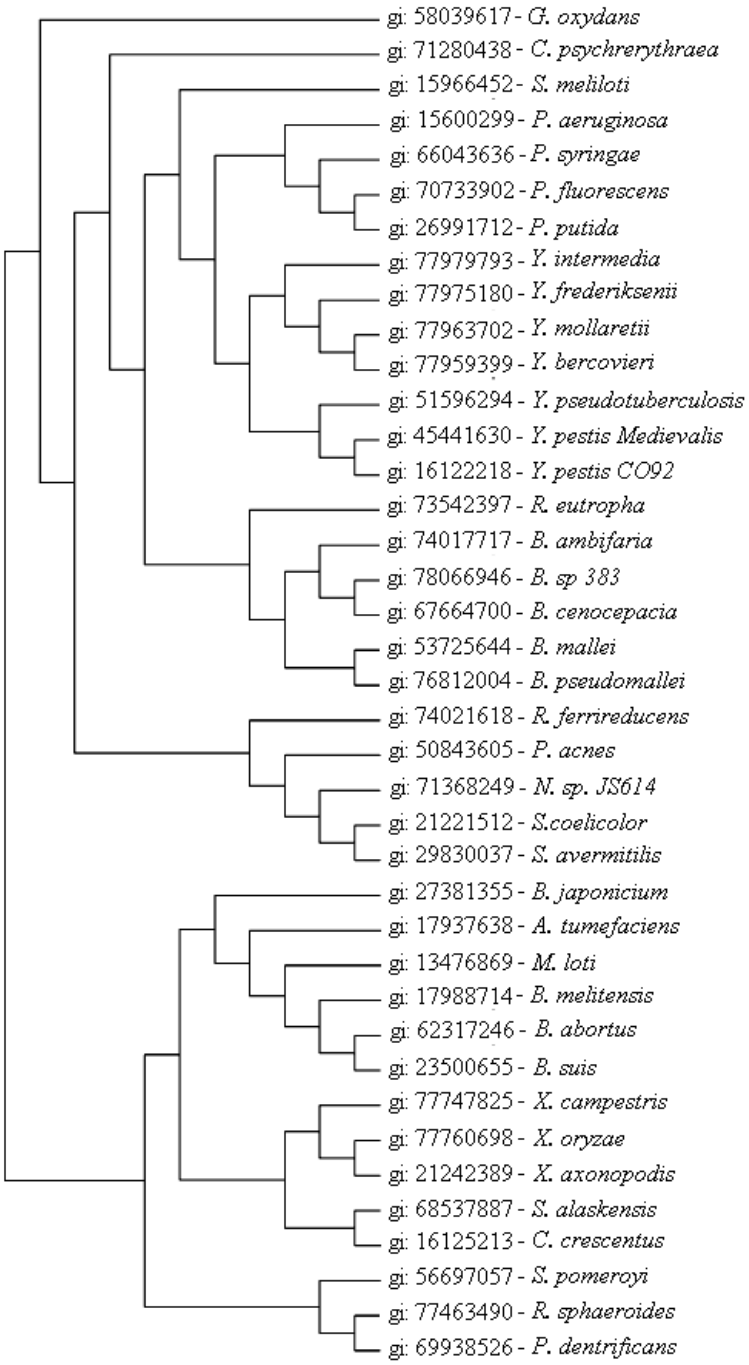

Figure 5.1: Dendrogram of the Pa5106 homologues obtained from the microbial genomes. The amino acid sequence identity of this group of enzymes is over 30%.

then an enzyme responsible for the deimination of *N*-formimino-L-glutamate should be present. This investigation demonstrates that Pa5106 completes the histidine degradation pathway in *Pseudomonas aeruginosa* and that it is likely that the other 38 homologous sequences in Figure 5.1 are *N*-formimino-L-glutamate deiminases. The gene encoding for the enzyme that performs this reaction has sometimes been referenced as HutF (*54, 80*).

From all of the 14 *N*-formimino amino acids that were tested as substrates, only formimino-L-glutamate was hydrolyzed by Pa5106 at a significant rate. Very low activity was detected for the D-enantiomer and no turnover was observed for the analogs lacking the two carboxylate groups from the glutamate moiety. The *N*-acyl derivatives of glutamic acid were not hydrolyzed by Pa5106. These derivatives included guanidino, formyl, acetyl, and carbamoyl functional groups. All of these compounds were tested for inhibition of the deimination of *N*-formimino-L-glutamate and the only two compounds with significant competitive inhibitors were *N*-guanidino-L-glutamate (**V**) and *N*-formimino-L-aspartate (**IX**).

The amino acid sequence alignment against other members of the amidohydrolase superfamily showed that Pa5106 closely resemble atrazine chlorohydrolase (AtzA) from *Pseudomonas* sp. and another unknown function protein found in *Thermotoga maritima*. This later protein is known as Tm0936. The amino acid sequence alignment of Pa5106 with AtzA and Tm0936 is shown in Figure 5.2. The overall sequence identity of Pa5106 to Tm0936 and AtzA is 21% and 20%, respectively. The x-ray crystal structure of Tm0936 (PDB entry codes P1M1 and 1j6p) has been solved

to high resolution. The amino acid sequence alignment of PA5106 with Tm0936 allows the assignment of the active site with a high reliability. The x-ray crystal structure of Tm0936 shows an $(\beta/\alpha)_8$-barrel fold with a single divalent cation bound to the active site. The metal is ligated by two histidines at the end of strand one, a histidine from strand five and an aspartate from strand 8. In Pa5106, the analog residues are His-56 and His-58 from the first strand, His-232 from the fifth, and Asp-320 from the eighth strand. Other members of the amidohydrolase superfamily with similar active site construction also conserve another histidine residue at the end of stand six (His-269) and a glutamate residue (Glu-235) found three residues beyond the conserved histidine from strand 5 (HxxE motif) (*6, 7, 34*). In adenosine deaminase (ADA) the histidine from strand six (analog to His-269 in Pa5106) is believed to participate in the activation of the hydrolytic water (*7*). The glutamate from the HxxE motif (Glu-235 in Pa5106) has been postulated in cytosine and adenosine deaminase to serve as a general acid/base catalyst for proton transfer to the ring nitrogen during deamination (*6, 7, 34*).

```
AtzA    MQTLSIQHGTLVTMDQYRRVLGDSWVHVQDGRIVALGVHAESVPPPADRV   5
Tm0936  -----MIIGNCLILKDFSSEPFWGAVEIENGTIKRVLQGEVKVD------   3
Pa5106  --MSAIFAERALLPEGWARN--VRFEISADGVLAEIRPDANADG------   4

AtzA    IDARGKVVLPGFINAHTHVNQILLRGGPSHGRQFYDWLFN---VVYPGQK   9
Tm0936  LDLSGKLVMPALFNTHTHAPMTLLRG-VAEDLSFEEWLFS---KVLPIED   8
Pa5106  AERLGGAVLPGMPNLHSHAFQRAMAGLAEVAGNPNDSFWTWRELMYRMVA   9

AtzA    AMRPEDVAVAVRLYCAEAVRSGITTINENADSAIYPGNIEAAMAVYGEVG  14
Tm0936  RLTEKMAYYGTILAQMEMARHGIAGFVD-----MYFHEEWIAKAVR-DFG  12
Pa5106  RLSPEQIEVIACQLYIEMLKAGYTAVAEFHYVHHDLDGRSY-ADPAELSL  13

AtzA    VRVVYARMFFDRMDGRIQGYVDALKARSPQVELCSIMEETAVAKDRITAL  19
Tm0936  MRALLTRGLVDSNG----------------------DDGGRLEENLKL  15
Pa5106  RISRAASAAGIGLTLLPVLYSHAGFGGQPASEGQRRFINGSEAYLELLQR  18

AtzA    SDQYHGTAGGRISVWPAPATTTAVTVEGMRWAQAFARDRAVMWTIHMAES  24
Tm0936  YNEWNGFE-GRIFVGFGPHSPYLCSEEYLKRVFDTAKSLNAPVTIHLYET  20
Pa5106  LRAPLE-AAG-HSLGLCFHSLRAVTPQQIATVLA-AGHDDLPVHIHIAEQ  23

AtzA    DHDER----IHGMSPAEYMECYGLLDERLQVAHCVYFDRKDVRLLHRHNV  29
Tm0936  SKEE---------YDLEDILNIGLKEVKTIAAHCVHLPERYFGVLKDIPF  24
Pa5106  QKEVDDCQAWSGRRPLQWLYENVAVDQRWCLVHATHADPAEVAAMARSGA  28

AtzA    KVASQVVSNAYLGSGVAPVPEMVERGMAVGIGTDNGNSNDSVNMIGDMKF  34
Tm0936  FVSHNPASNLKLGNGIAPVQRMIEHGMKVTLGTDGAASNNSLNLFFEMRL  29
Pa5106  VAGLCLSTEANLGDGIFPATDFLAQGGRLGIGSDSHVSLSVVEELRWLEY  33

AtzA    MAHIHR----AVHRDADVLTPEKILEMATIDGARSLGMDHEIGSIETGKR  38
Tm0936  ASLLQK----AQN--PRNLDVNTCLKMVTYDGAQAMGFK--SGKIEEGWN  33
Pa5106  GQRLRDRKRNRLYRDDQPMIGRTLYDAALAGGAQALGQP--IGSLAVGRR  38

AtzA    ADLILLDLRHPQTTPHH--HLAATIVFQAYGNEVDTVLIDGNVVMENRRL  43
Tm0936  ADLVVIDLDLPEMFPVQ--NIKNHLVHAFSG-EVFATMVAGKWIYFDGEY  38
Pa5106  ADLLVLDGNDPYLASAEGDALLNRWLFAGGDRQVRDVMVAGRWVVRDGRH  43

AtzA    SFLPPERELAFLEEAQSRATAILQRANMVANPAWRSL  474
Tm0936  PTIDSEE----VKRELARIEKELYSS-----------  406
Pa5106  AGEERS------ARAFVQVLGELLD------------  453
```

Figure 5.2: Amino acid sequence alignment of Pa5106, atrazine chlorohydrolase from *Pseudomonas* sp. and Tm0936 from *Thermotoga maritima* using CLUSTALW. The eight strands forming the barrel are highlighted in yellow and were assigned taking into in consideration the X-ray crystal structures of Tm0936 (PDB entry codes 1p1m and 1j6p). The conserved residues composing the active site of these proteins are highlighted in bold red letters. The HxxE motif at the end of strand 5 is indicated by a blue box. Pa5106 presents an overall sequence identity of 21% to Tm0936 and 20% to atrazine chlorohydrolase.

There appears to be multiple pathways for the degradation of *N*-formimino-L-glutamate (**I**) in *Pseudomonas aeruginosa.* This chapter discusses three proteins that form two different pathways for the conversion of *N*-formimino-L-glutamate to glutamate. The proteins Pa5106 and Pa 5091 are found within the Hut operon and enable the two-step degradation of *N*-formimino-L-glutamate to ammonia, formate and L-glutamate. The protein Pa5091 shows a high specificity toward the hydrolysis of *N*-formyl-L-glutamate (**II**). Of the fifteen compounds tested for activity, only *N*-formyl-L-glutamate and *N*-formyl-L-glutamine were hydrolyzed. The alternative pathway for the degradation *N*-formimino-L-glutamate to glutamate is composed of a single enzyme, identified in this investigation to be Pa3175. Purified Pa3175 was found to catalyze the direct hydrolysis of the formimino group of *N*-formimino-L-glutamate producing formamide and L-glutamate. An assortment of *N*-acyl L-amino acid derivatives were tested for catalytic activity turnover with Pa3175, showing that *N*-formimino-L-glutamate was the sole compound found to be a substrate. The reason for the existence of two different pathways for the degradation of *N*-formimino-L-glutamate (**I**) in *Pseudomonas aeruginosa* is unclear. The proximity of the genes encoding for Pa5091 and Pa5106 to the Hut operon suggests that the degradation of L-histidine in *Pseudomonas aeruginosa*, as reported for *Pseudomonas fluorescens* (*76*) and *Pseudomonas putida* (*80*), takes place by the formation and hydrolysis of the *N*-formyl-L-glutamate.

The similarities in the active site construction of Pa5106 with those of adenosine deaminase (ADA) and cytosine deaminase (CDA) allow the proposition of a mechanism

for the deimination of *N*-formimino-L-glutamate. Based on these similarities and the amino acid sequence alignments, a model of the active site of Pa5106 with the bound substrate were constructed (Figure 5.3). In this model the lone divalent cation is ligated to His-56, His-58, His-232, and Asp-320. The fifth ligand to the metal is a water molecule from solvent that is also hydrogen bonded to His-269 and Asp-320. From the annotation based on the amino acid sequence similarities with CDA and AtzA and the conservation of the HxxE motif, it was anticipated that Pa5106 would be responsible for the deamination of an aromatic base or similar compound. The formimino group in *N*-formimino-L-glutamate is a rather nice mimic of the exocyclic amino group found in adenosine, cytosine (see Scheme 5.1), and guanine. The analogous chemical properties of the formimino group and the exocyclic amino group in the aromatic bases provide grounds for the proposition of the chemical mechanism for the deimination of *N*-formimino-L-glutamate by Pa5106, based upon what has been previously postulated for adenosine and cytosine deaminase (*6, 7, 34*).

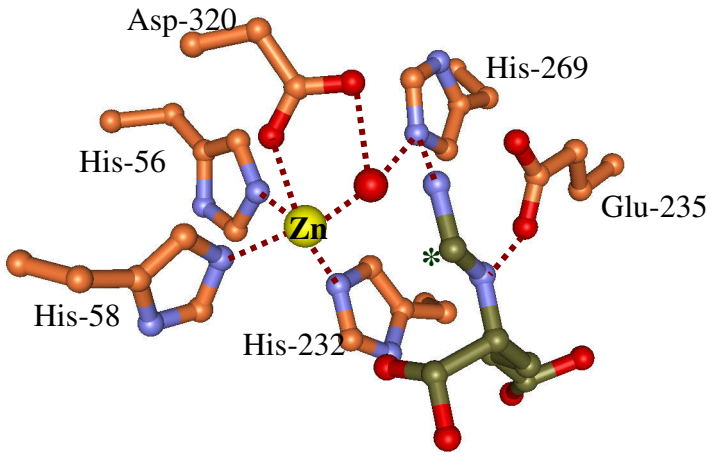

Figure 5.3: Possible model for *N*-formimino-L-glutamate binding to the active site of Pa5106. The amino acid side chains of the protein are depicted as gold bonds and the *N*-formimino-L-glutamate is highlighted in green bonds. The orientation of the residues in the active site was obtained from the alignment of the amino acid sequence of Pa5106 to the structure of Tm0936 (PDB entry codes 1p1m and 1j6p) using the CLUSTALW and Swiss-PbdViewer 3.7. The position of the substrate in the active site was obtained by aligning the Pa5106 model to the structure of 4-Hydroxy-3,4-Dihydro-1H-pyrimidin-2-one complexed to the active of cytosine deaminase (PDB entry code 1k7o). The position of the carbon center attacked during catalysis is indicated by the asterisk. The image was drawn with the program WebLab Viewer Pro.

Scheme 5.4 illustrates the working model for the mechanism of deimination of *N*-formimino-L-glutamate by Pa5106. The substrate, *N*-formimino-L-glutamate, binds to the active site and the reaction is initiated with the abstraction of a proton from the bound water by base catalysis of His-269. The enhanced solvent nucleophile then attacks the formimino carbon center creating a tetrahedral intermediate. The collapse of the tetrahedral intermediate is facilitated by base catalysis of Asp-320 and proton donation to the terminal amino substituent of the formimino group by the protonated

imidazolium side chain of His-269. The carbon-nitrogen bond is broken to generate ammonia and *N*-formyl-L-glutamate. The products dissociate and the active site is regenerated by the binding of a molecule of water from solvent. Alternative reaction mechanisms can also be proposed, depending on the ionization states of the three conserved residues in the active site (His-269, Glu-235 and Asp-320) and the tautomeric form of the substrate that initially binds to the active site. The following chapter (Chapter VI) presents experiments that discriminate among these alternative possibilities and the specific roles of the different residues and substrate species that may be influencing the mechanism of catalysis for Pa5106.

This chapter explored the final part of the histidine degradation pathway in *Pseudomonas aeruginosa*. The existence of two competing pathways for the conversion of *N*-formimino-L-glutamate to L-glutamate has been demonstrated. One of these pathways involved *N*-formimino-L-glutamate deiminase (Pa5106, HutF), a member of the amidohydrolase superfamily and *N*-formyl-L-glutamate deformylase (Pa5091, HutG). The genes for these two enzymes are found within the histidine degradation pathway genes and catalyze the degradation of *N*-formimino-L-glutamate (**I**) to ammonia, formate and L-glutamate. Due to the proximity of the genes encoding for Pa5106 (HutF) and Pa5091 (HutG) to the rest of the Hut operon, it is suggested that the degradation of L-histidine to L-glutamate in *Pseudomonas aeruginosa* proceeds through the pathway that includes HutH, HutU, HutI, HutF and HutG. A secondary pathway for the degradation of *N*-formimino-L-glutamate (**I**) to L-glutamate is found dislocated from the Hut operon. The protein Pa3175 (*N*-formimino-L-glutamase) is shown to catalyze

the direct hydrolysis of *N*-formimino-L-glutamate (**I**) to formamide and L-glutamate in a single step. A rational explanation for the existence of this secondary degradation pathway in *Pseudomonas aeruginosa* is unknown.

Scheme 5.4

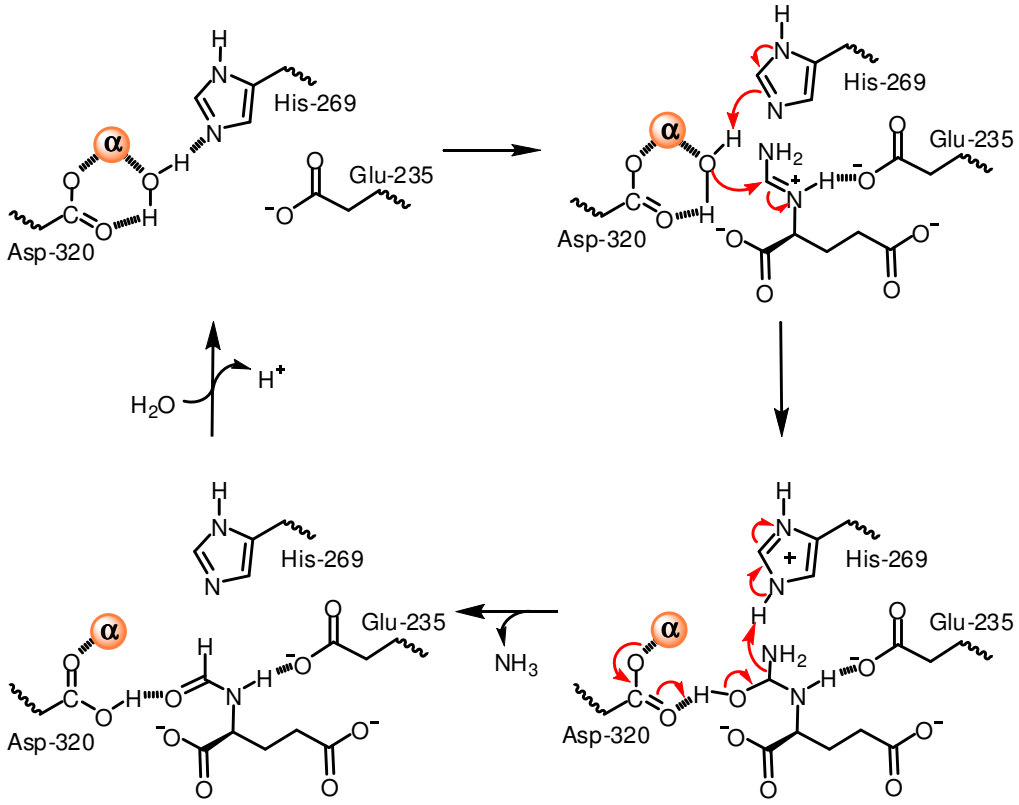

CHAPTER VI

MECHANISTIC CHARACTERIZATION OF *N*-FORMIMINO-L-GLUTAMATE IMINOHYDROLASE FROM *PSEUDOMONAS AERUGINOSA*

The amidohydrolase superfamily was first identified from the three-dimensional structural similarities found within the active sites and protein folds of urease (URE), phosphotriesterase (PTE), and adenosine deaminase (ADA) (*4*). Members of this functionally diverse superfamily are found in every organism sequenced (*1, 74*) and are characterized by their mononuclear or binuclear metal centers embedded within the C-terminal end of a $(\beta/\alpha)_8$-barrel structural fold (*4*). Large scale protein sequence comparisons suggested that *N*-formimino-L-glutamate iminohydrolase (HutF) is part of the amidohydrolase superfamily and most closely resembles cytosine deaminase and atrazine chlorohydrolase. *N*-formimino-L-glutamate iminohydrolase catalyzes the deimination of *N*-formimino-L-glutamate, an intermediate in the histidine degradation pathway (*53*).

The pathway for the degradation of histidine has been extensively studied (*9*). The pathway leading from L-histidine to *N*-formimino-L-glutamate is similar in very different types of organisms. L-Histidine is converted to urocanate and ammonia by histidine ammonia-lyase (HutH). Urocanase (HutU) then transforms urocanate to L-5-imidazolone-4-propionate, which is subsequently hydrolyzed to *N*-formimino-L-glutamate by imidazolonepropionate amidohydrolase (HutI). In all cases, *N*-formimino-

L-glutamate is further degraded to glutamate. The degradation of *N*-formimino-L-glutamate can occur by three independent paths. *N*-formimino-L-glutamate can be converted to glutamate in a single enzymatic reaction, or by a two step conversion. In animal liver, L-glutamate *N*-formimidoyltransferase can transfer the formimino group from *N*-formimino-L-glutamate to tetrahydrofolic acid (*51*). In *Aerobacter aerogenes*, *N*-formimino-L-glutamate is hydrolyzed to glutamate and formamide in a single hydrolysis reaction (*52*). For *Pseudomonas fluorescens* and *Pseudomonas putida*, the transformation of *N*-formimino-L-glutamate to glutamate occurs by two hydrolytic reactions. *N*-formimino-L-glutamate is deiminated to *N*-formyl-L-glutamate and ammonia by *N*-formimino-L-glutamate iminohydrolase (HutF) (*76, 80*) (Scheme 1), then *N*-formyl-L-glutamate is hydrolyzed to formate and L-glutamate by *N*-formyl-L-glutamate deformylase (HutG) (*54*).

Scheme 6.1

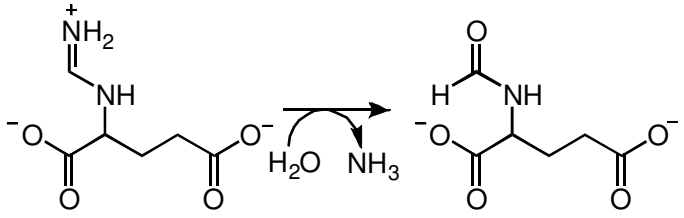

N-Formimino-L-glutamate iminohydrolase (HutF, PA5106 or gi: 15600299) was cloned from *Pseudomonas aeruginosa* PAO1. The 49 kDa protein is composed of 453 amino acids and gel filtration chromatography has suggested that HutF behaves as a

dimer in solution (*2*). Amino acid sequence alignments between homologous proteins and other members of the amidohydrolase superfamily suggested that the active site of HutF is formed by His-56, His -58, His -232, His -269 and Asp-320. The amino acid sequence alignments also identify the existence of other highly conserved residues within the active site of HutF that are analog to the catalytic residues identified in cytosine deaminase and adenosine deaminase and are suggested to be important for the catalytic proficiency of the enzyme. HutF from *Pseudomonas* sp. had been previously purified by Wickner and co-workers (*53*). The specific activity determined for the catalytic hydrolysis of *N*-formimino-L-glutamate was 10 s^{-1} with a Michaelis constant of about 120 μM. HutF exhibited little or no activity against the deimination of other *N*-substituted amino acids. Inhibition experiments demonstrated that the enzymatic activity can be suppressed by incubation with tetranitromethane (*53*), and competitive inhibition was observed in the presence of *N*-formimino-L-acetate and *N*-guanidino-L-glutamate (*2*).

The current investigation presents the biochemical characterization of the mechanism of reaction of HutF from *Pseudomonas aeruginosa*. The functional roles of the residues anticipated to be directly involved in catalysis and substrate specificity were addressed by the construction and characterization of site-directed mutant enzymes. The role of the active site metal was interrogated by formation and reconstitution of apo-HutF with an array of divalent cations. This chapter presents the formation of metal-free species of HutF and its reconstitution with different divalent metals such as Cd^{2+}, Co^{2+}, Cu^{2+}, Mn^{2+}, Ni^{2+}, and Zn^{2+}. pH-rate profiles of the native and metal reconstituted HutF,

as well as the catalytic properties of some mutant enzymes, were analyzed to study the pH dependence of the catalytic activity.

MATERIALS AND METHODS

Materials. All chemicals were obtained from Sigma-Aldrich, unless otherwise stated. The genomic DNA from *Pseudomonas aeruginosa* was purchased from the American Type Culture Collection (ATCC). The oligonucleotide synthesis and DNA sequencing reactions were performed by the Gene Technology Laboratory of Texas A&M University. The pET30a(+) expression vector and the BL21(DE3)star cells were acquired from Novagen. The Quick Change site-directed mutagenesis kit was purchased from Stratagene.

Cloning and Site-Directed Mutagenesis. The gene encoding for PA5106 (HutF) was cloned from *Pseudomonas aeruginosa* PA01 into a pET30a(+) expression vector as described in the previous chapter. Site-directed mutagenesis of HutF at residues Glu-235, His-269, and Asp-320 was accomplished using the Quick Change site-directed mutagenesis kit. The wild-type and mutant HutF were expressed in BL21(DE3)star cells.

Purification of Wild-Type and Mutant HutF. A single colony was grown overnight in 50 mL of LB media containing 50 μM kanamycin and was used to inoculate 4L of the same media. Cell cultures were grown at 37 °C with a rotatory shaker until an A_{600} of ~ 0.6 was reached, after which induction was initiated by the addition of 1.0 mM isopropyl-thiogalactoside (IPTG). The culture was incubated overnight at 30 °C. The

bacterial cells were isolated by centrifugation at 6500 × *g* for 15 min at 4 °C. The pellet was re-suspended in 50 mM HEPES buffer at pH 7.5 (buffer A) and 0.1 mg/mL of the protease inhibitor (PMSF) per gram of cells, and disrupted by sonication. The soluble protein was separated from the cell debris by centrifugation at 12,000 × *g* for 15 min at 4 °C. Nucleic acids were precipitated by the addition of protamine sulfate to a 1.5% (W/V) solution. The protein solution was fractionated between 40% and 60% saturated ammonium sulfate solutions. The precipitated protein from the 40-60% saturated ammonium sulfate solution was re-suspended in buffer A and loaded onto a High Load 26/60 Superdex 200 prep grade gel filtration column (GE Health Care) and eluted with buffer A. Fractions containing the *N*-formimino-L-glutamate deiminase activity were pooled and loaded onto a 6 mL Resource Q ion exchange column (GE Health Care) and eluted with a gradient of NaCl in 20 mM HEPES at pH 8.5 (buffer B). The fractions that contained HutF were pooled and reprecipitated with a 65% saturated ammonium sulfate solution, centrifuged at 12 000 × *g* for 15 min at 4 °C, and re-suspended in a minimal amount of Buffer A. The final step in the purification was accomplished with a High Load 26/60 Superdex 200 prep grade gel filtration column where the protein was eluted with buffer A. The purity of the protein during the isolation procedure was monitored by SDS-PAGE.

The purification of HutF mutants were performed as described above for the wild-type HutF with some modifications. These amendments include the induction of protein overexpression using 500 μM IPTG and growing the cells at 20 °C. The nucleic acids were digested by the addition of 5 U/mL of Benzonase followed by incubation for

1 hour. The protein solution was fractionated between 30% and 65% saturated ammonium sulfate solutions. The remaining purification steps were unchanged.

Specific Activity Determination. The specific activity of HutF toward the deimination of N-formimino-L-glutamate was followed by coupling the production of ammonia to the oxidation of NADH. The decrease in the concentration of NADH was followed spectrophotometrically at 340 nm using a SPECTRAmax-340 microplate spectrophotometer (Molecular Devices Inc.). The standard assay was modified from that reported by Muszbek *et al.* (*77*) and contained 100 mM HEPES at the desired pH, 100 mM KCl, 7.4 mM α-ketoglutarate, 0.4 mM NADH, 6 units of glutamate dehydrogenase, 20 nM of HutF, and the appropriate *N*-formimino-L-amino acid in a final volume of 250 μL at 30 °C.

Metal Analysis. Metal-free HutF (apo-HutF) was prepared and reconstituted with different divalent metal cations, as previously described (*2*). Purified HutF was treated with 3 mM dipicolinate at 4 °C and pH 5.6 for 48 hours. The chelator was removed by loading the protein/chelator mixture onto a PD10 column (GE Health Care) and eluting with metal-free buffer A. The apo-HutF was reconstituted with 1.0 equivalent of the desired divalent metal (Zn^{2+}, Co^{2+}, Ni^{2+}, Cd^{2+}, and Mn^{2+}) in 50 mM HEPES at pH 7.5. The metal content of the apo-HutF and reconstituted enzymes were verified using a Perkin-Elmer AAnalyst 700 atomic absorption spectrometer and inductively coupled plasma emission-mass spectrometry (ICP-MS).

pH-Rate Profiles. The pH dependence of the kinetic parameters was determined for the Zn, Cd, Cu and Ni forms of the wild-type HutF using *N*-formimino-L-glutamate

as the substrate. pH-rate profiles were also made for the Zn form of the E235Q and E235A mutants. The pH range for the enzymatic assays was between 6.1 and 9.5 in 0.2 pH unit increments. The buffers MES (pH 6.1 and 6.5) PIPES (pH 6.7 to 7.3), HEPES (pH 7.3 to 8.3), TAPS (pH 8.3 to 8.9), and CHES (8.9 and 9.5) were used at a concentration of 100 mM concentration. The pH was measured after completion of the assay to verify the pH.

Data Analysis. The kinetic parameters, k_{cat} and k_{cat}/K_m were determined by fitting the initial velocity data to equation 6.1 (*62*), where v is the initial velocity, E_T is the enzyme concentration, k_{cat} is the turnover number, S is the substrate concentration, and K_m is the Michaelis constant.

$$v / E_T = \frac{k_{cat} S}{K_m + S} \tag{6.1}$$

The pK values were obtained by fitting the k_{cat} or k_{cat}/K_m values (y) to equation 6.2 (*62*), where c is the pH independent value of y, K_a and K_b are the dissociation constants of the ionizable groups and H is the hydrogen–ion concentration.

$$\log y = \log\left(\frac{c}{1 + \frac{H}{K_a} + \frac{K_b}{H}} \right) \tag{6.2}$$

For the cases where the ionization of two groups with similar ionization constants at high pH were implicated, the decrease in activity at high pH presented a slope of about 2, therefore $K_b = (K_{b1} + K_{b2})/2$, and the data were fit to equation 6.3.

$$\log y = \log\left(\frac{c}{1+\frac{H}{K_a}+\frac{K_b}{H}+\frac{(K_b)^2}{H^2}}\right) \qquad 6.3$$

When the ionization of two groups with similar ionization constants at low pH were implicated, the decrease in activity at low pH presented a slope of about 2, therefore $K_a = (K_{a1} + K_{a2})/2$, and the data were fit to equation 6.4.

$$\log y = \log\left(\frac{c}{1+\frac{H}{K_a}+\frac{K_b}{H}+\frac{H^2}{(K_a)^2}}\right) \qquad 6.4$$

RESULTS

Metal Analysis. The study of the role of the metals in the active site of HutF was probed by formation and reconstitution of apo-HutF. The purified protein contained 0.5 equivalent of Zn^{2+} per active site with a specific activity of 5.2 s^{-1}. Chelation of the metal from the active site of HutF resulted in a 99% decrease in catalytic activity with a k_{cat} lower than 0.1 s^{-1} and ~0.03 equivalent of Zn^{2+} per active site. The metal center was reconstituted with 1 equivalent of Cd^{2+}, Cu^{2+}, Ni^{2+} and Zn^{2+} in about 10 minutes. The reconstitution of apo-HutF resulted in catalytically active enzyme with the tendency of $Cd^{2+} > Ni^{2+} > Zn^{2+} > Cu^{2+}$ with respect to the activity. The reconstitution of apo-HutF with Co^{2+} and Mn^{2+} could not be accomplished after a few days of incubation with up to 10 equivalents of metal per subunit. The average metal content per subunit of the reconstituted proteins was 1.2, 0.8, 1.2, and 1.7 for the Zn-, Ni-, Cd-, and Cu-substituted

forms of HutF, respectively. The kinetic parameters for the different forms of metal reconstituted HutF are presented in Table 6.1.

Table 6.1: Kinetic Parameters for Metal-Reconstituted HutF and Mutants[a]

HutF (M)	equivalents of M^{2+}/A.S.	K_m (mM)	k_{cat} (s^{-1})	k_{cat}/K_m ($M^{-1}s^{-1}$)
WT (Zn)	1.2	0.22 ± 0.03	13.2 ± 0.4	(6.0 ± 0.1) x 10^4
WT (Ni)	0.81	2.7 ± 0.1	21.3 ± 0.3	(8.0 ± 0.3) x 10^3
WT (Cd)	1.2	2.1 ± 0.3	31.0 ± 0.1	(1.5 ± 0.2) x 10^4
WT (Cu)	1.7	1.2 ± 0.1	8.5 ± 0.1	(7.3 ± 0.4) x 10^3
E235A (Zn)	0.62	2.2 ± 0.1	(1.0 ± 0.2) x 10^{-1}	(4.7 ± 0.6) x 10^1
E235D (Zn)	0.51	0.66 ± 0.05	(5.0 ± 0.1) x 10^{-3}	7.9 ± 0.6
E235Q (Zn)	0.77	19 ± 2	(1.2 ± 0.1) x 10^{-1}	6.3 ± 0.8
H269A (Zn)	0.12	—	—	(1.6 ± 0.1) x 10^{-1}
H269C (Zn)	0.95	—	—	(7.3 ± 0.1) x 10^{-1}
H269N (Zn)	0.17	—	—	(1.8 ± 0.1) x 10^{-1}
D320A (Zn)	0.50	—	—	< 2.0 x 10^{-2}
D320C (Zn)	1.0	—	—	< 2.0 x 10^{-2}

[a]The kinetic parameters were determined with *N*-formimino-L-glutamate as the substrate at pH 8.0, 30 °C and fit to eq 6.1.

Site-Directed Mutagenesis. The roles of the residues His-269 and Asp-320 in the active site of HutF were studied by their mutation to alanine, asparagine and cysteine. The role of Glu 235 was addressed by mutating the glutamate side chain to alanine, aspartate and glutamine. The mutant proteins were purified to homogeneity and the zinc content varied from 0.17 to 1.0 equivalents of Zn^{2+} per enzyme subunit. The effects of these mutations on the kinetic parameters are presented in Table 6.1. The catalytic activity obtained for the His-269 mutants was very low, about 5 orders of magnitude lower than the wild type enzyme. The mutation of Glu-235 to glutamine showed a considerable loss of catalytic activity and a large increase in the Michaelis constant, with values determined to be 0.12 s^{-1} and 19 mM, respectively, compared with 13 s^{-1} and 0.2 mM for the wild-type enzyme. Site-directed mutagenesis of the Asp-320 to asparagine resulted in insoluble protein, whilst mutation to alanine and cysteine resulted in soluble protein with no detectable catalytic activities ($< 2.0 \times 10^{-2}$ $M^{-1}s^{-1}$). Similar effects were found in other members of the amidohydrolase superfamily when aspartate from strand 8 was mutated (*6, 7, 34-36*).

pH-Rate Profiles. The ionization constants (pK_a and pK_b) were determined from the pH dependence of the kinetic parameters, k_{cat} and k_{cat}/K_m. The pH-rate profiles for wild-type HutF with different metal substitutions (Figure 6.1) present notable losses in activity at low and high pH, causing the plots of log k_{cat} vs. pH and log k_{cat}/K_m vs. pH to appear as bell shape curves. This demonstrates the requirement of a protonated and a deprotonated group for maximal activity. The variation of the native Zn metal in the active site of the wild-type HutF for Cu and Ni did not showed significant effects on the

pK values obtained from the log k_{cat} vs. pH and log k_{cat}/K_m vs. pH (Table 6.2). The substitution of the Zn for Cd caused the pK values to approximate to each other causing difficulties in the differenciation of them. In this case, the fits to equation 6.2 give an average for the two pK values and comparisons to the other metal-substituted species of HutF is ambiguous. The pH profile obtained from the log k_{cat}/K_m for E235Q, presents a shift in the pK_b from 8.5 for the wild-type to over 9.4 for the mutant enzyme. In addition, mutations at this position cause the decrease in activity seen at low pH to be more drastic, increasing the slope of the acidic side of the bell shaped curve to two (Figure 6.2). This suggests the ionization of a two groups at low pH.

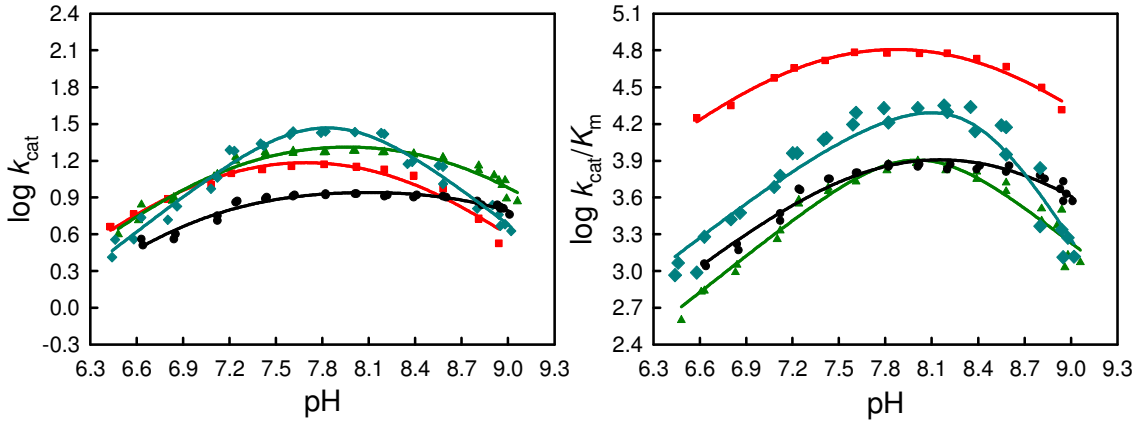

Figure 6.1: pH-rate profiles of k_{cat} and k_{cat}/K_m for different metal reconstituted wild-type HutF (■ Zn, ● Cu, ▲ Ni and ♦ Cd). The kinetic constants were obtained for Zn, Cu, Ni, and Cd. The data obtained for the Zn-, Cu- and Ni-HutF using *N*-formimino-L-glutamate as the substrate were fit to equation 6.2, while the data from Cd-HutF were fit to equation 6.3. Additional details are provided in the text and in Table 6.2.

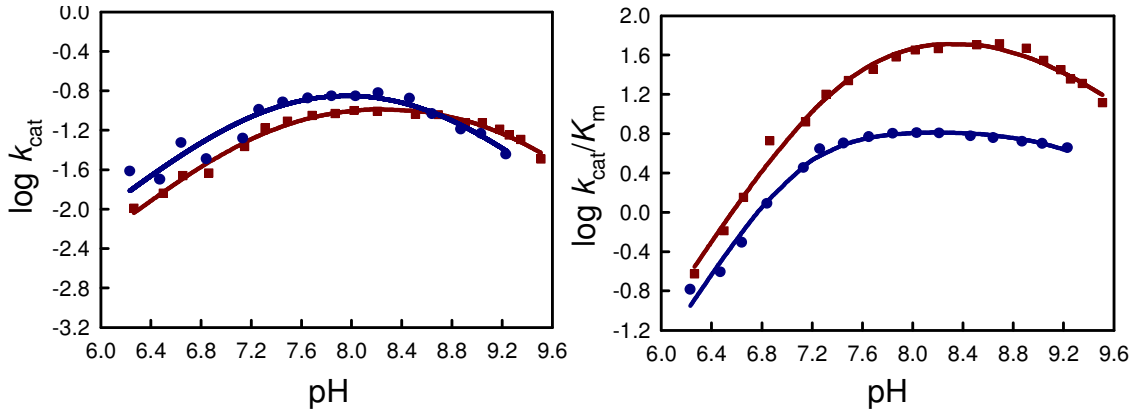

Figure 6.2: pH-rate profiles of k_{cat} and k_{cat}/K_m for the mutant forms of HutF; E235A (●) and E235Q (■). The kinetic constants were obtained for the Zn-forms of the HutF mutant enzymes. The data obtained using *N*-formimino-L-glutamate as the substrate was fit to equation 6.2 for log k_{cat} vs. pH, and equation 6.4 for log k_{cat}/K_m vs. pH. Additional details are provided in the text and in Table 6.2.

Table 6.2: Ionization Constants for Metal-Substituted HutF from pH-Rate Profiles[a]

HutF	log k_{cat} vs. pH		log k_{cat}/K_m vs. pH	
	pK_a	pK_b	pK_a	pK_b
WT (Zn)	7.0 ± 0.1	8.3 ± 0.1	7.3 ± 0.1	8.5 ± 0.1
WT (Ni)	7.2 ± 0.2	8.7 ± 0.1	8.1 ± 0.1	8.1 ± 0.1
WT (Cd)	7.9 ± 0.1	7.9 ± 0.1	7.7 ± 0.3[b]	8.7 ± 0.2[b]
WT (Cu)	7.0 ± 0.1	8.8 ± 0.2	7.5 ± 0.3	8.8 ± 0.3
E235A (Zn)	7.4 ± 0.1	9.1 ± 0.1	7.5 ± 0.2[c]	8.9 ± 0.1[c]
E235Q (Zn)	7.3 ± 0.4	8.6 ± 0.2	7.1 ± 0.2[c]	> 9.4[c]

The kinetic constants were determined using *N*-formimino-L-glutamate as the substrate and fits of the data to eq 6.2[a], 6.3[b], and 6.4[c].

DISCUSSION

The degradation of histidine is the first metabolic pathway found to contain multiple members of the amidohydrolase superfamily catalyzing consecutive steps in the pathway. Imidazolonepropionate amidohydrolase (HutI) and *N*-formimino-L-glutamate iminohydrolase (HutF) are members of the amidohydrolase superfamily involved in the histidine degradation pathway. In *Pseudomonas aeruginosa,* the pathway for the degradation of histidine begins with the deamination of L-histidine to urocanate; then urocanate is converted to L-5-imidazolone-4-propionate and subsequently hydrolyzed to *N*-formimino-L-glutamate. The deimination of *N*-formimino-L-glutamate is performed by HutF, forming *N*-formyl-L-glutamate and ammonia. Finally, *N*-formyl-L-glutamate is hydrolyzed to formate and L-glutamate.

HutF has a high specificity toward the deimination of *N*-formimino-L-glutamate. Thirteen other *N*-formimino containing compounds were tested as substrates and presented extremely low or no turnover. A K_m of 200 μM and a k_{cat} of 13.3 s^{-1} were found for *N*-formimino-L-glutamate. Several substrate analogs were tested as inhibitors. From these, only *N*-formimino-L-aspartate and *N*-guanidino-L-glutamate showed competitive inhibition (Chapter V). These observations confirm the high specificity and the exclusivity of the construction of the active site of HutF for the accommodation of the *N*-formimino-L-glutamate substrate.

The amidohydrolase superfamily contains several proteins involved in the deamination of nucleotides, such as in the deamination of cytosine and adenosine by cytosine deaminase (*6*) and adenosine deaminase (*12*), respectively. These nucleotides

contain motifs that are homologous to the formimino carbon center in *N*-formimino-L-glutamate. The mechanism of reaction of adenosine deaminase had been widely studied through biochemical, crystallographic and computational methods (*7, 9, 34, 81-83*). In those studies, several residues within the active site have been recognized to be directly involved in binding and catalysis. These residues include but are not restricted to Asp-295, His-138, and Glu-217. Residues that are believed to posses the same function have been found in cytosine deaminase (*6*), guanidine deaminase (*1*) and AMP deaminase (*1*). Amino acid sequence alignments have identified analogous residues conserved within the active site of HutF. These residues are Glu-235, His-269 and Asp-320. Site-directed mutagenesis of these residues in conjunction with metal analysis and pH-rate profiles have provided valuable information leading toward the elucidation of the mechanism of deimination of *N*-formimino-L-glutamate by HutF.

The formation and reconstitution of apo-HutF with Cd^{2+}, Cu^{2+}, Ni^{2+}, and Zn^{2+} allow us to address about the role of the metal in the active site. The loss of activity of apo-HutF reveals the importance of the metal in catalysis. This also suggests that the metal center is utilized by the enzyme to activate the hydrolytic solvent molecule and/or the substrate. This behavior is also found in other members of the amidohydrolase superfamily (*6, 7, 12, 84*). The proposed reaction mechanism (Scheme 6.2) points to the basic catalytic activation of the solvent molecule via His-296. The loss of activity of HutF at low pH indicates the protonation of a single group with a pK_a of approximately 7. Taking in consideration that the substrate is not ionizable a this pH (*76*), and the relatively small dependence of the kinetic pK_a on the identity of the divalent cation

(Table 6.2), it is likely that this ionization must originate within the enzyme. The loss of activity is consistent with the protonation of His-269, which makes the enzyme incapable of activating the solvent molecule for nucleophilic attack. This conclusion is supported by the loss of catalytic activity through mutations of His-269 to alanine, asparagine and cysteine. The crystal structures of cytosine deaminase (*6*) and adenosine deaminase (*7, 34*) show that a water molecule bridges the histidine from strand 6 and the active site metal. A very similar active site construction is expected for HutF. Site-directed mutagenesis of His-269 to alanine and asparagine resulted in a decrease in the metal occupancy of the active site of HutF. The decrease in the metal occupancy suggests that the orientation of the water molecule in position to act as a metal ligand by His-269 is important for the binding of the metal. When the imidazolium side chain of His-269 is mutated to cysteine, the metal occupancy is regenerated, but the lack of basic catalysis by the cysteine side chain causes the catalytic activity of the enzyme to remain very low.

The decrease in catalytic activity at high pH implies the deprotonation of a group with a pK_a around 9. Based on the what has been observed in the crystal structures of cytosine deaminase (*6*) and adenosine deaminase (*7, 34*) and the comparison of their amino acid sequences with the amino acid sequence of HutF, there is no apparent residue within the active site of HutF that might be responsible for the decrease in activity at high pH. The pK_a value for the formimino group of *N*-formimino-L-glutamate has been reported to be 11.2 (*76*) and is the group with the closest pK_a to that found for the loss of catalytic activity at high pH.

The p*K* values obtained from the pH profile of the mutations at Glu-235 present little deviations from those of the wild type enzyme. The significant decrease in catalytic activity and the increase of K_m by mutations at Glu-235 demonstrate the importance of the carboxylate in binding, orientation and the stabilization of the reaction intermediate. While the p*K* values for the pH-rate profiles of E285A mutant remain relatively unchanged in comparison to the wild-type, mutations at this position cause the decrease in activity at low pH to be more drastic, increasing the slope of the acid side of the bell shaped curve to two (Figure 6.2). This suggests the ionization of a second group at low pH. This second ionizated group at low pH is more likely to be the Asp-320. Site-directed mutagenesis of Asp-320 to alanine and cysteine results in catalytically deficient enzyme, and confirm its critical function. The pH-rate profile for the log k_{cat}/K_m vs. pH of the E235Q mutant showed a shift on the p*K* at high pH from around 8.9 to over 9.4. This apparent shift can be explained by the instability of the mutant protein at this high pH, at pH higher than 9.4 the mutant protein start to precipitate making the analysis of the catalytic activity imposible.

Scheme 6.2 is a representation of the proposed mechanism for the deimination of *N*-formimino-L-glutamate by HutF. Upon the binding of the substrate to the active site, the reaction is initiated by the base catalysis of His-269, which abstracts a proton from the metal bound solvent molecule. The enhanced solvent nucleophile attacks the formimino carbon center creating a tetrahedral intermediate. The tetrahedral intermediate is stabilized through interactions with the metal, Glu-235, His-269, and Asp-320. The collapse of the tetrahedral intermediate is facilitated by base catalysis via

Asp-320 and proton donation to the terminal amino substituent of the formimino group by the protonated His-269. The carbon-nitrogen bond breaks, the products are released and the active site is regenerated by the binding of a molecule of water from solvent. This mechanism of reaction is analogous to that previously proposed for cytosine deaminase (*6*) and adenosine deaminase (*34*). A more complete picture of the molecular determinants for substrate specificity and catalysis will emerge once the structure of the enzyme has been solved in the presence of appropriate substrate analogues. These investigations are currently underway.

Scheme 6.2

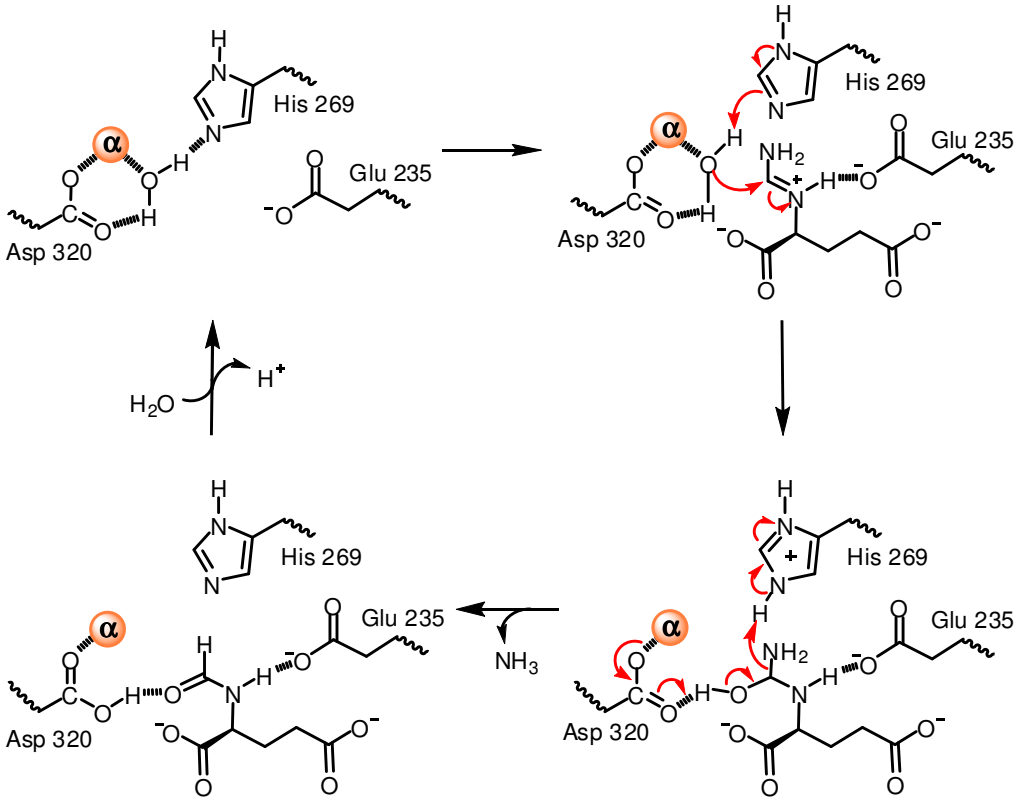

CHAPTER VII

SUMMARY AND CONCLUSIONS

The amidohydrolase superfamily is a functionally diverse group of enzymes composed of predominantly hydrolytic enzymes. This superfamily operates on a wide range of substrates containing amines, imides, amides, phosphotriesters, ureas, carbon and phosphorus centers (*1, 3*) and its members are found in every organism sequenced to date (*1, 74*). Since the discovery of the amidohydrolase superfamily by Holm and Sander in 1997, the three-dimensional structural similarities among this group of proteins have been a key tool in the identification and classification of the members of the superfamily (*4*). The landmark for this superfamily is the conservation of a $(\beta/\alpha)_8$-barrel structural fold with the catalytic active site at the C-terminal end of the barrel. The assortment of catalytic activities exhibited by the amidohydrolase superfamily is represented in Scheme 7.1. Over 2000 sequences have been identified as members of this superfamily among the partially and completely sequenced bacterial genomes. Due to the diversity of substrates and reactions of the amidohydrolase superfamily, a significant fraction of the identified members of the superfamily remain with unknown function.

The biochemical, computational and structural characterization of the members of the amidohydrolase superfamily have identified strong similarities within the active sites of the members of the superfamily as well as the mechanism of catalysis. The

Scheme 7.1

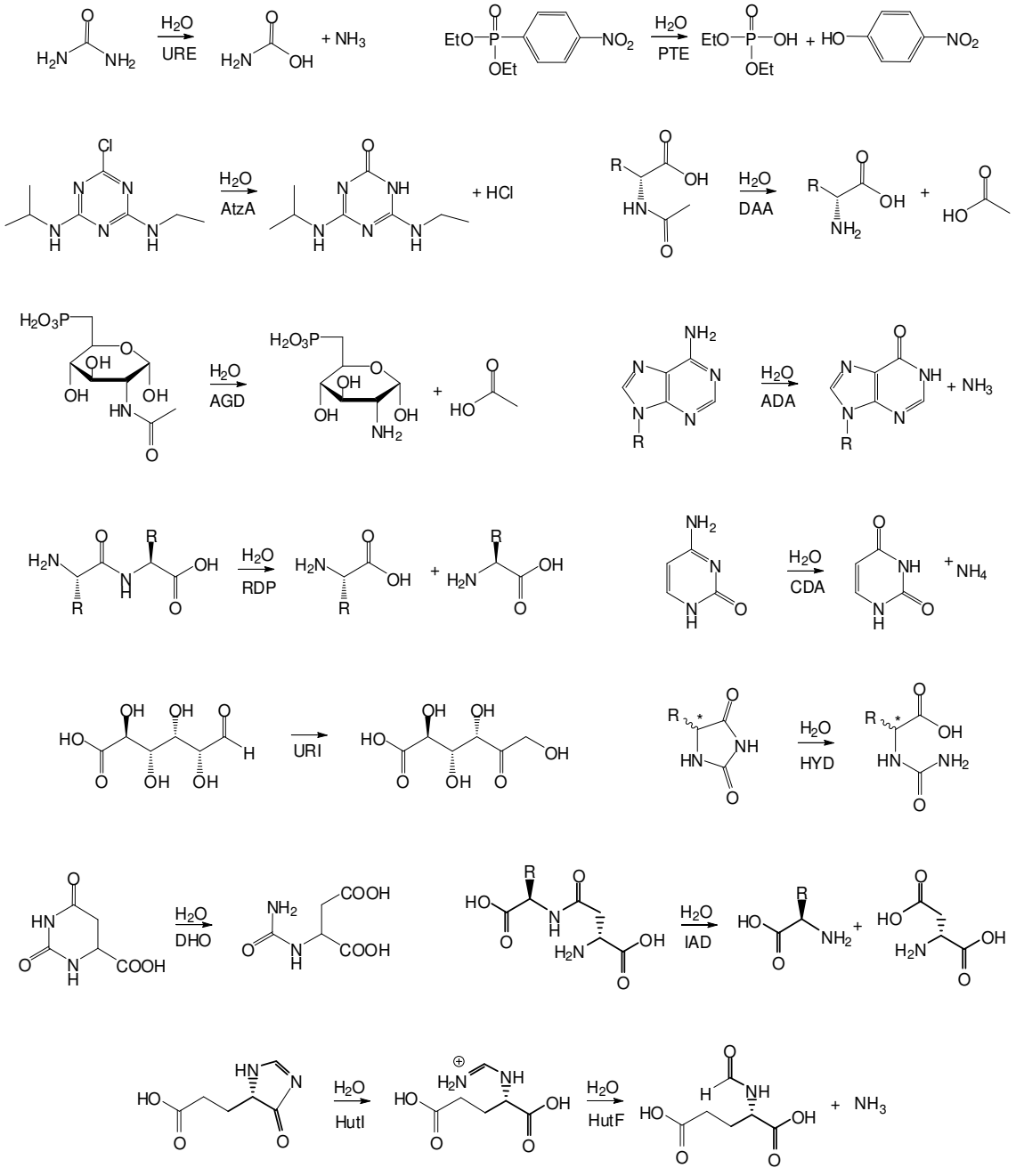
H2O
URE
+ NH3
EtO
P
NO2
OEt
H2O
PTE
OH
HO
Cl
N
NH
H
H2O
AtzA
+ HCl
R
HN
H2O
DAA
NH2
H2O3P
OH
H2O
AGD
H2O3P
NH2
H2O
ADA
+ NH3
R
H2O
RDP
H2O
CDA
+ NH4
URI
H2O
HYD
H2O
DHO
COOH
H2O
IAD
H2O
HutI
H2O
HutF
+ NH3

analysis of the X-ray crystal structures of this catalytically diverse group of enzymes has highlighted the existence of at least nine slightly different active site architectures. This information is expected to widely expand the range of active sites architectures found within the amidohydrolase superfamily members. The most common of the active site constructions within the superfamily are the mononuclear and binuclear metal centers composed of four histidines and an aspartate. Two of the histidine residues extend from the first strand, the other two histidines from strands 5 and 6, respectively. The aspartate residue originates from strand 8 and is mostly responsible for the general basic catalysis within the reaction mechanism. A solvent molecule is commonly found ligated to the mono or binuclear metal center, which plays a vital role in its nucleophilic activation. The members of the superfamily that contain a binuclear metal center, contain a carboxylated lysine side chain from strand 4 bridges the two divalent metal ions in the active site. In some cases, this carboxylated lysine is replaced for a glutamate residue which can originate from either strand 3 or 4 (*1*).

The most common of the active sites within the superfamily is the binuclear metal center found in PTE, DHO, IAD, URE, and HYD (*1*). The active site of members of the amidohydrolase superfamily containing binuclear metal center are virtually identical and their proposed mechanism of reaction are very similar as well. There are several variations within the active sites of members of the amidohydrolase superfamily that contain a single divalent metal center. The two major differences are the position and ligands of the single metal ion within the active site on the enzyme. In some cases the single metal ion is virtually in the same position as the α-metal from the binuclear

metal center mentioned above, as found for ADA, CDA, and HutF. In others, the divalent metal ion is located in a position equivalent to the β-metal, as found for AGD, and DAA. This suggests at least three possible mechanisms of reaction for the members of the amidohydrolase superfamily with these active site constructions. The general mechanism of reaction for members of the amidohydrolase superfamily with the binuclear metal center and the mononuclear metal center in the α-position were previously presented in chapter one, based on the analysis of various publications (*1, 6, 7, 34-36, 44, 85*). This dissertation presents the characterization of the mechanism of reaction of isoaspartyl dipeptidase (IAD), which contains a binuclear metal center, and *N*-formimino-L-glutamate iminohydrolase (HutF), with a mononuclear metal center located at the α-position. However, the mechanism of catalysis for the members of the superfamily with the mononuclear metal center in the β-position is yet to be characterized.

Isoaspartyl dipeptidase (IAD) catalyzes the hydrolysis of dipeptides formed from the β-carboxylate group of aspartic acid (*8*). IAD contains a binuclear metal center and is similar to that previously described for phosphotriesterase (*18*), dihydroorotase (*19*), and urease (*39*). The best substrate was β-Asp-Leu with a k_{cat}/K_m of ~1.0 x 10^5 M^{-1} s^{-1}. The X-ray structures of the resting enzyme, the bound substrate (β-Asp-His), the bound hydrolysis product (aspartate) and the phosphonate inhibitor have been solved to 1.65 Å, 2.0 Å, 2.1 Å and 3.3 Å (*63*), respectively. The three-dimensional X-ray structures of the different species of IAD and the kinetic experiments have laid the groundwork for the reaction mechanism (Scheme 7.2).

Scheme 7.2

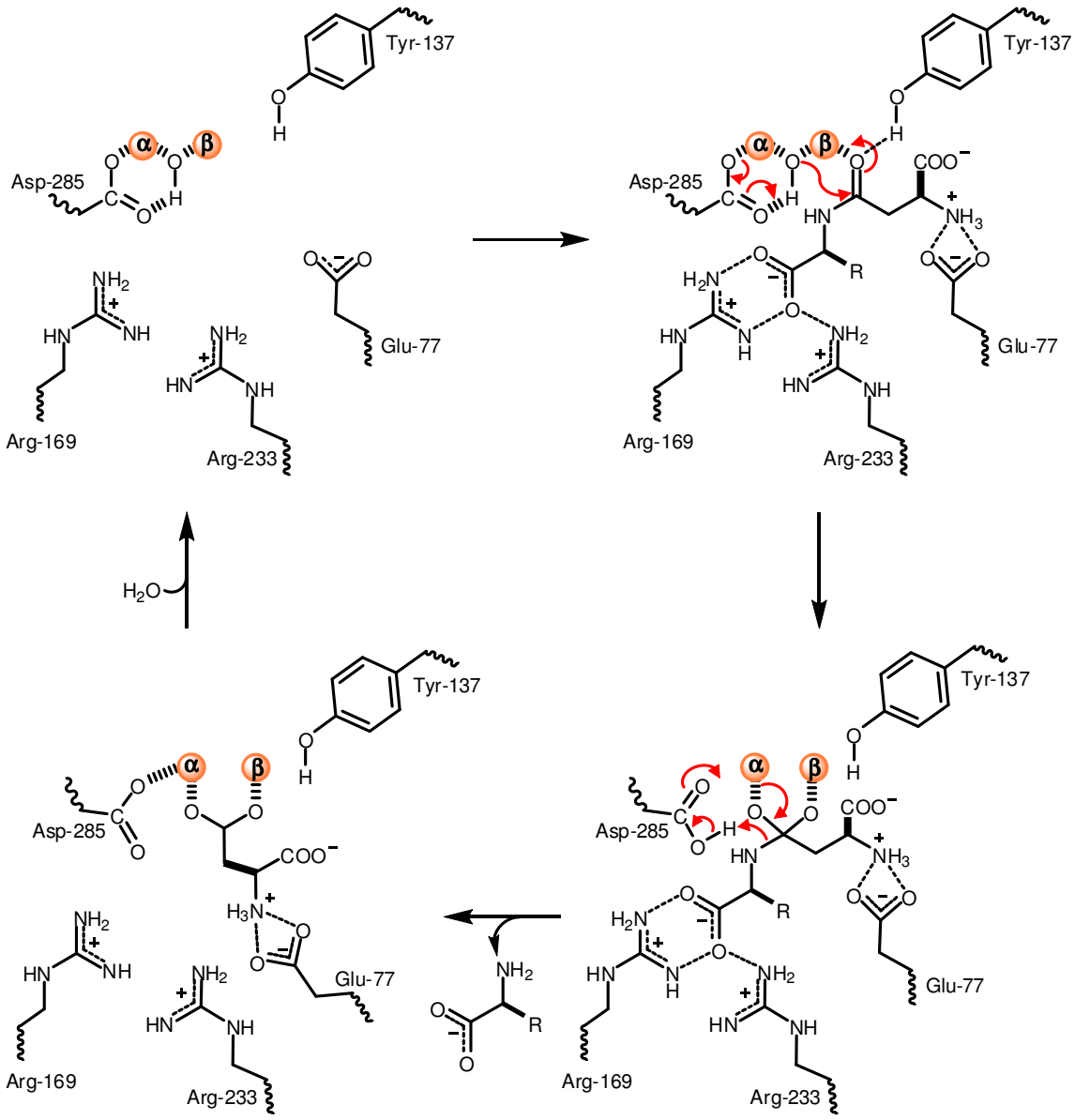

The mechanism for the hydrolysis of β-aspartyl dipeptides by IAD represented in Scheme 7.2, suggests the activation of the solvent molecule bridging the two metals

through the general base catalysis via Asp-285. Site directed mutagenesis of Asp-285 to alanine and asparagine resulted in catalytically inactive enzyme and allowed the successful crystallization of the mutant protein with the bound substrate, β-Asp-His. pH-rate profiles were used to address the identity of the solvent molecule that bridges the two divalent metals. The pH-rate profiles obtained for the hydrolysis of the peptide bond in β-Asp-Leu by IAD shows a significant decrease in catalytic activity at pH values lower than 6 and higher than 9. The dependence of the first kinetic pK_a on the identity of the metal forming the binuclear center is consistent with the protonation of the bridging hydroxide (*35, 36, 66*). In contrast, the kinetic pK_a for the group that must be protonated for catalytic activity appears to be independent of the specific metal ion bound to the active site.

The analysis of the amino acid sequence alignments between IAD from different organisms as well as the analysis of various X-ray crystal structures has demonstrated that in addition to the metal ligands, there are two other highly conserved residues within the active site that may be implicated with the catalytic efficiency of the enzyme. These residues are Glu-77 and Tyr-137. The position of the γ-carboxylate of Glu-77 relative to the bound substrate suggests an ion pair interaction with the α-amino group of the substrate. The X-ray crystal structure of the substrate bound to the active site of IAD demonstrates that the carbonyl of the side chain of Glu-77 is in position to help orient the α-amino group of the aspartate moiety of the substrate within the active site. This interaction has shown to be important since the

removal of the α-amino group from the substrates results in the total loss of catalytic activity.

The X-ray crystal structure of D285N mutant bound with the β-Asp-His substrate demonstrates that the oxygen of the phenolic side chain of Tyr-137 is within 2.4 Å from the carbonyl oxygen of the peptide bond and about 2.4 Å from the β-metal. Tyr-137 can function as a fifth ligand to the β-metal and/or participate in the polarization of the peptidic carbonyl via Lewis acid catalysis. The pK_a for the loss of the catalytic activity at high pH is around 9 for both IAD mutants. Consequently, it is unlikely for these residues to be responsible for the loss of catalytic activity at high pH. However, the significant drop in catalytic activity for the E77Q and Y137F mutants suggest a critical role for the γ-carboxylate side chain of Glu-77 and the phenolic hydroxyl group of Tyr-137 in catalysis. The X-ray crystal structures of the E77Q and Y137F mutant enzymes demonstrate that mutation at these positions did not create any significant conformational change, therefore it is unlikely that a conformational difference between the mutant enzymes and the wild type is the root cause for the attenuation of the catalytic activity.

Based on the observations from several X-ray structures and the biochemical characterization of wild-type and mutant forms of IAD, a self consistent mechanism of reaction for the hydrolysis of β-aspartyl dipeptides can be proposed. In the resting state of the enzyme, a hydroxide molecule bridges the two divalent cations and the carboxylate side chain of Asp-285 is ligated to the α-metal and hydrogen bonded to the metal bridging hydroxide. The substrate binds to the active site in an orientation that

positions the carbonyl oxygen of the scissile bond adjacent to the β-metal ion and within hydrogen bonding distance to Tyr-137. These interactions polarize the carbonyl group and enhance the electrophilic character of the carbonyl carbon. The ion pair interaction between the side chain carboxylate of Glu-77 and the α-amino group of the substrate facilitates the binding and orientation of β-aspartyl dipeptides. Additional ion pair interactions between the α-carboxylate of the leaving group product and the guanidinium groups of Arg-169 and Arg-233 contribute to the orientation of the substrate in the active site. The enzymatic reaction is initiated by the nucleophilic attack of the bridging hydroxide to the *re* face of the amide bond concomitant with proton transfer from the hydroxide to the side chain carboxylate of Asp-285. This forms a tetrahedral intermediate, which then collapses after the proton transfer to the α-amino group of the departing amino acid by the lately protonated Asp-285. The reaction finalizes with the departing of the leaving group and the newly formed carboxylate on the side chain of the aspartate product, coordinated to the binuclear metal center, as observed in the X-ray structure of the complexed product.

N-formimino-L-glutamate iminohydrolase (HutF) from *Pseudomonas aeruginosa* is an example of an amidohydrolase superfamily member that contains a mononuclear metal center. The proposed reaction mechanism for these type of amidohydrolase is slightly different from the mechanism for IAD, which contains a binuclear metal center. In *Pseudomonas aeruginosa*, HutF performs the fourth step of the histidine degradation pathway. *N*-formimino-L-glutamate iminohydrolase is highly specific toward the deimination of *N*-formimino-L-glutamate. An amino acid sequence alignment between

HutF and other members of the amidohydrolase superfamily containing mononuclear metal centers has identified homologous residues conserved within their active sites. The residues within the active site of HutF have been identified to be His-56, His-58, His-232, Glu-235, His-269, and Asp-320. From these residues His-56, His-58, and His-232 have been suggested to be directly related to metal binding, whilst Glu-235, His-269, and Asp-320 were proposed to be involved in substrate binding and/or catalysis. The role of the mononuclear metal center in HutF was investigated by the formation and reconstitution of apo-HutF with various divalent metal ions. The loss of activity of apo-HutF reveals the importance of the metal in catalysis and suggests that the metal center acts in the activation of the hydrolytic solvent molecule and/or the substrate. Site-directed mutagenesis of Glu-235, His-269, and Asp-320, in conjunction with the analysis of active site metal substitution and pH-rate profiles have provided valuable information for the proposal of a mechanism of deimination of *N*-formimino-L-glutamate by HutF (Scheme 7.3).

Scheme 7.3:

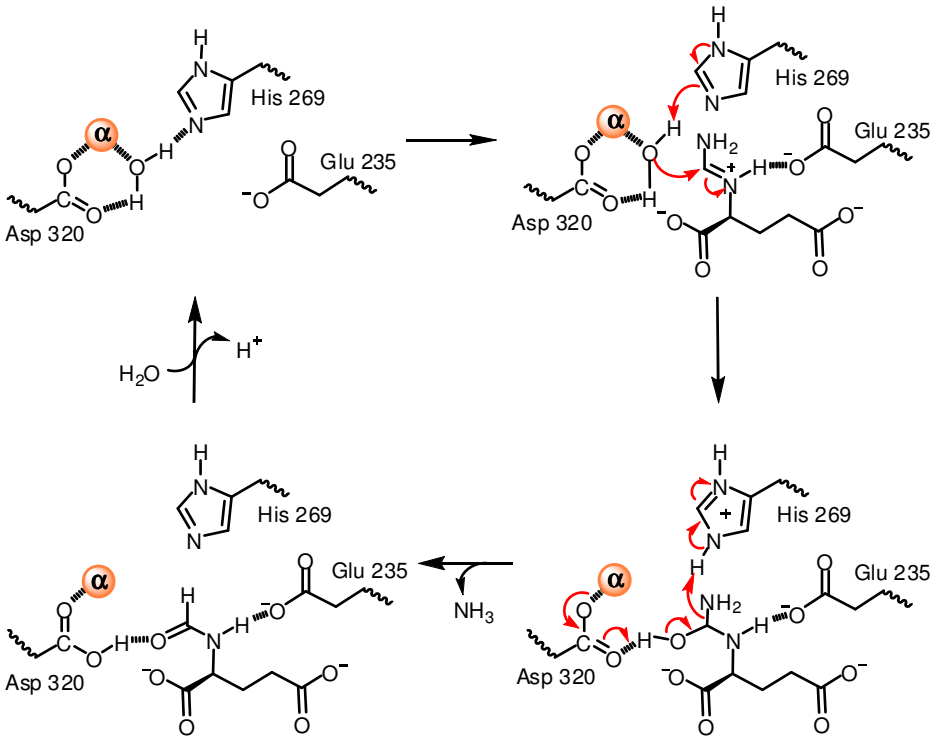

The pH-rate profile obtained for the hydrolysis of *N*-formimino-L-glutamate by HutF shows that a group must be protonated and another deprotonated for catalytic activity. The loss of activity of HutF at low pH indicates the protonation of a single group with a pK_a of approximately 7. Taking into consideration that the substrate is not ionizable at this pH (*76*) and the low dependence of the metal identity of the catalytic pK_a obtained at low pH, it is likely that this ionization must originate from the protonation of the imidazolium side chain of His-269. Scheme 7.3 proposes that the activation of the solvent molecule occurs through general base catalysis via His-296. The site-directed mutagenesis of His-269 to alanine, asparagine, and cysteine resulted in

catalytically inactive enzyme, suggesting that His-269 is important for the activation of the water molecule, in conjunction with the divalent metal center.

The decrease in catalytic activity at high pH implies the deprotonation of a group with a pK_a around 9. There is no apparent residue within the active site of HutF that might be responsible for the decrease in activity at high pH. The pK_a value for the formimino group of *N*-formimino-L-glutamate has been reported to be 11.2 (*76*) and it appears to be the group with the closest pK_a to that found for the loss of catalytic activity at high pH. The pH-rate profiles of the E235A and E235Q mutant enzymes present little deviations from those of the wild type enzyme. The significant decrease in catalytic activity and the increase of K_m by mutations at Glu-235 demonstrate the importance of the carboxylate in binding, orientation and in the stabilization of the reaction intermediate.

Scheme 7.3 illustrates a working model for the mechanism of deimination of *N*-formimino-L-glutamate by HutF. In the resting state of the enzyme, a solvent molecule is ligated to the divalent cation as well as the Asp-320, which is also hydrogen bonded to the solvent molecule. The substrate is bound to the active site in an orientation that positions the hydrogen in the α-amino group of the glutamate within hydrogen bonding distance to Glu-235. This hydrogen bond interaction favors the positive charge to be on the α-amino group of the glutamate rather than the nitrogen of the iminium group. Upon the binding of the substrate to the active site, the reaction is initiated through the activation of the hydrolytic water with base catalysis via His-269. The enhanced solvent nucleophile attacks the formimino carbon center creating a tetrahedral intermediate by

the addition of a hydroxide. The tetrahedral intermediate is stabilized through interactions with the metal, Glu-235, His-269, and Asp-320. The collapse of the tetrahedral intermediate is facilitated by base catalysis via Asp-320 and proton donation to the terminal amino of the iminium group by the lately protonated imidazolium side chain of His-269. The carbon-nitrogen bond then breaks, and the products are released. A solved X-ray crystal structure of HutF in the presence of the appropriate substrate analogues will present a more complete picture of the molecular determinants for substrate specificity and catalysis.

REFERENCES

1. Seibert, C. M., and Raushel, F. M. (2005) Structural and catalytic diversity within the amidohydrolase superfamily, *Biochemistry 44*, 6383-91.
2. Marti-Arbona, R., Xu, C., Steele, S., Weeks, A., Kuty, G. F., Seibert, C. M., and Raushel, F. M. (2006) Annotating enzymes of unknown function: *N*-formimino-L-glutamate deiminase is a member of the amidohydrolase superfamily, *Biochemistry 45*, 1997-2005.
3. de Souza, M. L., Sadowsky, M. J., and Wackett, L. P. (1996) Atrazine chlorohydrolase from *Pseudomonas* sp. strain ADP: Gene sequence, enzyme purification, and protein characterization, *J. Bacteriol. 178*, 4894-900.
4. Holm, L., and Sander, C. (1997) An evolutionary treasure: Unification of a broad set of amidohydrolases related to urease, *Proteins 28*, 72-82.
5. Gerlt, J. A., and Raushel, F. M. (2003) Evolution of function in $(\beta/\alpha)_8$-barrel enzymes. *Curr. Opin. Chem. Biol. 7*, 252-64.
6. Ireton, G. C., McDermott, G., Black, M. E., and Stoddard, B. L. (2002) The structure of *Escherichia coli* cytosine deaminase, *J. Mol. Biol. 315*, 687-97.
7. Wang, Z., and Quiocho, F. A. (1998) Complexes of adenosine deaminase with two potent inhibitors: X-ray structures in four independent molecules at pH of maximum activity, *Biochemistry 37*, 8314-24.
8. Haley, E. E. (1968) Purification and properties of a β-aspartyl peptidase from *Escherichia coli*, *J. Biol. Chem. 243*, 5748-52.

9. Borek, B. A., and Waelsch, H. (1953) The enzymatic degradation of histidine, *J. Biol. Chem. 205*, 459-74.

10. Dumas, D. P., Caldwell, S. R., Wild, J. R., and Raushel, F. M. (1989) Purification and properties of the phosphotriesterase from *Pseudomonas diminuta*, *J. Biol. Chem. 264*, 19659-65.

11. Akana, J., Fedorov, A. A., Fedorov, E., Novak, W. R., Babbitt, P. C., Almo, S. C., and Gerlt, J. A. (2006) D-Ribulose 5-phosphate 3-epimerase: Functional and structural relationships to members of the ribulose-phosphate binding $(\beta/\alpha)_8$-barrel superfamily, *Biochemistry 45*, 2493-503.

12. Babbitt, P. C., Mrachko, G. T., Hasson, M. S., Huisman, G. W., Kolter, R., Ringe, D., Petsko, G. A., Kenyon, G. L., and Gerlt, J. A. (1995) A functionally diverse enzyme superfamily that abstracts the alpha protons of carboxylic acids, *Science 267*, 1159-61.

13. Copley, R. R., and Bork, P. (2000) Homology among $(\beta/\alpha)_8$-barrels: Implications for the evolution of metabolic pathways, *J. Mol. Biol. 303*, 627-41.

14. Wise, E., Yew, W. S., Babbitt, P. C., Gerlt, J. A., and Rayment, I. (2002) Homologous $(\beta/\alpha)_8$-barrel enzymes that catalyze unrelated reactions: Orotidine 5'-monophosphate decarboxylase and 3-keto-L-gulonate 6-phosphate decarboxylase, *Biochemistry 41*, 3861-9.

15. Murzin, A. G. (1993) Sweet-tasting protein monellin is related to the cystatin family of thiol proteinase inhibitors, *J. Mol. Biol. 230*, 689-94.

16. Gerlt, J. A., and Babbitt, P. C. (2001) Divergent evolution of enzymatic function: Mechanistically diverse superfamilies and functionally distinct suprafamilies, *Annu. Rev. Biochem. 70*, 209-46.

17. Benini, S., Rypniewski, W. R., Wilson, K. S., Miletti, S., Ciurli, S., and Mangani, S. (1999) A new proposal for urease mechanism based on the crystal structures of the native and inhibited enzyme from *Bacillus pasteurii*: Why urea hydrolysis costs two nickels, *Structure 7*, 205-16.

18. Benning, M. M., Shim, H., Raushel, F. M., and Holden, H. M. (2001) High resolution X-ray structures of different metal-substituted forms of phosphotriesterase from *Pseudomonas diminuta*, *Biochemistry 40*, 2712-22.

19. Thoden, J. B., Phillips, G. N., Jr., Neal, T. M., Raushel, F. M., and Holden, H. M. (2001) Molecular structure of dihydroorotase: A paradigm for catalysis through the use of a binuclear metal center, *Biochemistry 40*, 6989-97.

20. Abendroth, J., Niefind, K., May, O., Siemann, M., Syldatk, C., and Schomburg, D. (2002) The structure of L-hydantoinase from *Arthobacter aurescens* leads to an understanding of dihydropyrimidinase substrate and enantio specificity, *Biochemistry 41*, 8589-97.

21. Abendroth, J., Niefind, K., and Schomburg, D. (2002) X-ray structure of a dihydropyrimidinase from *Thermus* sp. at 1.3 A resolution, *J. Mol. Biol. 320*, 143-56.

22. Cheon, Y. H., Kim, H. S., Han, K. H., Abendroth, J., Niefind, K., Schomburg, D., Wang, J., and Kim, Y. (2002) Crystal structure of D-hydantoinase from

Bacillus stearothermophilus: Insight into the stereochemistry of enantioselectivity, *Biochemistry 41*, 9410-7.

23. Nitanai, Y., Satow, Y., Adachi, H., and Tsujimoto, M. (2002) Crystal structure of human renal dipeptidase involved in β-lactam hydrolysis, *J. Mol. Biol. 321*, 177-84.

24. Vincent, F., Yates, D., Garman, E., Davies, G. J., and Brannigan, J. A. (2004) The three-dimensional structure of the *N*-acetylglucosamine-6-phosphate deacetylase, NagA, from *Bacillus subtilis*: A member of the urease superfamily, *J. Biol. Chem. 279*, 2809-16.

25. Schwarzenbacher, R., Canaves, J. M., Brinen, L. S., Dai, X., Deacon, A. M., Elsliger, M. A., Eshaghi, S., Floyd, R., Godzik, A., Grittini, C., Grzechnik, S. K., Guda, C., Jaroszewski, L., Karlak, C., Klock, H. E., Koesema, E., Kovarik, J. S., Kreusch, A., Kuhn, P., Lesley, S. A., McMullan, D., McPhillips, T. M., Miller, M. A., Miller, M. D., Morse, A., Moy, K., Ouyang, J., Robb, A., Rodrigues, K., Selby, T. L., Spraggon, G., Stevens, R. C., van den Bedem, H., Velasquez, J., Vincent, J., Wang, X., West, B., Wolf, G., Hodgson, K. O., Wooley, J., and Wilson, I. A. (2003) Crystal structure of uronate isomerase (TM0064) from *Thermotoga maritima* at 2.85 A resolution, *Proteins 53*, 142-5.

26. Liaw, S. H., Chen, S. J., Ko, T. P., Hsu, C. S., Chen, C. J., Wang, A. H., and Tsai, Y. C. (2003) Crystal structure of D-aminoacylase from *Alcaligenes faecalis* DA1. A novel subset of amidohydrolases and insights into the enzyme mechanism, *J. Biol. Chem. 278*, 4957-62.

27. Thoden, J. B., Marti-Arbona, R., Raushel, F. M., and Holden, H. M. (2003) High-resolution X-ray structure of isoaspartyl dipeptidase from *Escherichia coli, Biochemistry 42*, 4874-82.

28. Buchbinder, J. L., Stephenson, R. C., Dresser, M. J., Pitera, J. W., Scanlan, T. S., and Fletterick, R. J. (1998) Biochemical characterization and crystallographic structure of an *Escherichia coli* protein from the phosphotriesterase gene family, *Biochemistry 37*, 5096-106.

29. Shim, H., and Raushel, F. M. (2000) Self-assembly of the binuclear metal center of phosphotriesterase, *Biochemistry 39*, 7357-64.

30. Lai, W. L., Chou, L. Y., Ting, C. Y., Kirby, R., Tsai, Y. C., Wang, A. H., and Liaw, S. H. (2004) The functional role of the binuclear metal center in D-aminoacylase: One-metal activation and second-metal attenuation, *J. Biol. Chem. 279*, 13962-7.

31. Benning, M. M., Kuo, J. M., Raushel, F. M., and Holden, H. M. (1994) Three-dimensional structure of phosphotriesterase: An enzyme capable of detoxifying organophosphate nerve agents, *Biochemistry 33*, 15001-7.

32. Li, T., Iwaki, H., Fu, R., Hasegawa, Y., Zhang, H., and Liu, A. (2006) alpha-amino-β-carboxymuconic-ε-semialdehyde decarboxylase (ACMSD) is a new member of the amidohydrolase superfamily, *Biochemistry 45*, 6628-6634.

33. Li, T., Walker, A. L., Iwaki, H., Hasegawa, Y., and Liu, A. (2005) Kinetic and spectroscopic characterization of ACMSD from *Pseudomonas fluorescens*

reveals a pentacoordinate mononuclear metallocofactor, *J. Am. Chem. Soc. 127*, 12282-90.

34. Wilson, D. K., and Quiocho, F. A. (1993) A pre-transition-state mimic of an enzyme: X-ray structure of adenosine deaminase with bound 1-deazaadenosine and zinc-activated water, *Biochemistry 32*, 1689-94.

35. Aubert, S. D., Li, Y., and Raushel, F. M. (2004) Mechanism for the hydrolysis of organophosphates by the bacterial phosphotriesterase, *Biochemistry 43*, 5707-15.

36. Porter, T. N., Li, Y., and Raushel, F. M. (2004) Mechanism of the dihydroorotase reaction, *Biochemistry 43*, 16285-92.

37. Barnum, D. W. (1983) Hydrolysis of cations - formation-constants and standard free-energies of formation of hydroxy complexes, *Inorg. Chem. 22*, 2297-2305.

38. He, C., and Lippard, S. J. (2000) Modeling carboxylate-bridged dinuclear active sites in metalloenzymes using a novel naphthyridine-based dinucleating ligand, *J. Am. Chem. Soc. 122*, 184-185.

39. Jabri, E., Carr, M. B., Hausinger, R. P., and Karplus, P. A. (1995) The crystal structure of urease from *Klebsiella aerogenes*, *Science 268*, 998-1004.

40. Benini, S., Ciurli, S., Rypniewski, W. R., Wilson, K. S., and Mangani, S. (1998) Crystallization and preliminary high-resolution X-ray diffraction analysis of native and beta-mercaptoethanol-inhibited urease from *Bacillus pasteurii*, *Acta. Crystallogr. D. Biol. Crystallogr. 54*, 409-12.

41. Benini, S., Rypniewski, W. R., Wilson, K. S., Ciurli, S., and Mangani, S. (2001) Structure-based rationalization of urease inhibition by phosphate: Novel insights into the enzyme mechanism, *J. Biol. Inorg. Chem. 6*, 778-90.

42. Benini, S., Rypniewski, W. R., Wilson, K. S., Mangani, S., and Ciurli, S. (2004) Molecular details of urease inhibition by boric acid: Insights into the catalytic mechanism, *J. Am. Chem. Soc. 126*, 3714-5.

43. Barrios, A. M., and Lippard, S. J. (2001) Phthalazine-based dinucleating ligands afford dinuclear centers often encountered in metalloenzyme active sites, *Inorg. Chem. 40*, 1060-4.

44. Estiu, G., and Merz, K. M., Jr. (2004) Enzymatic catalysis of urea decomposition: Elimination or hydrolysis?, *J. Am. Chem. Soc. 126*, 11832-42.

45. Mack, E., and Villars, D. S. (1923) The action of urease in the decomposition of urea, *J. Am. Chem. Soc. 45*, 505-510.

46. Estiu, G., and Merz, K. M., Jr. (2006) Catalyzed decomposition of urea. Molecular dynamics simulations of the binding of urea to urease, *Biochemistry 45*, 4429-43.

47. Geiger, T., and Clarke, S. (1987) Deamidation, isomerization, and racemization at asparaginyl and aspartyl residues in peptides. Succinimide-linked reactions that contribute to protein degradation, *J. Biol. Chem. 262*, 785-94.

48. Fu, J. C., Ding, L., and Clarke, S. (1991) Purification, gene cloning, and sequence analysis of an L-isoaspartyl protein carboxyl methyltransferase from *Escherichia coli*, *J. Biol. Chem. 266*, 14562-72.

49. Lowenson, J. D., and Clarke, S. (1991) Structural elements affecting the recognition of L-isoaspartyl residues by the L-isoaspartyl/D-aspartyl protein methyltransferase. Implications for the repair hypothesis, *J. Biol. Chem. 266*, 19396-406.

50. Stover, C. K., Pham, X. Q., Erwin, A. L., Mizoguchi, S. D., Warrener, P., Hickey, M. J., Brinkman, F. S., Hufnagle, W. O., Kowalik, D. J., Lagrou, M., Garber, R. L., Goltry, L., Tolentino, E., Westbrock-Wadman, S., Yuan, Y., Brody, L. L., Coulter, S. N., Folger, K. R., Kas, A., Larbig, K., Lim, R., Smith, K., Spencer, D., Wong, G. K., Wu, Z., Paulsen, I. T., Reizer, J., Saier, M. H., Hancock, R. E., Lory, S., and Olson, M. V. (2000) Complete genome sequence of *Pseudomonas aeruginosa* PA01, an opportunistic pathogen, *Nature 406*, 959-64.

51. Tabor, H., and Wyngarden, L. (1959) The enzymatic formation of formiminotetrahydrofolic acid, 5,10-methenyltetrahydrofolic acid, and 10-formyltetrahydrofolic acid in the metabolism of formiminoglutamic acid, *J. Biol. Chem. 234*, 1830-46.

52. Magasanik, B., and Bowser, H. R. (1955) The degradation of histidine by *Aerobacter aerogenes*, *J. Biol. Chem. 213*, 571-80.

53. Wickner, R. B., and Tabor, H. (1972) *N*-Formimino-L-glutamate iminohydrolase from histidine-adapted *Pseudomonas*. Purification and properties, *J. Biol. Chem. 247*, 1605-9.

54. Hu, L., Mulfinger, L. M., and Phillips, A. T. (1987) Purification and properties of formylglutamate amidohydrolase from *Pseudomonas putida*, *J. Bacteriol. 169*, 4696-702.

55. Gary, J. D., and Clarke, S. (1998) β-Aspartyl dipeptidase, in *Handbook of Proteolytic Enzymes,* pp 1461-1465, Academic Press, London.

56. Gary, J. D., and Clarke, S. (1995) Purification and Characterization of an Isoaspartyl Dipeptidase from *Escherichia coli*, *J. Biol. Chem. 270*, 4076-4087.

57. Hejazi, M., Piotukh, K., Mattow, J., Deutzmann, R., Volkmer-Engert, R., and Lockau, W. (2002) Isoaspartyl dipeptidase activity of plant-type asparaginases, *Biochem. J. 364*, 129-36.

58. Benning, M. M., Kuo, J. M., Raushel, F. M., and Holden, H. M. (1995) Three-dimensional structure of the binuclear metal center of phosphotriesterase, *Biochemistry 34*, 7973-8.

59. Gary, J. D., and Clarke, S. (1995) Purification and characterization of an isoaspartyl dipeptidase from *Escherichia coli*, *J. Biol. Chem. 270*, 4076-87.

60. Brynes, S., Burckart, G. J., and Mokotoff, M. (1978) Potential inhibitors of L-asparagine biosynthesis. 4. Substituted sulfonamide and sulfonylhydrazide analogues of L-asparagine, *J. Med. Chem. 21*, 45-9.

61. Schmidt, D. M., Hubbard, B. K., and Gerlt, J. A. (2001) Evolution of enzymatic activities in the enolase superfamily: Functional assignment of unknown proteins in *Bacillus subtilis* and *Escherichia coli* as L-Ala-D/L-Glu epimerases, *Biochemistry 40*, 15707-15.

62. Cleland, W. W. (1979) Statistical analysis of enzyme kinetic data, *Methods Enzymol 63*, 103-38.

63. Jozic, D., Kaiser, J. T., Huber, R., Bode, W., and Maskos, K. (2003) X-ray structure of isoaspartyl dipeptidase from *E. coli*: A dinuclear zinc peptidase evolved from amidohydrolases, *J. Mol. Biol. 332*, 243-56.

64. Dawson, R. M. C., Elliott, D. C., Elliott, W. H., and Jones, K. M. (1986) *Data for Biochemical Research,* 3rd ed., pp 1-31, Oxford Science Publications, Oxford , U.K.

65. Benning, M. M., Hong, S. B., Raushel, F. M., and Holden, H. M. (2000) The binding of substrate analogs to phosphotriesterase, *J. Biol. Chem. 275*, 30556-60.

66. Marti-Arbona, R., Fresquet, V., Thoden, J. B., Davis, M. L., Holden, H. M., and Raushel, F. M. (2005) Mechanism of the reaction catalyzed by isoaspartyl dipeptidase from *Escherichia coli*, *Biochemistry 44*, 7115-24.

67. Porter, T., Li, Y., and Raushel, F. (2004) Mechanism of the dihydroorotase reaction. *Biochemistry 43*, 16285-16292.

68. Benning, M., Shim, H., Raushel, F., and Holden, H. (2001) High resolution X-ray structures of different metal-substituted forms of phosphotriesterase from *Pseudomonas diminuta*, *Biochemistry 40*, 2712-2722.

69. Wise, E. L., and Rayment, I. (2004) Understanding the importance of protein structure to nature's routes for divergent evolution in TIM barrel enzymes, *Acc. Chem. Res. 37*, 149-58.

70. Yang, Z., Savchenko, A., Yakunin, A., Zhang, R., Edwards, A., Arrowsmith, C., and Tong, L. (2003) Aspartate dehydrogenase, a novel enzyme identified from structural and functional studies of TM1643, *J. Biol. Chem. 278*, 8804-8.

71. Akita, M., Kayatama, K., Hatada, Y., Ito, S., and Horikoshi, K. (2005) A novel beta-glucanase gene from *Bacillus halodurans* C-125. *FEMS Microbiol. Lett. 248*, 9-15.

72. Thoden, J. B., Taylor Ringia, E. A., Garrett, J. B., Gerlt, J. A., Holden, H. M., and Rayment, I. (2004) Evolution of enzymatic activity in the enolase superfamily: Structural studies of the promiscuous *O*-succinylbenzoate synthase from *Amycolatopsis*, *Biochemistry 43*, 5716-27.

73. Wang, Z., Wei,H., Yu, Y., Sun, J., Yang, Y., Xing, G., Wu, S., Zhou, Y., Zhu, Y., Zhang, C., Zhou, T., Zhao, X., Sun, Q., and Hea, Z. . (2004) Characterization of Ceap-11 and Ceap-16, two novel splicing-variant-proteins, associated with centrosome, microtubule aggregation and cell proliferation, *J. Mol. Biol. 343*, 71-82

74. Roodveldt, C., and Tawfik, D. S. (2005) Shared promiscuous activities and evolutionary features in various members of the amidohydrolase superfamily, *Biochemistry 44*, 12728-36.

75. Tabor, H., and Rabinowitz, J. C. (1957) Formiminoglycine, formimino-L-aspartic acid, formimino-L-glutamic acid, *Biochemical Preparations 5*, 100-105.

76. Tabor, H., and Mehler, A. H. (1954) Isolation of *N*-formyl-L-glutamic acid as an intermediate in the enzymatic degradation of L-histidine, *J. Biol. Chem. 210*, 559-68.

77. Muszbek, L., Polgar, J., and Fesus, L. (1985) Kinetic determination of blood coagulation Factor XIII in plasma, *Clin. Chem. 31*, 35-40.

78. Nanba, H., Takaoka, Y., and Hasegawa, J. (2003) Purification and characterization of formate dehydrogenase from *Ancylobacter aquaticus* strain KNK607M, and cloning of the gene, *Biosci. Biotechnol. Biochem. 67*, 720-8.

79. Beutler, H.-O. (1990) L-Glutamate, colorimetric method with glutamate dehydrogenase and diaphorase, in *Methods of Enzymatic Analysis*, 3rd ed., *8*, pp 369-376, Verlag Chemie, Weinheim, Germany.

80. Hu, L., and Phillips, A. T. (1988) Organization and multiple regulation of histidine utilization genes in *Pseudomonas putida*, *J. Bacteriol. 170*, 4272-9.

81. Frick, L., Wolfenden, R., Smal, E., and Baker, D. C. (1986) Transition-state stabilization by adenosine deaminase: structural studies of its inhibitory complex with deoxycoformycin, *Biochemistry 25*, 1616-21.

82. Kinoshita, T., Nakanishi, I., Terasaka, T., Kuno, M., Seki, N., Warizaya, M., Matsumura, H., Inoue, T., Takano, K., Adachi, H., Mori, Y., and Fujii, T. (2005) Structural basis of compound recognition by adenosine deaminase, *Biochemistry 44*, 10562-9.

83. Kurz, L. C., Moix, L., Riley, M. C., and Frieden, C. (1992) The rate of formation of transition-state analogues in the active site of adenosine deaminase is encounter-controlled: Implications for the mechanism, *Biochemistry 31*, 39-48.

84. Seffernick, J. L., McTavish, H., Osborne, J. P., de Souza, M. L., Sadowsky, M. J., and Wackett, L. P. (2002) Atrazine chlorohydrolase from *Pseudomonas* sp. strain ADP is a metalloenzyme, *Biochemistry 41*, 14430-7.

85. Weiss, P. M., Cook, P. F., Hermes, J. D., and Cleland, W. W. (1987) Evidence from nitrogen-15 and solvent deuterium isotope effects on the chemical mechanism of adenosine deaminase, *Biochemistry 26*, 7378-84.

VITA

Name: Ricardo Martí Arbona

Address: 2409 Bandera Dr. Apt. D
College Station, Texas 77845

Alternative Address: P.O. Box 224
Angeles, P.R. 00611

Email. Address: r_marti07@yahoo.com

Education: Texas A&M University
College Station, Texas
Ph.D. Chemistry
December 2006

Universidad de Puerto Rico
Rio Piedras, Puerto Rico
B.S. Chemistry
May 2001